Copyright Warning & Restrictions

The copyright law of the United States (Title 17, United States Code) governs the making of photocopies or other reproductions of copyrighted material.

Under certain conditions specified in the law, libraries and archives are authorized to furnish a photocopy or other reproduction. One of these specified conditions is that the photocopy or reproduction is not to be "used for any purpose other than private study, scholarship, or research." If a, user makes a request for, or later uses, a photocopy or reproduction for purposes in excess of "fair use" that user may be liable for copyright infringement,

This institution reserves the right to refuse to accept a copying order if, in its judgment, fulfillment of the order would involve violation of copyright law.

Please Note: The author retains the copyright while the New Jersey Institute of Technology reserves the right to distribute this thesis or dissertation

Printing note: If you do not wish to print this page, then select "Pages from: first page # to: last page #" on the print dialog screen

ABSTRACT

IMPROVEMENT OF WATERJET AND ABRASIVE WATERJET NOZZLE

by
Zheng Li

This investigation is concerned with the improvement of the nozzle design for water and abrasive water jet machining. The mechanism of formation and characteristics of pure water and abrasive water jets are investigated in order to determine quasi-optimal process conditions.

To improve the pure water jet machining, a pulsed water jet nozzle, which employs the principle of the Helmholtz type resonator, is investigated experimentally and numerically. The experiments show the advantages of this nozzle over the commercial nozzle in cutting and cleaning. A numerical solution of the differential equations of continuity, momentum conservation, turbulent kinetic energy and dissipation for two dimensional axi-symmetric flow by employing the FIDAP package is developed and used for the numerical prediction of pulsed turbulent flow inside the nozzle. The determination of the optimal nozzle parameters aided by numerical simulation is carried out and the best ratios of the parameters are: h (cavity length) / d_1 (diameter of upstream nozzle) = 3.0 and d_2 (diameter of downstream nozzle) / d_1 (diameter of upstream nozzle) = 1.3. The results of simulation agree well with the experiments. The numerical prediction of the velocity at the exit of the pulsed nozzle is validated by the velocity measurement by a laser transit anemometer. The obtained velocity changes periodically and ranges from 190 m/s to 230 m/s. A numerical analysis enables us to evaluate nozzle design and the effectiveness of the numerical prediction is validated experimentally. The numerical solutions and experimental results present the improvement on the pure water cutting and cleaning and provide a technological basis for the improvement of pulsed water jet machining and technology.

To increase the efficiency of abrasive water jet machining, an improved abrasive water jet nozzle is developed and experimentally investigated. The performance of the abrasive water jet is improved by the modification of the abrasive particles path prior to the collision with the water jet. This modification is obtained by control of the angle (α) between the top-shaped surface of the focusing tube and the water flow direction and change of distance (H) between the water nozzle and focusing tube. The improvement of water-particles mixing increases the rate of material removal and simplifies the alignment procedure. It is found that the optimal parameters for the nozzle design are: $\alpha = 45^{0}$ and H = 1.587 mm. The experimental results and analysis show the potential of this modified nozzle for applications in abrasive water jet machining.

IMPROVEMENT OF WATERJET AND ABRASIVE WATERJET NOZZLE

by
Zheng Li

A Dissertation
Submitted to the Faculty of the
New Jersey Institute of Technology
in Partial Fulfillment of the Requirement for the Degree of
Doctor of Philosophy

Department of Mechanical and Industrial Engineering

October 1994

APPROVAL PAGE

AN INVESTIGATION OF THE IMPROVED AWJ NOZZLE AND PULSED WJ NOZZLE

Zheng Li

Dr. Ernest S. Geskin, Dissertation Advisor **Date**
Professor of Mechanical Engineering
of the Department of Mechanical and Industrial Engineering, NJIT

Dr, Rong Chen, Committee Member **Date**
Professor of Mechanical Engineering and Graduate Advisor
of the Department of Mechanical and Industrial Engineering, NJIT

Dr. Nouri Levy, Committee Member **Date**
Associate Professor of Mechanical Engineering
of the Department of Mechanical and Industrial Engineering, NJIT

Dr. Zhiming Ji, Committee Member **Date**
Assistant Professor of Mechanical Engineering
of the Department of Mechanical and Industrial Engineering, NJIT

Dr. Denis Blackmore, Committee Member **Date**
Professor of the Department of Mathematics, NJIT

BIOGRAPHICAL SKETCH

Author: Zheng Li

Degree: Doctor of Philosophy

Date: October 1994

Undergraduate and Graduate Education:

- Doctor of Philosophy in Mechanical Engineering, New Jersey Institute of Technology, Newark, NJ, 1994
- Master of Science in Power Engineering, Shanghai Institute of Mechanical Engineering, Shanghai, P.R.China, 1987
- Bachelor of Science in Power Engineering, Shanghai Institute of Mechanical Engineering, Shanghai, P.R.China, 1982

Major: Mechanical Engineering

Presentations and Publications:

Zheng Li and E.S. Geskin, 1994, "Computer Aided Simulation of Turbulent Flow in Pulsate Jet Nozzle". 14th International Computers in Engineering Conference, Hawaii.

Zheng Li and E. S. Geskin, 1994, "Investigation of the Performance of Self-Resonating Nozzle". 12th International Conference on Jet Cutting Technology, France.

Zheng Li, and E. S. Geskin and L. Tismenetskiy, 1994, "Improvement of Water-Particles Mixing in the Course of Abrasive Waterjet Formation". ASME Annual Symposium on Nontraditional Manufacturing Processes of the 1990's, Chicago.

Zheng Li and E. S. Geskin, 1994, "Numerical Analysis of Waterjet Flow in a Pulsate Jet Nozzle". 7th International Symposium on Transport Phenomena in Manufacturing Processes, Mexico.

BIOGRAPHICAL SKETCH
(Continued)

Zheng Li and E.S. Geskin, 1993, "Efficient Cleaning of Metal Surface by Pulsed Water Jet", ASME Graduate Student Technical Conference for Region I and II. Polytechnic University, New York.

Zheng Li and E.S. Geskin, 1992, "Experimental Study of Advanced Machining Using An Integrated Plasma, Oxyacetylene And Waterjet Workcell", ASME Graduate Student Technical Conference for Region I and II. Steven Institute of Technology, New Jersey.

Zheng Li, 1992, "Development of Masking Technology in Plasma Treatment", ASME Graduate Student Technical Conference for Region I and II. Steven Institute of Technology, New Jersey.

This dissertation is dedicated to
my parents

ACKNOWLEDGMENT

The author wishes to express his sincere gratitude to his advisor, Professor E. S. Geskin, for his guidance and constant supervision, many valuable suggestions, continuous support and friendship throughout this research.

Special thanks to Drs. R. Chen, N. Levy, Z. Ji and D. Blackmore for serving as members of committee, having kindly provided valuable suggestions in this study. Additionally, sincere thanks to Dr. A. Harnoy for his valuable suggestions, to Dr. Md. E. H. Khan for his timely help in this research and to Dr. Y. Q. Zhang for his initial help in this work.

The author wishes to thank the Department of Mechanical and Industrial Engineering, NJIT for funding this research and assistantship from Sep, 1990 to Sep, 1994 during Ph.D. program, Pittsburgh Super Computer Center and Sun Workstation of Department of Mechanical and Industrial Engineering, NJIT for giving computing support.

And finally, a grateful thank you to the author's family, especially, his wife, XiaoLin Wang, for the firm support and encouragement.

TABLE OF CONTENTS

TABLE OF CONTENTS
(Continued)

LIST OF TABLES

LIST OF TABLES
(Continued)

Table **Page**

LIST OF FIGURES

LIST OF FIGURES
(Continued)

Figure **Page**

LIST OF FIGURES
(Continued)

Figure **Page**

LIST OF FIGURES
(Continued)

Figure **Page**

LIST OF SYMBOLS

Symbols	Meaning
B	buoyancy generation term
c_1, c_2, c_3	empirical constants
c_ε, c_μ	empirical constants
d_1, d_2	diameters of upstream and downstream orifices
f_i	body force components per unit mass
G	shear generation term
g_i	gravitational force components
H	distance between orifice and focusing tube
h	cavity length
k	kinetic energy
l_m	Prandtl's mixing length
P	fluid pressure
r	radius of the orifice
t	time
t_0	reference time point
u	velocity component along axis of water flow direction
u_i	Eulerian fluid velocity component
u_t	characteristic velocity scale
v	velocity component along radius
x_i	Cartesian coordinates of a point in the fluid
y	coordinate normal to the wall
α	angle between tapered surface of the focusing tube and axial direction of the nozzle
β	thermal expansion coefficient

LIST OF SYMBOLS
(Continued)

Symbols	Meaning
θ	temperature of the fluid
θ_β	reference temperature
φ	shape function
ϕ	generic flow variable
ε	turbulent dissipation
$\varepsilon_F, \varepsilon_\mu$	tolerance of convergence
ρ	density
κ	Von Karman constant
δ_l	characteristic length scale
μ	dynamic viscosity
μ_t	eddy viscosity

CHAPTER 1

INTRODUCTION

1.1 Pulsed Water Jets

High pressure water jets have been used as an industrial tool for many years. This cutting method shows great potential not only in cutting and drilling minerals, rocks and concrete, but also in comparison with conventional cutting and drilling tools which are inherently limited by their lack of both strength and resistance to abrasion. This cutting technology has proved to possess many advantages such as low production cost, high cutting speed and low material loss. The application of high pressure water jet cutting technology has been traced back to the 1970's when the jet was used in cutting some soft materials (non-metal) with a pressurized pure water jet of 132 - 198 Mpa. This application began by using a high pressure and low flow rate water jet in cleaning, mining and cutting woods or paper products. A working pressure of the water jet at a maximum of 330.7 Mpa proved to be able to cut a variety of relatively soft material at a high cutting rate. At the present, the water jet (WJ) machining technology has found more applications in industry, including cleaning of deposits from the shell and tube side in heat exchangers, and removal of plastic explosives from unwanted locations. In order to increase the efficiency of WJ performance, a number of investigations have been undertaken in the development of the pulsed WJ techniques. It is demonstrated that a pulsed jet is an effective cleaning and machining tool and is superior to the continuous water jet. Periodical forces exerted on a target by such a jet induce high momentary stresses in the impingement zone. The increased erosivity afforded by causing a water jet to break up into a series of water slugs has long been recognized. Such interrupted or pulsed jets offer the following advantages, compared to the steady-flowing jets, for either cleaning a substance from a substrate or cutting into a bulk material:

(1) Larger impact stresses, due to the water hammer pressure, which enhance the local erosive intensity,

(2) Greater ratio of impacted area per volume of jetted water, thus exposing larger areas of the surface to the water hammer pressure,

(3) Cycling of loading: this promotes unloading stresses which may enhance the process of debonding the substance from the substrate, or fracturing the bulk material being cut, and

(4) Short duration loading, which tends to minimize energy losses within either the substrate being cleaned or the bulk material being cut, and hence increases the material removal per input energy.

It is unfortunate that to date an adequate model to prescribe the flow field of the high speed pulsed WJ has not been developed. Although a number of prior researches have been concerned with the analysis of pulsed jets, the available information is not sufficient to predict the WJ flow characteristics, such as distribution of pressure and velocity inside the nozzle. These parameters which are determined by the nozzle design strongly affect the performance of the pulsed WJ. Thus the optimal nozzle design, aided by experiments and numerical simulation, is the objective of the second part of this research.

1.2 Abrasive Water Jets

The rapid growth of harder and difficult-to-machine materials over the past two decades necessitates the development of compatible abrasive water jet (AWJ) machining techniques. A number of research works have been performed to find new applications of the jet cutting, to determine the jet properties, and to improve the jet performance. In the new applications, the AWJ cutting is more efficient, accurate and less material consuming than some other traditional cutting methods. In the beginning of the 1980's, it was found that by mixing the abrasive particles in the jet the cutting capability will be increased so that almost any type of materials can be cut. The jet developed through the entraining of solid particles is the abrasive water jet (AWJ). During this process, the abrasives are flowed into the

downstream of a pure water jet which guides the particles into a focusing tube where mixing takes place and forms the water jet stream. In the focusing tube the particles are accelerated and this means that the kinetic energy of the particles increases and this creates the high cutting capability of the developed two phase mixture. An AWJ consists of liquid water, bubbles and abrasive particles. When impinging at a target material, each of them is capable of causing damage on the target surface. During the study of AWJ machining, it is found that the effect of water and bubbles is too small to be of concern if compared with the effect of abrasive particles on the material removal. Thus, the erosion by solid particles which is defined as the mechanism of material removal in the course of particles impinging on a target surface is defined as the main mechanism of the AWJ machining processes. So, the extent of mixing between abrasive and water has an important effect on the AWJ performance.

The abrasive water jet (AWJ) has a potential of becoming one of the principal machining technologies. Unfortunately, at the present this process has found very limited application. The AWJ is used only if other machining technologies, such as conventional or thermal beam machining, fail. One of the main reasons impeding the commercial application of AWJ is low process efficiency. The productivity of AWJ machining is far below than that of milling or laser cutting. At the same time, the expansion of AWJ machining will have substantial and diverse effect on manufacturing. It will enhance the complementation of new materials, expand the use of existing hard-to-machine materials, make practical formation of complex sculptured surface, reduce the amount and severity of subsurface defects and increase flexibility of machining facilities. Material removal by AWJ is carried out by the particles impinging on the target, thus the process efficiency is determined by the particles momentum. Low AWJ efficiency is due to the high rate of energy dissipation in the course of the jet formation and water-particles momentum exchange. Analysis of the water jet pressure-velocity correlation shows that the principal cause of the energy dissipation in the course of particle acceleration is the process of mixing. The first step in

the formation of a slurry jet is injection of the abrasive particles into the focusing tube. This step determines to some extent interaction between water and particle flow and subsequent entrainment of the particles by the water jet. At the same time, at this stage of the stream formation, the particle flow can be readily guided. Thus improvement of the geometry of the region adjacent to the water-particle mixing constitutes an effective means for the improvement of the overall nozzle efficiency. Such an improvement is the objective of the first part of this research.

CHAPTER 2

LITERATURE SURVEY

The prior investigations of the WJ and AWJ machining technologies are discussed in this section.

2.1 Pulsed Water Jets

A variety of techniques have been used to interrupt water jets. Many investigators examined phenomena related to fluctuating jets, either self-excited or with an external means for stimulating or driving the pulsation in the jet flow. As described by Nebeker, et al.,1970-1980, a pulsed water jet has advantages over conventional ones in water jet cutting and cleaning. By exerting an alternating force on the targets, the pulsed jet can produce high momentary pressure and subsequently generate high tensile stresses in the impingement zone. This enhances unloading damage in the materials. There are several major kinds of devices which can generate the pulsed jets.

1. Percussive Jet:

The percussive jet (Fig. A.1) can be obtained by modulating the discharge of water through the jet nozzle, i.e., by cycling the discharge flow above and below its average value with some particular frequencies, amplitudes and wave forms. When this varying free flow strikes a target, the momentum flux through the nozzle is not transmitted as a steady force, but as a possibly discontinuous sequence of force peaks or percussive impacts.

2. Impulsive Water Cannon:

In this case (Fig. A.2), the reciprocating movement of the piston generates the discontinuous flow. When the piston moves towards the right, it pushes the water out of the nozzle. Because the cross sectional area of the piston cylinder is much larger than that

of nozzle, the high pressure in the cylinder can be transmitted into high kinetic energy of the flow at the nozzle exit. When the piston moves to the left, the water is supplied into the cylinder. By repeating the above cycle of the piston movement, the so called "water cannon" can be formed at the exit of the nozzle. The reciprocating time of the piston is controlled to modulate the frequency of the pulsed jet for different drilling or cutting applications.

3. Pulsed Jet Produced by Ultrasonic Vibration of the Nozzle:

A new concept for producing a discontinuous liquid jet is currently being developed by the use of ultrasonic axial nozzle vibration (Fig. A.3). An ultrasonic power generator is used in conjunction with a converter booster and horn in order to impose vibration on the nozzle. The high pressure water is induced into the horn and moved to the nozzle exit. When the nozzle is moving in the same direction as the continuous jets, it increases the absolute jet velocity. While the nozzle moves in the opposite direction of the jet, it decreases the absolute jet velocity. As a result, the jets breaks into segments at the point where high velocity particles hit the slow moving ones. In this way, a pulsed jet flow is generated.

4. The Fig. A.4 shows a pulsed jet produced by an oscillating piston installed upstream of the nozzle. At the initial stage, the steady flow enters the oscillating chamber. When the flow exits the oscillating chamber, the flow becomes the unsteady flow due to the vertically reciprocating movement of piston. Finally, the pulsed water flow is obtained at the exit of the nozzle because of the periodic movement of the piston.

5. A pulsed flow can be produced by installation of an oscillating mechanical valve into the nozzle body (Fig. A.5). The periodic opening and closing of the valve is mechanically or electronically controlled. So, the steady flow at the entrance of the nozzle can become pulsing flow at the exit of the nozzle.

6. Mechanical interruption of a continuous water jet can also be obtained by a perforated rotating disc (Fig. A.6). The perforated rotating disc is driven by a motor and placed

downstream of the nozzle. During the process of fluid flow from upstream to the downstream of the nozzle, the jet passes the hole of the disc or impinges on the disc surface alternately and thus the pulsed jet formed.

7. In the 1980's, V.E. Johnson and A.F. Conn developed a concept of the self-resonating cavitating jet which can result in pulsation by modifying the geometry of the nozzle body. The operation of the self-resonating cavitating nozzle is based on the theory of fluid transients and hydro-acoustics. When the fluid flows all the way to the exit of nozzle, a kind of surge pressure is formed due to the change of the cross sectional area of the pipe. The surge pressure is then fed back to the inlet of the pipe and superimposed on the pressure pulses of the incoming flow to form a standing wave. If the frequency of the surge pressure matches the natural frequency of the flow, pressure resonance will occur and the jet is converted into a system of discrete ring vortices, leading to the inception of cavitation. The large vortices and strong oscillation make it possible to generate stronger cavitation and thus the erosion and cleaning action is enhanced.

2.2 Abrasive Water Jets

In AWJ cutting, the nozzle plays a key role by converting high pressure to the high velocity necessary for cutting. The efficiency of this conversion process and the quality of the cut itself depends on the nozzle design, especially on the configuration of the mixing chamber. A number of studies are dedicated to the improvement of water and particles mixing.

1. A spiral nozzle was developed by Horri, 1990 (Fig. A.7) for use in efficient mixing of abrasive and improved focusing of spiral water jet streams in high pressure AWJ cutting applications. The development of this nozzle is based on the spiral flow theory. To obtain a focused jet flow, a nozzle is designed with an annular slit connected to a conical cylinder. Pressurized fluid is supplied through the slit (1) and the fluid, passing through the conical cylinder, is deformed into a spiral flow with the maximum axial flow on the axis.

Abrasive is fed from the inlet (2) in the nozzle. Turbulent pipe flow is deformed into a spiral flow as the flow passes through the conical cylinder.

2. An apparatus (Fig. A.8) for improving abrasive mixing was developed by Kiyoshige, 1991. In this apparatus the ejecting water passes through a special path. The nozzle orifice has an upstream tapered portion. The diameter of this orifice gradually increases toward an upstream opening at which the orifice is connected smoothly to the downstream end of the ejected water passageway. The abrasive suspension is supplied to and merges with the streamlined flow of ejecting water near the junction of the water passageway. The resulting dual-layer streamlined jet has better cutting performance.

3. A new AWJ assembly (Fig. A.9) was suggested by Yie (1984). When multiple fluid orifices are utilized, an area of lower pressure is formed in the central portion of the combined fluid stream thereby aiding in the mixing of the solids into the fluid stream. A flow shaping nozzle is provided at the exit of apparatus to increase the mixing of the solid within the fluid jet stream. The flow shaping nozzle has axial and radial freedom of movement for forming the fluid-solid stream and self-alignment. The apparatus and process of this study, in one preferred embodiment, involves introduction of the solids in the form of a foam into the fluid jet stream. The particulate-fluid mixing devices provide pressurized fluid flow through the central portion of a nozzle and particulate are introduced peripherally. Thus, the fluid flow is not disturbed and the peripheral portion of the nozzle may be readily adapted to accommodate a wide variety of particulate requirements.

4. As it is known, slight angular misalignment of the nozzle makes the jet impact the focusing tube first, before exit. This causes quick erosion and distortion of the focusing tube as well as poor cut quality, due to non-uniform mixing of the abrasive with water. Alignment is usually carried out on-line manual by adjustment of the focusing tube and sapphire nozzle and it may require several iterative adjustments before satisfactory alignment is obtained. This problem can be arduous, time-consuming and frustrating. An

alignable nozzle assembly was studied by Singh and Munoz, 1990. The alignable nozzle assembly described in this paper is comprised of the nozzle body, wear insert, focus tube, alignment screws, abrasive inlet fitting and nozzle. All parts are kept to a minimum manufacturing tolerances so that tolerance-based misalignment becomes acceptable. During operation, the alignment is carried out by tightening or loosening special screws around the nozzle holder.

2.3 Comments of the Previous Studies

1. All of the above mentioned types of pulsing water jets are subject to the excessive internal component wear, complicated construction and pressure losses associated with mechanically driven approaches. Also, up to the present, the available information is not sufficient for the prediction of the flow characteristics in the pulsed nozzle and for the optimal nozzle design. Because of this further improvement of pulsed water jet machining is impeded. To improve pulsed jet machining, a self-excited pulsed WJ nozzle which has the advantages of simple structure, small volume, no external excitation source and moving seals is developed and such characteristics of pulsed jets as pressure, velocity, turbulent kinetic energy and viscous dissipation which largely depend on the nozzle designs have been extensively investigated experimentally and numerically in this study.

2. Although a number of previous studies have been concerned with the modification of the AWJ nozzle to improve the AWJ performance, insufficient information about such improvement of the mixing chamber is available. Also, the above mentioned AWJ nozzles have some disadvantages, such as extra energy losses through thin annular slits or paths and complicated configuration of the nozzle. Since the mixing of water and abrasive particles has a stronger effect on the AWJ performance, investigation of water-particle mixing is a part of this research.

CHAPTER 3

EXPERIMENTAL APPARATUS AND PROCEDURES

The presented experimental study is concerned with the optimal nozzle design. The first series of experiments are related to the modification of the mixing chamber of the AWJ nozzle. The second series of experiments are involved with the improvement of the pulsed WJ nozzle design. The laser transit anemometer (LTA) is employed in the determination of water velocity at the exit of the pulsed nozzle. A machining system (Fig.3.1) employed in this investigation is manufactured by Ingersoll-Rand Inc. The major units of the system are described as follows:

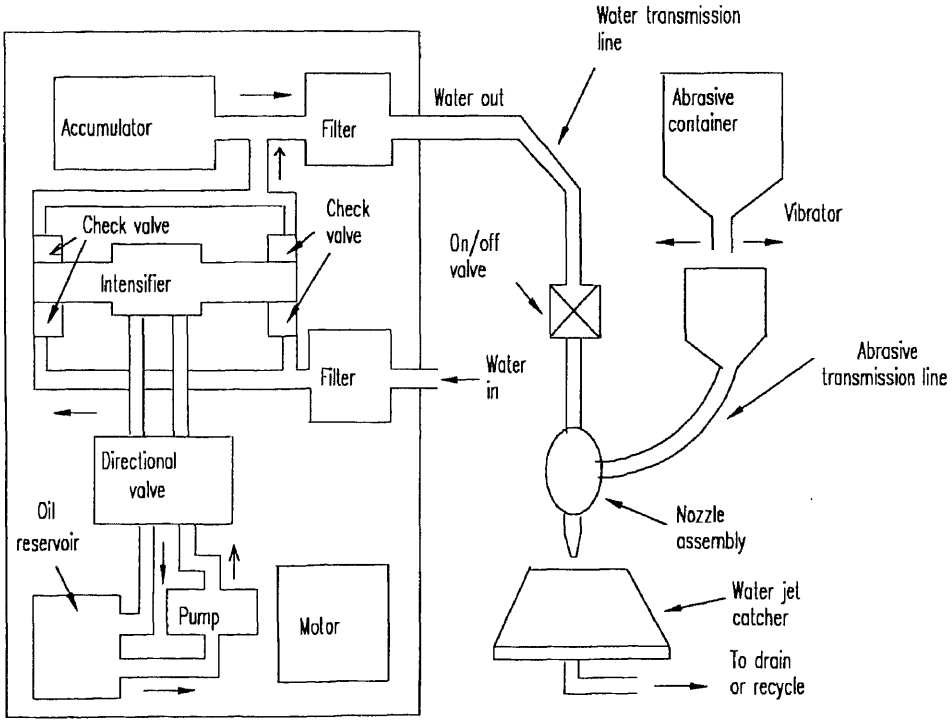

Figure 3.1 Water Jet Machining System

1. Water Preparation Unit

This unit includes a booster pump, prime mover, intensifier, filters, water softener, accumulator, control and safety instrumentation. To ensure continuous fluid flow into the high pressure cylinder, the booster pump feeds the water into the circulation pipe line at a low pressure (1.25 Mpa). The impurities such as iron and calcium compounds can dissolve in the water at the high pressure and thus destroy the orifice. Thus the low pressure filters (1 - 10 microns) and softener are employed to remove these impurities. A hydraulic oil driven intensifier (10 - 40 hp) develops pressure up to 345 Mpa in the water fed from the booster pump. The oil and water circuits are separated. The oil pressure of 20 Mpa developed by a rotary pump is used to drive an intensifier. The intensifier is a double acting reciprocating (15.24 cm diameter) type pump. It is operated periodically by an adjustable controller. The high pressure water from both sides of the intensifier is fed to an accumulator in which the pressure is stabilized. Because the water is not discharged uniformly from the intensifier at all piston positions due to the compressibility of 12 percent of water at the pressure of 345 Mpa, the accumulator can provide uniform discharge pressure and fluid flow.

2. High Pressure Water Distribution Unit.

The high pressure water from the accumulator is fed to the work station through a series of pipes, flexible joints, fittings and swivels. Under the pressure of 133 Mpa, a hose can be employed without swivels. This simplifies pumping. When the pressure exceeds 133 Mpa, hard pipes, swivels, flexible joints and fittings should be employed. The joints, elbows and the longer pipe length, increases line pressure drops. So it is better to centralize the water preparation unit in one or more work stations which are fixed in suitable places for different applications.

3. Work Station.

Here the actual cutting operations are performed. The station consists of the robotics work cell, abrasive feeder and catcher system. The robotics work cell is the gantry CNC 5-

axis robotics work cell controlled by the Allen-Bradley 8200R controller. The input can be received from keyboard entry, punched tape and magnetic tape with EIA standard RS-232, 244, 358 and 274. Also, the standard G, F and M codes are used. The abrasive feeder ensures continuous delivery of the abrasive into the mixing chamber of the nozzle body with a controlled rate. The bulk abrasive is stored in a hopper and the exit of the hopper faces an electrically adjustable vibrating tray. The tray can meter the flow of abrasive to a catch hopper by the control of the amplitude of vibration. The abrasive is then fed to the mixing chamber of the nozzle through the tube. The catcher unit is installed below the machining head to store the ejected jets which are mixed with abrasive, water and cutting debris. A drain near the base of the catcher tank ensures the water and abrasive flow into a settlement tank in which the water can be drained out and the grit left in the tank.

3.1 Experimental Study of the Improved AWJ Nozzle

The geometry of the mixing chamber of the AWJ nozzle is modified by shaping the upper part of the focusing tube and varying the distance between the focusing tube and water nozzle. The rate of material removal done by modified and commercial nozzles are compared. Results of the experiments are used to identify a way to improve the focusing tube design and the nozzle assembly.

In our experiments a commercial Ingersoll-Rand nozzle is modified in order to improve mixing conditions. The geometry of a modified nozzle assembly is shown in Figs. 3.2 - 3.3. In this nozzle design, the tungsten carbide focusing tube is processed to the taped shape with certain angles and the position of this tube is made variable. The experiments involved cutting steel samples using a commercial and modified nozzle. A comparison was done of the results. Low carbon steel #c 1020 and stainless steel #316 are used. The experiments were carried out at the Ingersoll-Rand's 5-axis water jet work cell. Barton-mines garnet is used as an abrasive material.

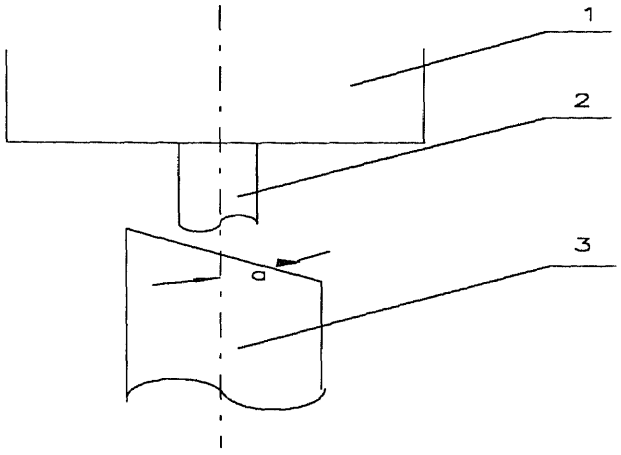

Figure 3.2 Schematic of the Improved Focusing Tube 1--water nozzle 2--water jet 3--focusing tube (carbide) α--angle between waterjet axes and tapered surface of focusing tube

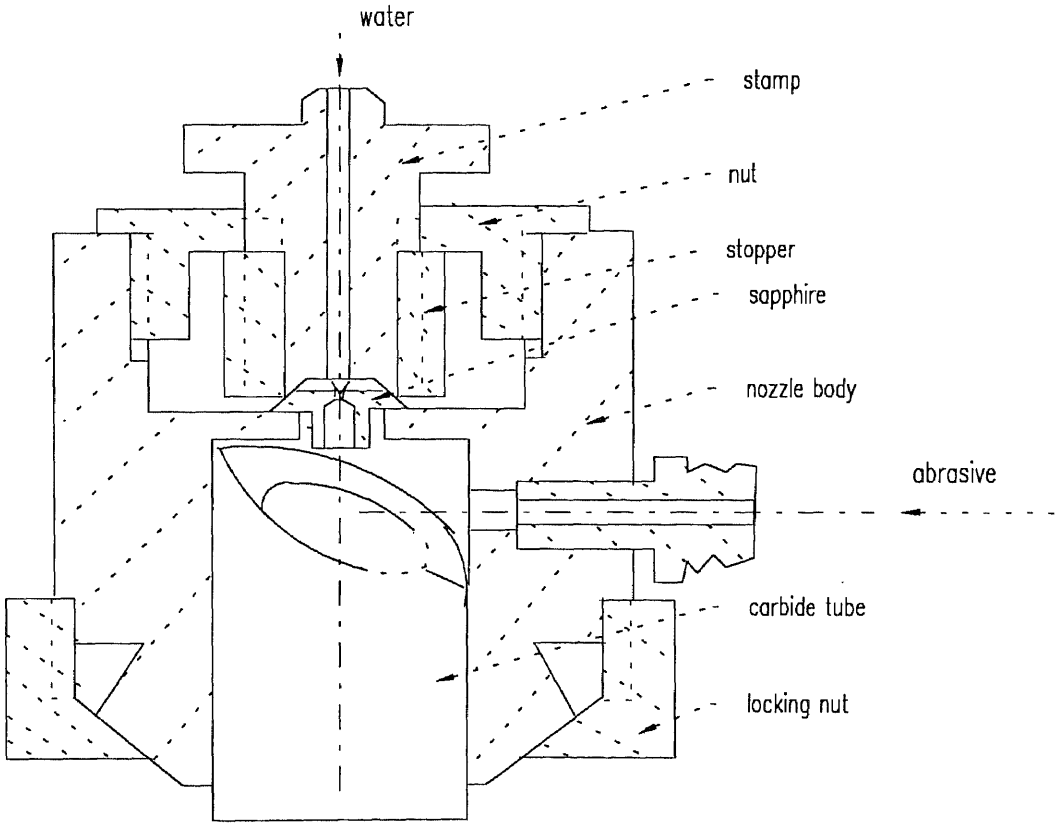

Figure 3.3 Schematic of the Improved AWJ Nozzle Assembly

The experiments were performed at the following operational conditions: Water pressure = 330.7 Mpa, diameter of the water nozzle = 0.254 mm, diameter of the focusing tube = 0.762 mm, stand off distance = 2.54 mm, traverse speed = 3 - 40 cm/min, abrasive size = 80 HP, 120 HP, 150 HP and abrasive flow rate = 100 - 700 g/min.

To determine the optimal design of this AWJ nozzle, the following different configurations of the mixing chamber were selected: the distances between the sapphire orifice and focusing tube (H) are 0.5 mm, 1.587 mm and 3.175 mm; the angle (α) determining the shape of the upper part of the focusing tube is equal to 30, 45 and 60 degree. At a commercial AWJ nozzle this angle is 90 degree.

In the course of cutting straight grooves were formed at the different operational conditions by the use of the modified and commercial AWJ nozzles. The depth of cut was measured by the use of a toolmaker microscope and a video matrix econoscope. The results of cutting enabled us to evaluate the effectiveness of the mixing chamber modification.

3.2 Experimental Study of the Pulsed WJ Nozzle

The operation of the fabricated pulsed WJ nozzle (Fig. 3.4) is examined. It is shown that the nozzle performance is determined by the dimensionless numbers h / d_1 and d_2 / d_1 . In our experiments, these parameters were selected as process variables. The selected variables of h / d_1 and d_2 / d_1 is shown in Table 3.1. The nozzle is constructed by inserting two commercial orifices into a special holder. The diameter of the orifices (d_1 and d_2) and the distance between the exit of the upstream and downstream orifices were changed in order to get the optimal nozzle design. The experimental study involved the cutting and cleaning of various samples using both the pulsed and commercial Ingersoll-Rand's nozzle and the experiments enable us to compare effectiveness of these nozzles.

Table 3.1 The Combination of Different Parameters of Improved Pulsed WJ Nozzle Used in Experiments

d2/d1	1.20	1.30	1.40
h/d1	2.50	3.00	3.50

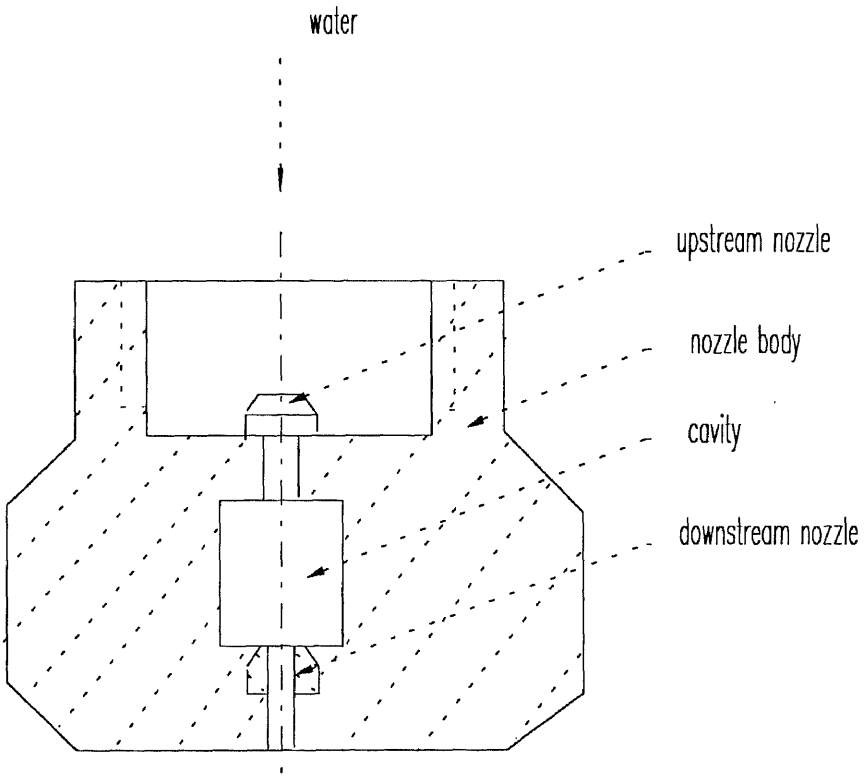

Figure 3.4 Schematic of Pulsed WJ Nozzle

The experiments included cutting aluminum 6061 and titanium 6A1/V4 samples as well as the removal of water, oil, epoxy paints and rust from a material surface by use of a commercial nozzle and pulsed nozzle. The experiments were carried out at the Ingersoll-Rand made 5-axes robotics work cell at the following operational conditions: water pressure = 330.7 Mpa, nozzle type = #9, #10, #12 and #14, traverse speed = 10 - 5100 cm/min. The results of cutting were evaluated by the measurement of the depth of penetrating into a material, while the cleaning results were determined by the measurement of the rate of the paint and rust removal. The rate of deposit removal is determined by the visual identification of the deposit free area.

3.3 Measurement of Water Velocity at the Exit of Pulsed Nozzle

Another experiment involved measuring the axial water velocity at the exit of the pulsed nozzle using a laser transit anemometer (LTA). A Dantec LTA with a 15 mw He-Ne laser as the beam source was employed to conduct the measurement. The LTA signal was processed and stored in a Nicolet 320 oscilloscope for further analysis.

CHAPTER 4

EXPERIMENTAL RESULTS AND DISCUSSIONS

The investigation is carried out using a wide range of process variables. The results of these experiments enable us to identify the effect of the nozzle parameter on the performance of the AWJ and pulsed WJ machining.

4.1 Improved AWJ Nozzle

The experimental comparison between the improved and commercial AWJ nozzle at different test conditions is presented in Figs. B.1 - B.6 and Tables B.1 - B.2. The effect of different abrasive flow rates on the cutting depth, with abrasive #80, #120 and #150 respectively, is shown in Figs. B.1(a) - B.1(c) and Table B.1. The effect of the transverse speed of the nozzle movement on the cutting depth is presented in Figs. B.2 - B.3. The effect of different nozzle combinations on the nozzle performance is shown in Figs. B4(a) - B.4(c) while the effect of variations of angle α and distance H on the cutting depth is given in Figs. B.5 - B.6 and Table B.2. The presented data (Figs. B.1 - B.3 and Table B.1) demonstrate definite improvement in the cutting results, obtained with the use of the modified AWJ nozzle. The most probable cause of this improvement is modification of the particles motion. The particles entering the modified mixing chamber are not halted at the corner around the upper part of the focusing tube, therefore a particle flow at the entrance of the focusing tube is better organized. This results in the uniform distribution of the abrasive particles in the flow and thus increases the rate of material removal.

The effect of the abrasive flow rates and nozzle parameters on the operational results is presented in Figs. B.4 - B.6. These figures evidently demonstrate the extreme effect of the α and H on the jet performance. Three deferent angles (α) of $30^0, 45^0$ and 60^0 are tested and the optimal angle is 45^0 (Figs.4.1 and B.5). The most probable reason for the

extreme system behavior is that a smaller angle results in the particles being halted at the lower corner of upper part of the focusing tube while a bigger angle causes particles to be halted at the lower and the upper corner of upper part of the focusing tube. The concentrated particle flow can be formed at the angle of 45^0 and then well mixed into the water flow. The effect of the distance (H) between sapphire orifice and focusing tube on the cutting performance is shown in Figs. 4.2 and B.6. Among H = 0.5 mm, 1.578 mm and 3.175 mm, the optimal performance is obtained at the distance of 1.578 mm. Probably the abrasive particles are partially blocked by the lower edge of the top part of focusing tube at smaller H and halted at the lower and upper corner of the top part of the focusing tube at a larger H.

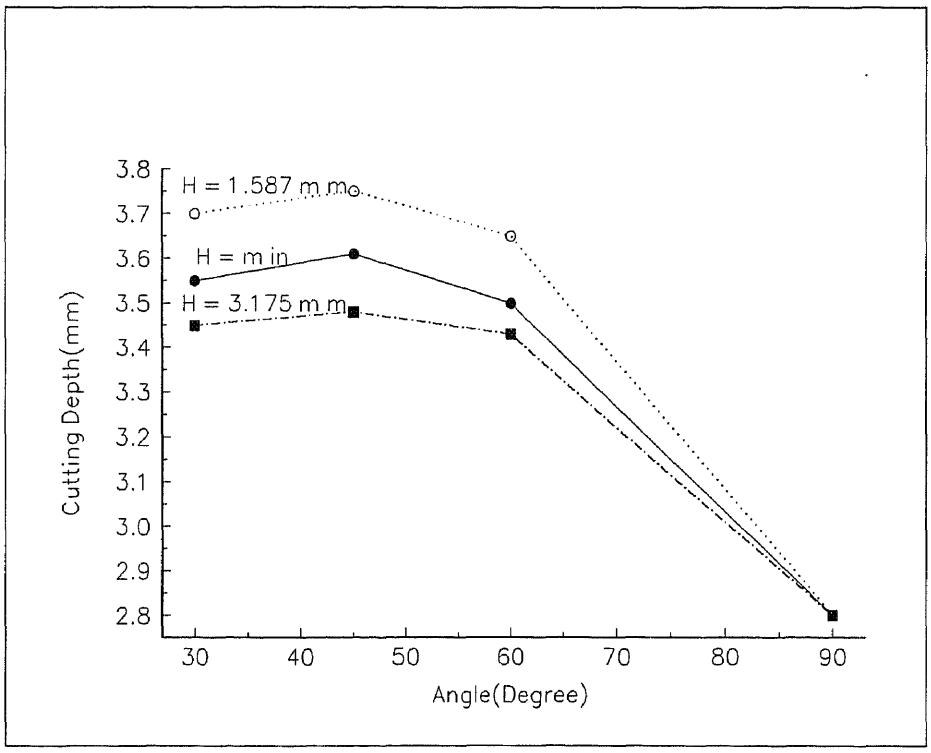

Figure 4.1 Effect of α on Cutting Depth (abrasive: 150 HP; abr flow: 558.50 g / min; sapphire: #10; focusing tube: #30; material: reg steel; trav spd: 25.4 cm / min; $\alpha = 30$, 45 and 60 degree at the modified nozzle; $\alpha = 90$ degree at the commercial nozzle; (H = min = 0.5 mm)); Optimal angle α is 45 degree.

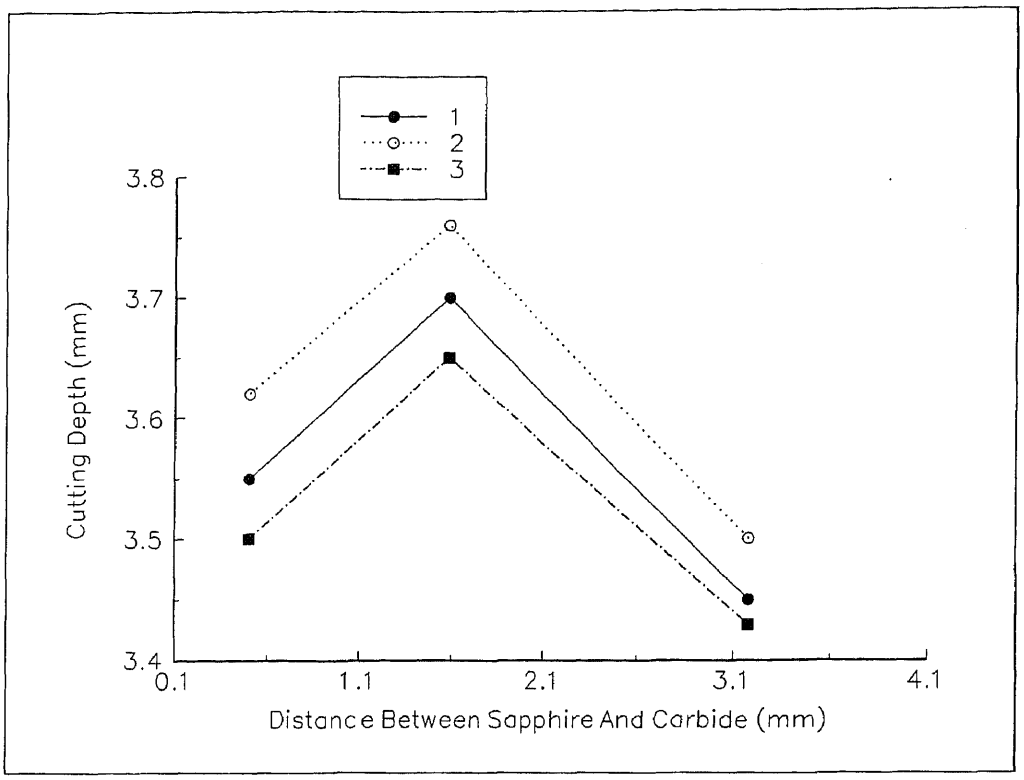

Figure 4.2 Effect of H on Cutting Depth (abrasive: 150 HP; abr flow: 558.50 g / min; sapphire: #10; focusing tube: #30; material: reg steel; trav spd: 25.4 cm / min; 1-- $\alpha = 30^0$; 2-- $\alpha = 45^0$; 3-- $\alpha = 90^0$) Optimal stand off distance is 1.587 mm.

Another important effect of this AWJ nozzle design is the increase of the flow stability in the focusing tube. This increase is demonstrated by the ability of this AWJ nozzle to be operated without any special alignment of the water nozzle and focusing tube. Thus the tolerance of the WJ orifice position is substantially increased and the operation of machining is simplified and eased.

Such "forgiveness" in the modified AWJ nozzle can also be explained by the better focusing of the abrasive particles entering the carbide tube. A smaller number of loss particles reduces the diameter of the slurry flow within the focusing tube and thus allows larger variation in the direction of the flow axis without destruction of the flow.

4.2 Pulsed WJ Nozzle

The experimental result in comparison between the pulsed and commercial WJ nozzle is presented in Figs. C.1 - C.6 and Tables C.1 - C.9. The Figs.C.1 - C.2 show the effect of the traverse speed on penetrating depth in cutting aluminum and titanium. The effect of nine different combinations of pulsed WJ nozzle on the cutting performance is presented in Figs. C.3(a) - C.3(b) and Table C.1(a) -C.1(b). The results of removal of water, oil and epoxy paints and rust from a material surface, under different stand off distances and traverse speed, are depicted in Figs. C.4(a) - C.5(d) and Tables C.2 - C.9. The cleaning results are evaluated by the correlation between the traverse speed and the critical stand off distance which is the maximum distance when deposit removal occurs. It is shown that at a small stand off distance the pulsed WJ nozzle is more efficient in cleaning than the commercial WJ nozzle. The cleaning results of oil and epoxy paint (Figs. C.4(e) - C.4(f)) obtained by people in our laboratory show the better performance of the commercial nozzle at an extended stand off distance since at large distance the impinging force of the pulsed jet exerted on the target decreased due to its characteristics of jet spreading after exiting the nozzle. The selection of different configuration parameters in this pulsed WJ nozzle results in different cleaning results and this related influence is presented in Figs. 4.3 and C.6(a) - C.6(c). Through the experiments, the configuration parameter of an optimal nozzle design is $h / d_1 = 3.0$ and $d_2 / d_1 = 1.3$.

The WJ velocity at the exit of the pulsed nozzle, measured by LTA, ranges between 190 - 230 m/s and this agrees well with the numerical solution in chapter 5.

The obtained data show the improvement in cutting and cleaning performance due to the use of the pulsed WJ nozzle. More detailed analysis and discussion of the performance of this nozzle is given in chapter 5.8.

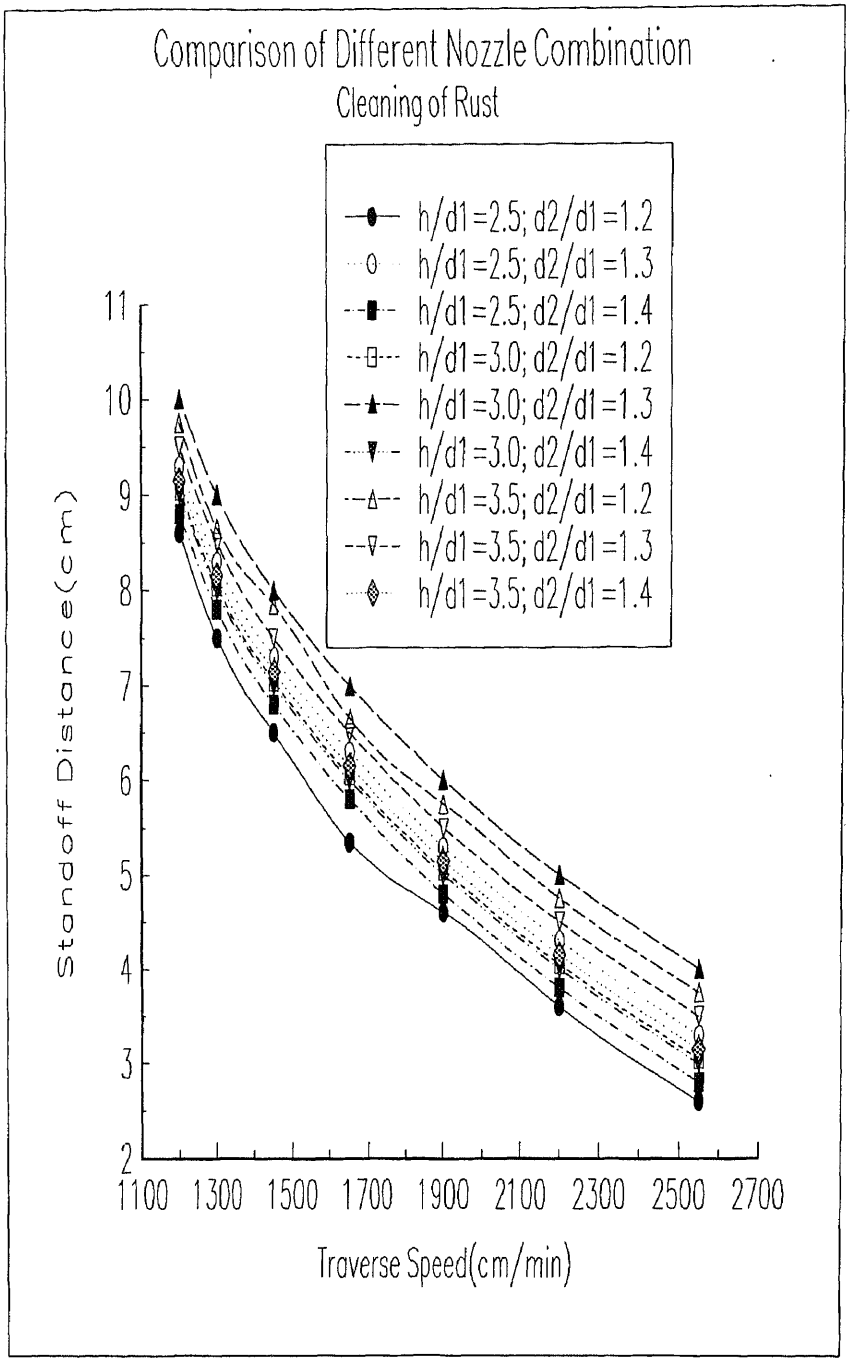

Figure 4.3 Effect of the Parameters of Pulsed WJ Nozzle on the Cleaning of Rust (by experiment, P = 330.7 Mpa)
Approximately linear correlation between stand off distance and traverse speed is presented at traverse speed 1900 - 2550 cm/min. Strong effect of cleaning presented at traverse speed less than 1900 cm/min and this is recommended speed zone. The optimal parameter of nozzle design is h/d1=3.0 and d2/d1=1.3.

CHAPTER 5

NUMERICAL SIMULATION OF PULSED FLOW INSIDE THE NOZZLE

Based on the principle of the Helmholtz resonator, a new type of pulsed WJ nozzle is designed and fabricated in order to improve the pure water jet machining and cleaning. Dynamic pulsation of the flow formed in the resonating cavity is generated by amplifying the unsteady perturbance in the shear layer near the separation point of the cavity. The pulsation is enhanced by the downstream cavity edge. The large vortices and strong pulsation enable this nozzle to produce strong cavitation which improves the processes of material removal. Understanding the pulsed turbulent flow characteristics is a necessity for designing and modifying this nozzle. At the present there is no practical experimental technique for the investigation of the pulsed flow inside of a nozzle However, computer simulation enables us to examine some elements of the flow behavior and evaluate the nozzle design characteristically. These subjects are focused on in the following chapter.

5.1 Mathematical Model of the Pulsed Turbulent Flow

Understanding and the subsequent simulation of turbulent flow is a growing and active area of research encompassing a diverse range of scientific disciplines. Pulsed turbulent flow is a highly complex multifaceted phenomenon. It is a highly nonlinear, time dependent and three dimensional flow. A fully developed turbulent motion is characterized by a large number of three dimensional entangled eddies (or vortex elements) of varying size that involve a wide spectrum of length and time scales. The largest eddies are generated as a result of hydrodynamic instabilities in the mean flow field, i.e., from shearing between two coflowing streams at different velocities, shearing between a stream and a solid boundary. These large eddies extract kinetic energy from the mean flow and by so doing provide the kinetic energy input that is necessary to maintain

turbulent motion. The largest eddies themselves become unstable and break down into progressively smaller eddies and transfer their kinetic energy, which is extracted from the mean flow, to smaller scales of motion. This nonlinear, three dimensional and transient process of eddy breakdown causes vortex-stretching and the associated process of turbulent kinetic energy transfer to progressively smaller scales of motion results in kinetic energy cascade. In cascading down to the fine scales of turbulent motion, the kinetic energy of turbulence is finally "destroyed" by viscous dissipation. Also, turbulence is a stochastic phenomenon since the exact detailed spatial and temporal evolution of a turbulent flow can never be replicated. It is useful to think of turbulent flows as being composed of mean and fluctuating parts. Defining the generic flow variable Φ, this decomposition is represented mathematically as: $\tilde{\Phi} = \overline{\Phi} + \Phi'$, where the superscripts (~), (-) and (') denote respectively instantaneous, mean and fluctuating quantities. The mean quantity $\overline{\Phi}$ can be obtained from applying one of the following two commonly used appropriate averaging procedures.

time averaging: $$\overline{\Phi} = \frac{1}{t_s} = \int_{t_0}^{t_0+t_s} \tilde{\Phi} dt \qquad (5.1)$$

ensemble averaging: $$\overline{\Phi} = \frac{1}{N} \sum^{N} \tilde{\Phi}(t_n) \qquad (5.2)$$

Here, t_0 is a reference point in time and t_s is the sampling interval over which the instantaneous quantity is averaged. In equation (5.2), $\tilde{\Phi}(t_n)$ is the value of the instantaneous flow quantity. Turbulent kinetic energy k is defined as the half sum of the variances of the three fluctuating velocity components, viz.

$$k = (\overline{u'^2} + \overline{v'^2} + \overline{w'^2}) / 2 \qquad (5.3)$$

Also, the viscous dissipation rate of turbulent kinetic energy ε is defined as

$$\varepsilon = \frac{\mu}{\rho} \overline{\frac{\partial u_i'}{\partial x_j} \frac{\partial u_i'}{\partial x_j}} \qquad (5.4)$$

An experimental setup for the study of a pulsed WJ nozzle is presented in Fig. 3.4. The nozzle consists of two orifices connected by a cavity. When a steady high pressure water stream flows from the upstream nozzle into the cavity, the fluid surrounding the jet is drawn into the jet. The shear layer is formed due to the momentum and heat energy exchange between the jet and fluid. Vorticity is induced since the fluid around the shear layer is entrained by the water. Then these induced vorticities move as vortex rings. Unsteady disturbances (vorticity oscillation) can be amplified by the instability of the shear layer in the cavity. As these disturbances move to the downstream nozzle and impinge on the downstream edge, the disturbances are limited and enforce an effect force on the flow and lead to pressure and velocity changing near the downstream zone. Oscillating pressure fields are produced in the impinging region and these disturbances then feed back to the separation region in which new perturbances are introduced since this zone is very sensitive to the disturbances. If the feedback is an effective or a positive one, it will induce some new disturbances at the separation region in phase with the original disturbances and enhance more instability of the disturbances. This can provide energy for maintaining or increasing oscillations.

In most turbulent flow problems of practical interest, only the overall effect of the turbulent flow field is usually considered. Because of this, an available computational technique is designed for evaluating the average flow characteristics. A mean flow field has a much smoother variation in space and time than the instantaneous flow field, thus significantly coarser meshes can be used for the numerical solution. The mean flow equations, in this case, are obtained from the application of time averaging to the instantaneous flow equations. The governing equations are

Continuity: $$\partial u_i / \partial x_i = 0 \qquad (5.5)$$

Momentum: $$\rho [(\partial u_i / \partial t) + u_j (\partial u_i / \partial x_j)] = -(\partial P / \partial x_i) + \rho f_i + \rho g_i [1 - \beta(\theta - \theta_\beta)] + \partial [\mu((\partial u_i / \partial x_j) + (\partial u_i / \partial x_i)) - \rho \overline{u_i' u_j'}] / \partial x_j \quad (5.6)$$

Because the flow involved in this study is axi-symmetric, incompressible, isothermal and chemically homogeneous, the energy and specie equations can be omitted. In equations (5.5) - (5.6), u_i , P and θ are the components of the mean velocity vector, the mean pressure and mean temperature respectively. Also, in the above equations, f_i is the mean component of a given body force field, g_i is the component of the gravitational acceleration vector, β is the thermal expansion coefficient and θ_β is the reference temperature at which the buoyancy force is zero. The term $\overline{u_i' u_j'}$ is the statistical correlation manifesting the effects of the turbulence (or fluctuating) field on the mean flow process. The second moment correlation $\rho\overline{u_i' u_j'}$ appearing in the momentum equation, which is a second order symmetric tensor, may be interpreted as the representation of the turbulent flux of the x_i component of momentum in the x_j direction, or owing to the symmetric nature of the tensor, the turbulent flux of the x_j component of momentum in the x_i direction. Alternatively, this tensor can be defined as an additional stress term, known as the Reynolds stress tensor, in the mean momentum equation. The Reynolds stress tensor is expanded below in terms of its nine elements in a three dimensional Cartesian framework

$$\rho\overline{u_i' u_j'} = \rho \begin{bmatrix} \overline{u'^2} & \overline{u'v'} & \overline{u'w'} \\ \overline{v'u'} & \overline{v'^2} & \overline{v'w'} \\ \overline{w'u'} & \overline{w'v'} & \overline{w'^2} \end{bmatrix} \quad (5.7)$$

The diagonal terms, which are the variances of the fluctuating components of the velocity vector multiplied by density, act as normal stresses on the fluid in much the same way as the pressure does. The off-diagonal terms, which are the covariance of the components of

a fluctuating velocity field multiplied by density, act as shear stresses in the fluid and produce shearing of the velocity profiles in three principal directions.

5.2 Modeling of the Turbulence

Turbulent modeling is the task of providing additional equations to describe the temporal and spatial evolution of the turbulent flux $\overline{u_i' u_j'}$. Thus, the turbulent flux can be solved simultaneously with the mean flow equations to produce a solution to the mean flow field if the turbulence model has been described. In general, the more sophisticated the turbulence model is, the more accurate is the prediction. But, it is also true that an increase in the degree of sophistication of a turbulence model often entails a significant increase in the overall computational cost for obtaining a prediction.

There are different eddy viscosity models adopted in practical use ranging from the simplest so called zero equation models (algebraically prescribed eddy viscosity models, mixing length type models, etc.) to the two equation type models (k - ε and variants) which are the most sophisticated turbulence models of this class. The Boussinesq eddy viscosity concept assumes that the turbulent fluxes of momentum can be approximated reasonably well by the following analogous expressions.

$$\rho \overline{u_i' u_j'} = \mu_t \left[\left(\partial u_i / \partial x_j \right) + \left(\partial u_i / \partial x_i \right) \right] - (2/3) \rho k \delta_{i,j} \qquad (5.8)$$

Here, μ_t is the eddy viscosity. Unlike μ which is property of the fluid, μ_t is not a fluid property but depends on the state of turbulence and it typically varies significantly within the flow field and from one flow to another. The above eddy viscosity concept in essence shifts the emphasis from modeling the individual unknown turbulent fluxes to that of modeling only a single unknown in the form of μ_t . The turbulence modeling relates μ_t to the large scale turbulent eddies via the following expression

$$\mu_t \propto \rho u_l \delta_l \qquad (5.9)$$

where u_l is characteristic velocity scale and δ_l is characteristic length scale. As u_l and δ_l are physically tangible quantities, it is generally easier to prescribe their variation in a given flow field than it is to prescribe u_l . Depending on the number of partial differential equations that are employed to model the scales u_l and δ_l , eddy viscosity models are classified into three groups,

(i). zero - equation models

(ii). one - equation models

(iii). two - equation models

Zero - equation models use only algebraic expressions to solve the equations and get the value of u_l and δ_l. In the one - equation class of models, one additional semi - empirical transport equation is introduced which governs (directly or indirectly) the level of one of the characteristic turbulent scaled u_l and δ_l. Two - equation models introduce two additional semi - empirical transport equations to model the spatial and temporal variation of both turbulent scales u_l and δ_l. These are considerably more universal than zero - and one - equation models and can be applied in complex flow situations with a reasonable degree of confidence.

The most popular two - equation turbulence model in practical use, the so called k - ε turbulent model, has been employed in this simulation. In the context of the k - ε turbulent model, the characteristic turbulent velocity scale u_l and length scale δ_l are related to the turbulent kinetic energy k and its rate of viscous dissipation ε through the following expressions,

$$u_l \propto k^{1/2} \tag{5.10}$$

$$\delta_l \propto k^{3/2} / \varepsilon \tag{5.11}$$

Substituting equations (5.10) and (5.11) into equation (5.9) leads to the following so called Kolmogorov - Prandtl expression

$$\mu_t = c_\mu \rho k^2 / \varepsilon \tag{5.12}$$

which relates μ_t directly to k and ε. Here c_μ is an empirical constant and k and ε can be derived from the following semi - empirical transport equations:

$$\rho Dk/Dt = \partial [(\mu_t / \sigma_k) (\partial k / \partial x_j)] / \partial x_j + \rho G + \rho B - \rho \varepsilon \tag{5.13}$$

$$\rho D\varepsilon / Dt = \partial [(\mu_t / \sigma_\varepsilon) (\partial \varepsilon / \partial x_j)] / \partial x_j + c_1 \rho (\varepsilon / k) G + c_1 (1 - c_3) \rho (\varepsilon / k) B - c_2 \rho \varepsilon^2 / k \tag{5.14}$$

These two equations are modeled forms of the exact (but intractable) transport equations for k and ε which can be derived from manipulations of the instantaneous flow equations. In the above equations, G is the shear generation term which expresses the production of turbulent kinetic energy generated from interactions between the mean flow patterns and the turbulent field, and B represents the buoyancy generation term generated from the varying temperature field. The exact expressions for these two terms are:

$$G = - \overline{u_i' u_j'} \, \partial u_i / \partial x_j \tag{5.15}$$

and

$$B = - \beta \overline{\mu_i' \theta' g_i} \tag{5.16}$$

Substituting the eddy viscosity expression of equation (5.8) into the equations (5.15) and (5.16), the following equations are obtained:

$$\rho G = \mu_t [(\partial u_i / \partial x_j) + (\partial u_i / \partial x_i)] \partial u_i / \partial x_j \tag{5.17}$$

$$\rho B = \beta (\mu_t / \sigma_t) (\partial \theta / \partial x_i) g_i \tag{5.18}$$

Compared with the equation of turbulent kinetic energy, the modeling of the source / sink terms in the equation of energy dissipation does not strongly depend on the corresponding terms of the exact energy dissipation equation. In the above equations, $c_1 \rho (\varepsilon / k) G$ and

$c_2 \rho \varepsilon^2 / k$ are the shear generation and viscous dissipation processes of ε, respectively, and c_1 and c_2 are empirical constants. The right hand side of equations (5.13) and (5.14), thus, contain modeled diffusion terms and modeled source / sink terms mimicking the local processes of turbulence production / destruction resulting from mean shear, thermal stratification and viscous dissipation. From the equations of (5.13) and (5.14), the temporal and spatial evolution of the characteristic turbulent and length scales can be determined. So, these variables are controlled by mean advection and diffusion, and also by the local processes of turbulent generation and destruction. Determined in this way, μ_t is significantly more representative of the local turbulent state at a spatial point than the value determined by zero- or one equation models.

5.3 Simulation of Pulsed Turbulent Flow Using k - ε Model

All nozzle combinations used in this research and some modified nozzle designs recommended for improving performance of the pulsed WJ nozzle have been simulated with the k - ε turbulent model. The corresponding governing equations used for this two dimensional, isothermal, incompressible pulsed turbulent flow without consideration of body forces inside the nozzle are:

$$\rho\,(u_{i,t} + u_j u_{i,j}) = P_{,j} + [\mu(u_{i,j} + u_{j,i}) - \rho\,\overline{u_i' u_j'}]_{,j} \tag{5.19}$$

$$\rho\,(k_{,t} + u_j u_{i,j}) = [\mu_t k_{,j} / \sigma_k]_{,j} + \mu_t (u_{i,j} + u_{j,i}) u_{i,j} \tag{5.20}$$

$$\rho\,(\varepsilon_{,t} + u_j \varepsilon_{,j}) = (\mu_t \varepsilon_{,j} / \sigma_\varepsilon)_{,j} + c_1 \varepsilon \mu_t (u_{i,j} + u_{j,i}) u_{i,j} / k - c_2 \rho\ \varepsilon^2 / k \tag{5.21}$$

Here, i , j = 1, 2, and total viscosity is identified with the sum of the laminar and eddy viscosity, $\mu = \mu_0 + \mu_t$. Again, the eddy viscosity μ_t is defined by equation (5.12). The above equations contain empirical constants c_1 , c_2 , σ_k , σ_ε and c_μ . The k - ε turbulence

model has over the years been tested, optimized, and fine tuned against a wide range of flow scenarios of practical interest. For the pulsed water flow through the nozzle involved in this research, the recommended set of empirical constants has been selected as: $c_1 = 1.44$, $c_2 = 1.92$, $\sigma_k = 1.00$, $\sigma_\varepsilon = 1.30$ and $c_\mu = 0.09$.

The important aspect of the k - ε model simulation that sets it apart from the corresponding zero-equation simulation is that appropriate boundary conditions must be prescribed for k and ε on the boundaries of the computational domain.

The inlet plane of this problem is positioned before the upstream nozzle where the flow field is undisturbed by any nearby obstacles. The inlet boundaries of k and ε can be empirically prescribed by the following expressions:

$$k = 0.1\, u^2 \tag{5.22}$$

$$\varepsilon = k^{3/2} / (0.05\, r) \tag{5.23}$$

where r is the radius of the orifice. The inlet condition for u which can be calculated from the measured water flow rate is considered to be uniform at the inlet plane.

The Neumann boundary condition (i.e., the zero gradient or zero flux in the axial direction) is appropriate for the outlet boundary of u, k and ε in this problem.

Since the pulsed flow investigated here is symmetric flow, the Neumann boundary condition can be applied to the variables in the radial direction.

In defining the boundary conditions for k and ε , the near-wall modeling method is employed in a one element thick layer near the wall region which includes the transitional and viscous sub layer. The Neumann and Dirichlet boundary conditions are applied, respectively, to the near wall region as

$$\partial k / \partial y = 0 \tag{5.24}$$

$$\varepsilon = (c_\mu^{1/2} k)^{3/2} / \kappa y \qquad (5.25)$$

and u, k and ε are set to zero on the solid wall. For the initial conditions, non-zero initial guesses for the u, k and ε are assumed, and the intermediate values obtained from equations (5.22) - (5.23) can be employed as the initial guess.

5.4 Modeling of Near-wall Flow

When simulating turbulent flows using the k - ε model, it is particularly challenging to use the near-wall modeling methodology to simulated the viscosity affected boundary regions. A major reason is that in order to resolve the sharply varying flow variables in near-wall regions, a disproportionately large number of grid points would be required in the immediate vicinity of the solid boundary. For most typical flow scenarios this leads to prohibitively expensive computations. A second reason is that the standard k - ε model which is employed to simulate the turbulent flow is of the high Reynolds number type and therefore can not be used in the near-wall regions. In this near-wall modeling scheme, the computational domain is extended to the physical boundary and the full set of elliptic mean flow equations is solved all the way down to the wall. A one element thick layer of special elements is then employed in the near-wall region between the fully turbulent flow field and the physical boundary. In these elements, specialized shape functions are used to simulate the sharp variations of mean flow variables (i.e., velocities) in this viscosity affected near-wall zone. These specialized sharp functions, which are based on the universal near wall profiles, are functions of the characteristic turbulence Reynolds numbers and adjust automatically during the course of the computations to accurately resolve the local flow profiles. Since use is still made of the standard high Reynolds number type of k - ε model, the k and ε equations are not solved in the layer of special near-wall elements; instead, the variation of the turbulent diffusivities of momentum is modeled using Van Driest's mixing length approach. The variation of the turbulent viscosity μ_t can be defined as

$$\mu_t = \rho\, l_m^2 \; \{[(\partial u_i / \partial x_j) + (\partial u_i / \partial x_i)]\, \partial u_i / \partial x_j\}^{1/2} \qquad (5.26)$$

where l_m is the Van Driest's mixing length defined as

$$l_m = \kappa\, y\, [\, 1 - \exp(-y_u^+ / A)\,] \qquad (5.27)$$

Here, A is an empirical constant which assumes a value of about 26 for smooth walls in the near-wall layers, κ is a Von Karman constant with a value of 0.41, and y_u^+ is the dimensionless normal distance from the wall, viz.,

$$y_u^+ = \rho\, (c_\mu^{1/2}\, k)^{1/2} / \mu \qquad (5.28)$$

The special one dimensional basis functions of 2 nodes in the y direction are:

$$\varphi_1(y) = 1 - A(y) \qquad (5.29)$$

$$\varphi_2(y) = A(y) \qquad (5.30)$$

Here, A(y) is an expression which is based on the universal profiles of semi-empirical form of Reichardt law. When applying for velocity interpolation,

$$A(y) = A_1 / A_2 \qquad (5.31)$$

where

$$\begin{aligned} A_1(y) = {} & (1/\kappa)\, \ln[\, 1 + 0.2\, \Delta_u^+ (1 + y)] + 7.8 \\ & [1 - \exp(-\Delta_u^+ (1+y) / 22) - \Delta_u^+ (1+y) \\ & \exp(-0.165\, \Delta_u^+ (1 + y)) / 22)\,] \end{aligned} \qquad (5.32)$$

$$A_2 = A_1 (y = 1) \qquad (5.33)$$

In the above equations, Δ_u^+ is the dimensionless characteristic height of the element in the y direction and is prescribed as

$$\Delta_u^+ = \rho \, (c_\mu^{1/2} \, k)^{1/2} \, \Delta / \mu \qquad (5.34)$$

Here Δ is the actual average dimensional height of the element above the wall and k is the turbulent kinetic energy at the top of the element, where y = 1. Δ_u^+ may alternatively be thought of as the characteristic element Reynolds number. The larger this number, the thinner the viscous sub layer will be with respect to the height of the special element.

5.5 Formulation of the Discrete Problem

The objective of the finite element method is to reduce the continuous problem (infinite number of degrees of freedom) of equations to a discrete problem (finite number of degree of freedom) prescribed by a system of algebraic equations. The finite element procedure begins with the division of the continuum zone of interest into a number of simply shaped zones which are alternatively called elements. Within each element, the dependent variables u_i , P, k and ε are interpolated by functions of compatible order, in terms of values to be computed on a set of nodal points. For the purpose of developing the equations for these nodal point unknowns, an individual element may be separated from the assembled system. For each element, u, P, k and ε fields are approximated by

$$\begin{aligned} u_i \, (x, t) &= \varphi^T \, U_i \, (t) \\ P \, (x, t) &= \psi^T \, P \, (t) \\ k \, (x, t) &= \varphi^T \, K \\ \varepsilon \, (x, t) &= \varphi^T \, E \end{aligned} \qquad (5.35)$$

Substitution of these approximations into the field equations and boundary conditions yields a set of nonlinear algebraic equations. In the above equations, the same basis functions are employed for components of u, k and ε with an unnecessary but cost

effective restriction. Also, U_i , P, K and E are column vectors of unknowns of element nodal point.

Of central importance to the development of a finite element program is the choice of the particular element to be included in the element library. Elements for fluid flow are usually categorized by the combination of velocity-pressure approximation used in the element. In this research, the four node quadratic and two dimensional elements are employed. The interpolation (or shape, or basis) function is prescribed by normalized a coordinate r and natural coordinate s. The value of r and s range from -1 to +1. For the four node quadrilateral element, the velocity component u_i is approximately prescribed by bilinear shape functions, viz.,

$$\varphi = \begin{bmatrix} 1/4(1-r)(1-s) \\ 1/4(1+r)(1-s) \\ 1/4(1+r)(1+s) \\ 1/4(1-r)(1+s) \end{bmatrix} \tag{5.36}$$

It is possible to use two types of pressure discretizations with this element: first is a bilinear continuous approximation with the pressure degree of freedom located at the nodes on four corners; second is a piece wise constant discontinuous pressure approximation with the pressure degree of freedom located at the element centroid.

5.6 Solution Procedures

Typically, the application of the Galerkin finite element procedure to the transient Navier - Stokes equations when an implicit time integrator is employed, results in a set of nonlinear algebraic equations that may be represented in matrix form as

$$\mathbf{K}(u)\,u = \mathbf{F} \tag{5.37}$$

where **K** is the global system matrix, u is the global vector of unknowns (i. e., velocities, pressures, etc.) and **F** is a vector which includes the effects of body forces and boundary conditions.

At present, there are mainly two different solution methodologies utilized for solving the nonlinear equation system described above. The first approach solves all conservation equations in a simultaneous coupled manner, while the second approach solves each equation separately in a sequential segregated manner. Here, a segregated algorithm with implicit time integration is used in the numerical solution of the discretized equations which result from the application of the Galerkin finite element scheme to the transit governing equations. The segregated solution algorithm is designed to address large-scale simulation. The most important difference from the other methods is that the segregated algorithm avoids the direct formation of a global system matrix. Instead, this matrix is decomposed into smaller sub-matrices each governing the nodal unknowns associated with only one conservation equation. These smaller sub-matrices are then solved in a sequential manner using either direct Gaussian elimination or conjugate gradient type schemes. The segregated algorithm with mixed velocity-pressure formulation is employed in this study. This formulation comprises three main steps. At the beginning of a given iteration, an approximation to the pressure is determined from the solution of a Poisson type pressure matrix using the most recent available values of the field variables. Then all the other components in the momentum and conservation equations prescribed in the flow problem are determined in a sequential manner using the latest field variables. Finally, the velocity field is mass adjusted (forced to satisfy the incompressibility constraint) via an irrotational projection onto a divergence free sub-space at the end of the iteration. This final step includes the determination of a further Poisson type pressure matrix for a pressure correction vector Δ P. The implicit segregated algorithm employed in this numerical simulation needs a relaxation factor of 0.5 for the equations of mean velocities, kinetic energy and viscous dissipation. The density of mesh in the computational domain is

varied to make the solution grid independent. The density of the mesh is reasonably re-adjusted to avoid "wiggle" if spurious spatial oscillations exists in the flow variable because of the large grid Reynolds number.

Three major sources of instability of the solution of the k - ε model simulation, exist if left untreated. The first kind of instability is associated with the dissipation (or sink) term in the k and ε equation. In the course of numerical simulation, when the interim solution field is considerately different from the fully converged solution, the dissipation terms may strongly outweigh the generation terms and can momentarily generate destabilizing negative nodal value of k and ε. The second kind of instability is associated with the advection terms in the k and ε equations. They can cause the stream wise oscillations in the related flow variables under the large Reynolds number. A negative nodal value of kinetic energy and viscous dissipation is produced if these oscillations are large compared to the local value of kinetic energy and viscous dissipation. The third kind of instability exists if k - ε model is employed in the prescription of flows that include both turbulent and laminar regions. Solution strategies of streamline upwinding and clipping are used to suppress the above three kinds of instabilities. Streamline upwinding is a numerical technique which introduces stabilizing false numerical diffusion along the stream wise direction. The upwinding factors for mean velocities are 1 and for k and ε are 5, respectively. The clipping is also a numerical technique by which the first and third kinds of instabilities can be avoided, and the nodal value of k and ε are ensured not to fall below the preassigned lower bound positive values. The lower bound value below which the nodal values of k and ε can be clipped are set to fifty thousand times smaller than the maximum nodal values of k and ε . Since the measures of streamline upwinding and clipping are the artificial stability enhancing methods which interface with the process of the numerical solution, the strategy employed in this simulation is to get a stable solution at the beginning with proper large values of the upwinding factors. Then the strategy

works to reduce the factor's value at points where the stream wise oscillations start to appear in the solution.

5.7 Convergence Criteria

Since the segregated algorithm is used in solving the equations, an appropriate convergence criteria is employed to terminate the iteration. Two important variables for use in designing termination criteria are the solution vector $\mathbf{u}_i$ (at iteration i) and the residual vector R ($\mathbf{u}_i$). It is of course desired that $\mathbf{u}_{i-1}$ be within a given tolerance , ε_u , of the accurate solution vector **u** at the end of each iteration. Hence, a realistic convergence criterion, depended on relative error, is defined as

$$\| \Delta \mathbf{u}_i \| / \| \mathbf{u} \| \leq \varepsilon_u \tag{5.38}$$

where $\Delta \mathbf{u}_i = \mathbf{u}_i - \mathbf{u}$, and $\| \cdot \|$ is an appropriate norm. Since **u** is not known at first, this value must be approximated, and the obvious selection is $\| \mathbf{u} \|$ replaced by $\| \mathbf{u}_i \|$ in equation (5.38) and **u** by $\mathbf{u}_{i-1}$ in the expression of $\Delta \mathbf{u}_i = \mathbf{u}_i - \mathbf{u}_{i-1}$.

Another more suitable convergence criterion which depends on the residual vector and tends to zero with $\mathbf{u}_{i-1}$ tending to **u**, is also employed in this numerical solution. Such a criterion is defined as

$$\| R (\mathbf{u}_i) \| / \| R_0 \| \leq \varepsilon_F \tag{5.39}$$

where $R_0 = R (u_0)$, is a reference vector.

Both of these two checks is employed in the involved numerical solution which provides an effective overall convergence criterion for all possible situations, since both $\Delta \mathbf{u}_i$ and R ($\mathbf{u}_i$) tend to zero near the solution. In the course of iteration of this pulsed turbulent flow, the solution is considered to be convergent if the normalized residuals are smaller than 0.0005.

5.8 Analysis and Discussion

The numerical simulation shows the jet pulsation generated in the nozzle cavity which is subsequently enhanced through the downstream region. The flow is separated in the expansion area from the downstream nozzle and vortices are induced around the pulsed jet core. The simulation results at time 0.5 x 10^{-3} second after initiation of the pulsed flow are presented in Figs. D.1 - D.6. Since the description of the pulsed WJ flow is a transient problem, the flow behavior depends on time. Fig. D.7a - D.7d show the flow characteristics at time of 0.1 x 10^{-3}, 0.5 x 10^{-2}, 0.1 x 10^{-2} and 0.5 x 10^{-1} second, respectively. Fig. D.1 clearly shows that the stream line pattern is smooth and parallel but there is a minor separation at the corner of the step change. Also, the circulation is induced in the resonant cavity, expansion is formed at the downstream nozzle, and then the flow is separated from the wall. The circulation generated from the diverging portion of the nozzle travels all the way to the exit. Figs. D.2 - D.3 show that turbulent kinetic energy reaches its peak value at the entrance of upstream nozzle and then dissipates through the nozzle. The turbulent kinetic energy plot indicates that the turbulent fluctuation increases in the radial direction. The pressure distribution is depicted in Fig. D.4. The pressure has the maximum value at the entry of the upstream nozzle and the pressure drop is achieved through the upstream, resonating cavity and downstream nozzle. Figs. D.5 - D.6 present that the axial velocity of the pulsed flow reaches its maximum at the entrance of the upstream nozzle and is almost constant through the upstream nozzle section. Further the velocity drops due to the pulsed effect of the flow in the resonating cavity and the decreases through the downstream nozzle region due to the friction in this zone. Flow separation in the expansion area and dissipation of turbulent kinetic energy through this section are also depicted. From the velocity plot, it follows that the tendency of flow separation in the orifice is insignificant. The variation of axial velocity at the nozzle exit with the time is prescribed in Fig. D.8. Maximum velocity is achieved in the centerline and the velocity decreases gradually in the radial direction towards the wall. The maximum

velocity of 190 - 230 m/s in the centerline is obtained periodically at every time interval. This numerical solution of velocity is validated by the measurement of LTA in the previous chapter. The effect of the parameters of the pulsed WJ nozzle on jet performance is depicted in Fig. 5.1. The presented data in this graph demonstrate that the maximum pulsation (or maximum velocity) is obtained with ratios of $h/d_1 = 3.0$ and $d_2 / d_1 = 1.3$, and this result is in good agreement with the experimental results determined in the previous chapter. Thus, the obtained computational results can be used for the practical process examination. It also follows that at $d_2 / d_1 < 1.15$, the pulsating amplitude at the nozzle exit is small. It is not clear if it is a self-excited oscillation or turbulent oscillation of the jet. After $d_2 / d_1 > 1.15$, the stronger pulsation can be observed and the optimal ratio of d_2 / d_1 at which the best performance of the pulsed flow can be obtained is 1.3. When the ratio of d_2 / d_1 exceeds 1.3, the pulsation amplitude decreases. As the ratio of the cavity length h over the diameter d_1 of upstream nozzle changes from 0.0 to 2.0, the mode of the flow at the nozzle exit changes from steady to pulsating. At the early stage, the pulsed frequency is very high and pulsed amplitude is very small. When the ratio of h/d_1 nears 2.7, the pulsation suddenly becomes strong and then reaches the maximum at ratio h/d_1 of 3.0. When h/d_1 exceeds 3.5, the pulsation amplitude decreases evidently. It results from that the disturbances are not content with the condition of feedback due to jet working unregularily.

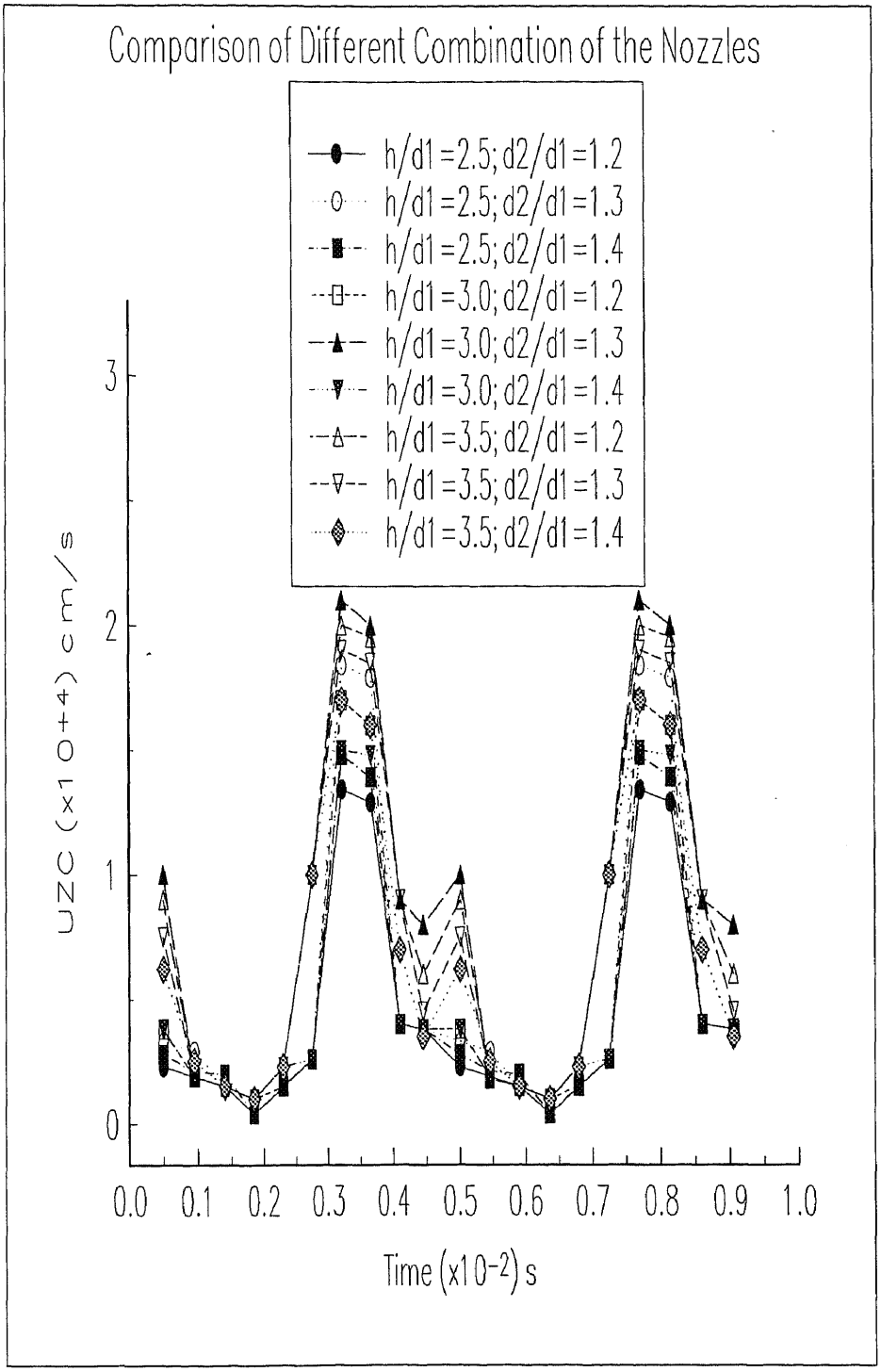

Figure 5.1 Effect of the Parameters of Pulsed WJ Nozzle on Jet Pulsation (axial velocity at nozzle exit) by Numerical Simulation (Test conditions are identical those in Fig. D.1) Optimal parameter of nozzle design is h/d1 = 3.0 and d2/d1 = 1.3.

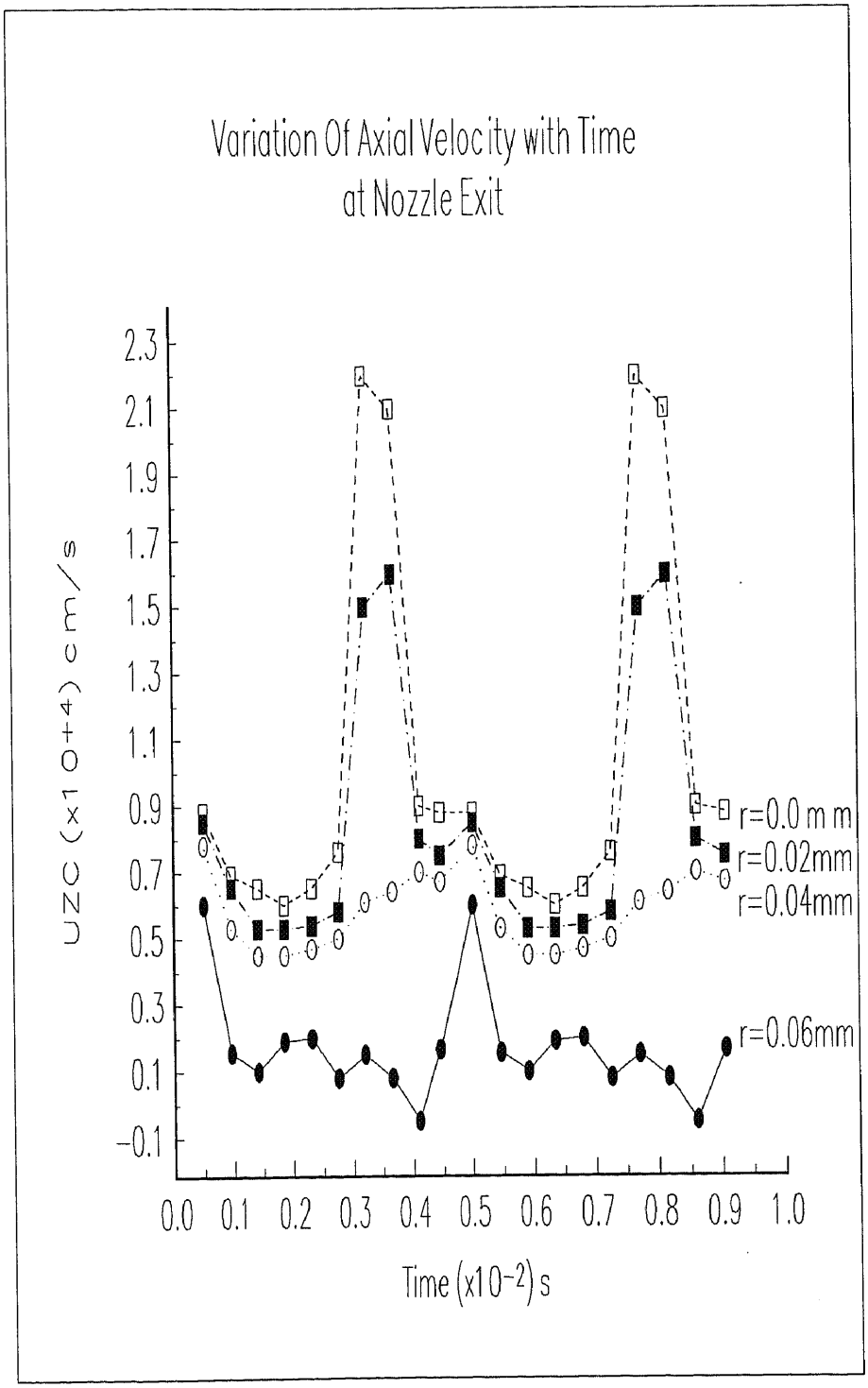

Figure 5.2 The Length of Downstream Nozzle is 3 mm

The length of the downstream nozzle also has an effect on the jet performance and these partial results are shown in Figs. 5.2 and D.9a - D.9b. It follows that a proper short length of this section keeps a higher momentum at the nozzle exit. The reason is that the vortices produced after expansion do not have enough time to absorb the kinetic energy from the core stream of the jet. But, when the length of this section is too short (i.e., 2 mm), the jet at the nozzle exit does not have the higher momentum since the flow does not have sufficient time to be fully developed.

CHAPTER 6

CONCLUDING REMARKS AND RECOMMENDATIONS

6.1 Concluding Remarks

6.1.1 Concluding Remarks for Improved AWJ Nozzle

The performed research shows that there is a significant potential for improving the efficiency of AWJ machining and the improvement involved in this research is attained by modifying the mixing chamber. The following concluding remarks are obtained from our results:

1. Modification of the shape at the top part of the focusing tube and control of the distance between the orifice and focusing tube well organize the solid particle flow and this results in uniform distribution of the abrasive in the water flow.

2. It is not necessary to make alignment between the orifice and focusing tube because of better focusing of the abrasive particles entering the focusing tube in this nozzle and this improves the operation of the AWJ machining.

3. It appears that the nozzles with different angles of the focusing tube and the distance between sapphire nozzle and the focusing tube lead to different penetration abilities. The optimal combination of a nozzle which has maximum efficiency of cutting is of angle of 45^0 and distance of 1.578 mm, on the basis of experiments.

From the above discussion and analysis, performing cuts with this improved AWJ nozzle is practical for industrial applications.

6.1.2 Concluding Remarks for Pulsed WJ Nozzle

The presented results for the pulsed WJ nozzle show that it is more efficient, with a deeper cutting depth and higher cleaning rate, in machining and cleaning than commercial WJ nozzle. The agreement between experimental and computational data demonstrates

the potential of this nozzle. The following conclusions are given based on the above studies:

1. Implementation of this nozzle design will provide an advanced cleaning techniques.

2. The computational technique developed in this research is validated by experiments and it is possible to use it for the study of other kinds of unsteady fluid flow.

3. The water velocity at the nozzle exit is obtained by measurement of the velocity using LTA and numerical simulation. The results determined by these two methods are well in agreement and this implies that the technologies involved in this research are useful for the investigation of the characteristics of the pulsed flow.

4. The diameter d_1 of upstream nozzle, diameter d_2 of downstream nozzle and cavity length h have an important effect on nozzle performance, since the different configurations lead to different conditions of disturbance feedback and compatibility of amplification of pulsation amplitude. The optimal configuration of nozzle design, validated by both computational and experimental results, is: $d_2 / d_1 = 1.3$ and $h / d_1 = 3.0$.

5. The length of the downstream nozzle has an effect on the behavior of the pulsed flow. Properly short the length improves the nozzle performance due to the water having higher momentum at the nozzle exit. The best value obtained in this study is 3 mm.

6. The pulsed nozzle is not suitable for the cleaning at an extended stand off because the larger the distance is, the lower the cleaning efficiency is due to more spread of the pulsed jet in free space.

6.2 Recommendations

6.2.1 Recommendation for Improved AWJ Nozzle

It is worth investigating the characteristics of water-particle mixing flow in this improved AWJ nozzle by computational techniques and thus will enable us to study this nozzle by theoretical methodology, in addition to the experimental scheme.

6.2.2 Recommendation for Pulsed WJ Nozzle

1. The geometry of the downstream edge in the resonating cavity also plays an important role in enhancing the pulsation of flow through this nozzle. Several kinds of geometry of the downstream edge are involved in investigation by numerical simulation. The partial computational results are presented in Figs. E.1 - E.3. The obtained information demonstrates that a downstream edge with geometry of concave shape is better than the convex shape and plate surface due to its convergent shape enhancing the focusing of the jet and thus increasing the jet velocity. Among the designs of concave shape nozzle, the best performance is at the angle of 75^0 . The probable reason is that the convergent effect is not sufficient at an angle smaller than 75^0 and pulsation is poorly affected due to the lager change of the cavity length at an angle larger than 75^0 . This phenomena should be further studied to improve the nozzle design.

2. The pulsed AWJ nozzle is worthy of study in order to improve AWJ machining technology. The initial design of this nozzle is finished and is ready for further manufacturing.

APPENDIX A

CONFIGURATION OF NOZZLES

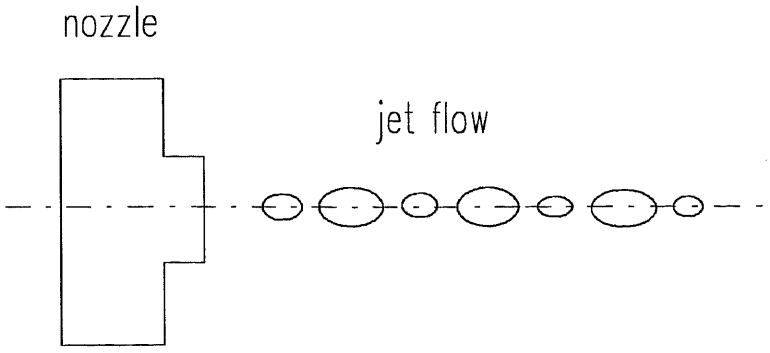

Figure A.1 Percussive Jet Device

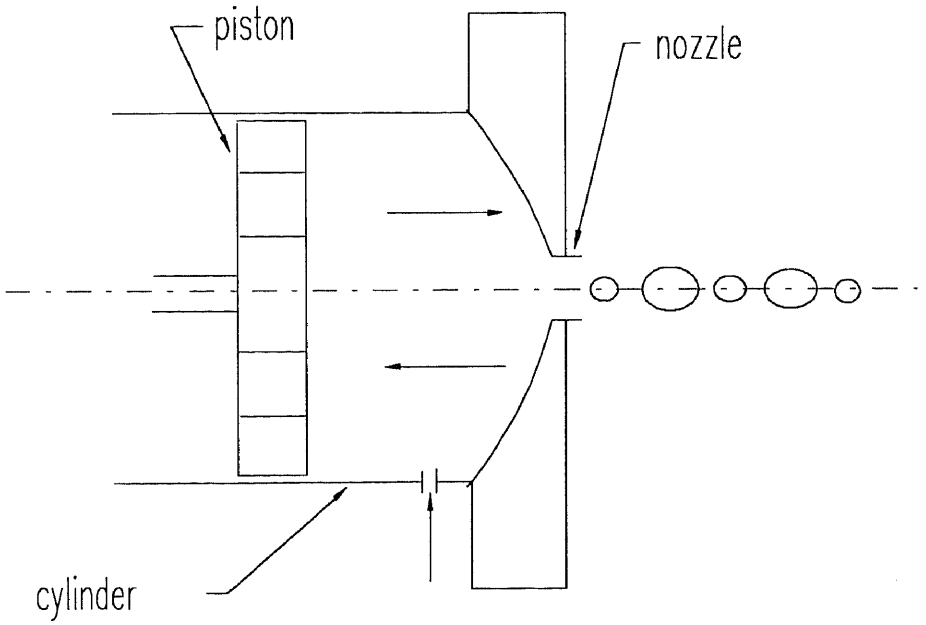

Figure A.2 Impulsive Water Cannon

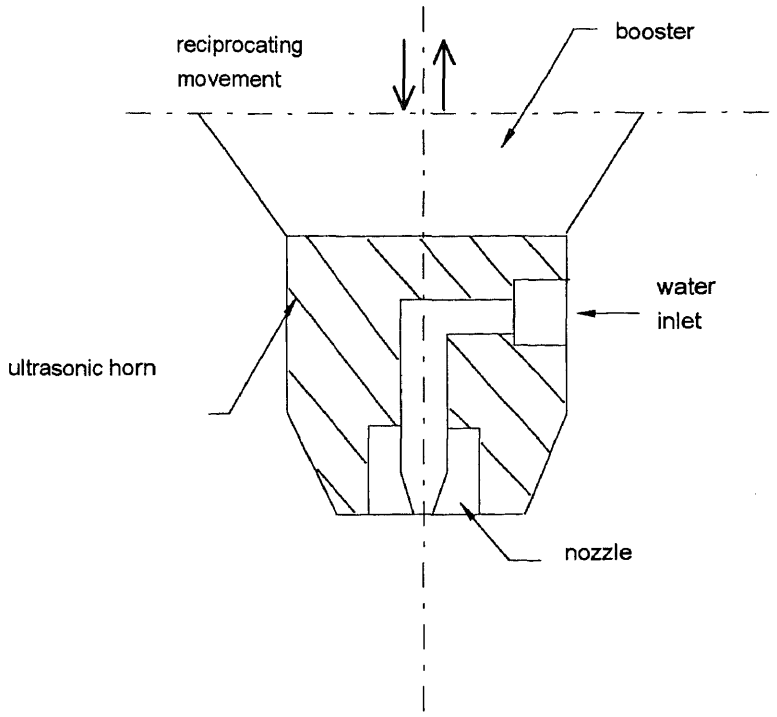

Figure A.3 Ultrasonic Vibration WJ Nozzle

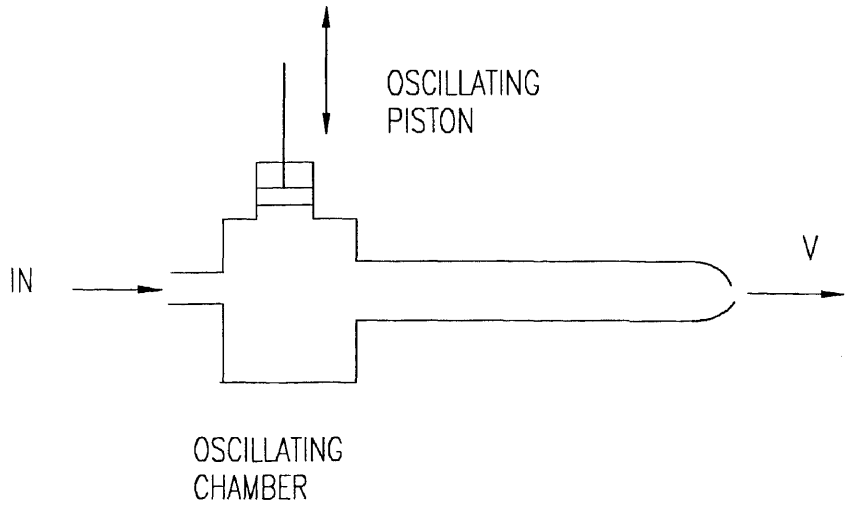

Figure A.4 WJ Nozzle with a Oscillating Piston

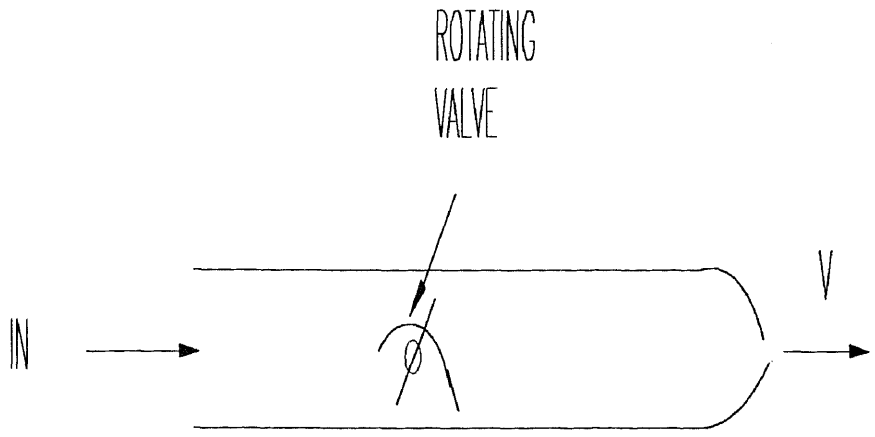

Figure A.5 WJ Nozzle with a Oscillating Mechanical Valve

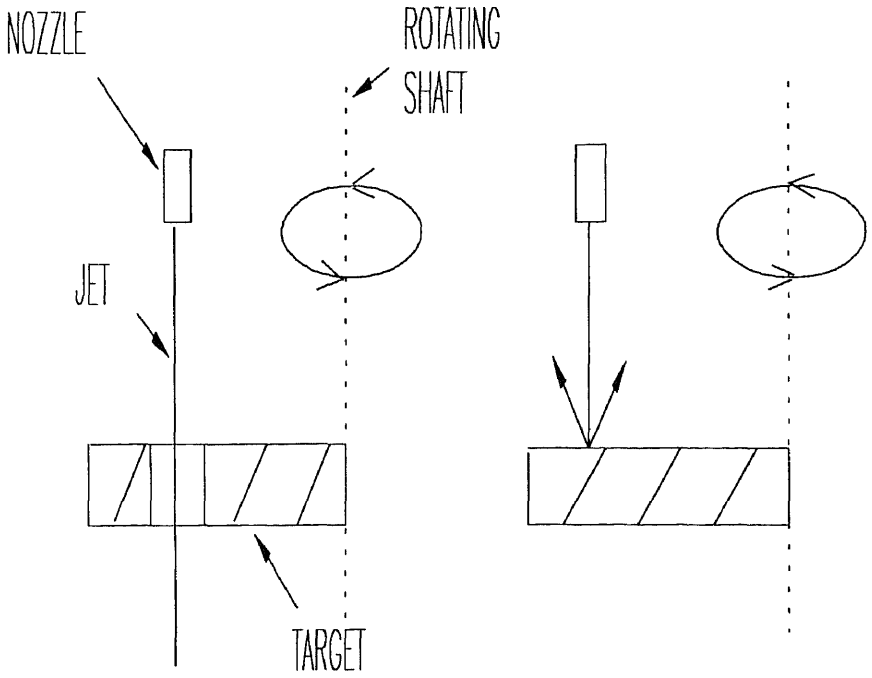

Figure A.6 Schematic Showing the Mechanism of Interrupting a Continuous Jet by a Rotating Disc

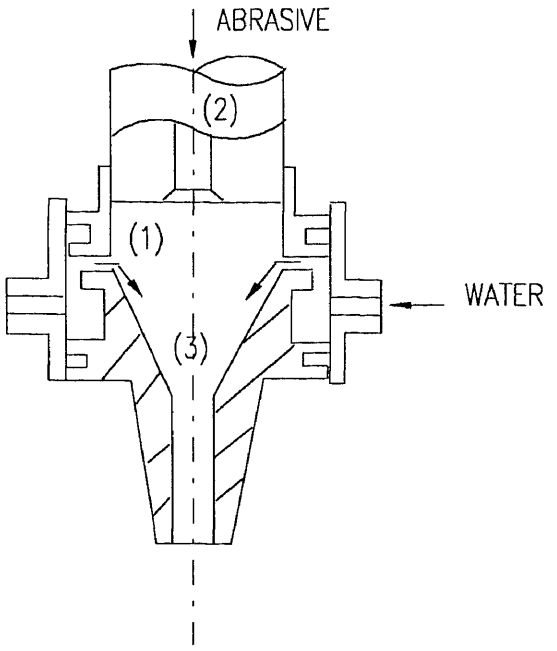

Figure A.7 Schematic of Spiral Nozzle

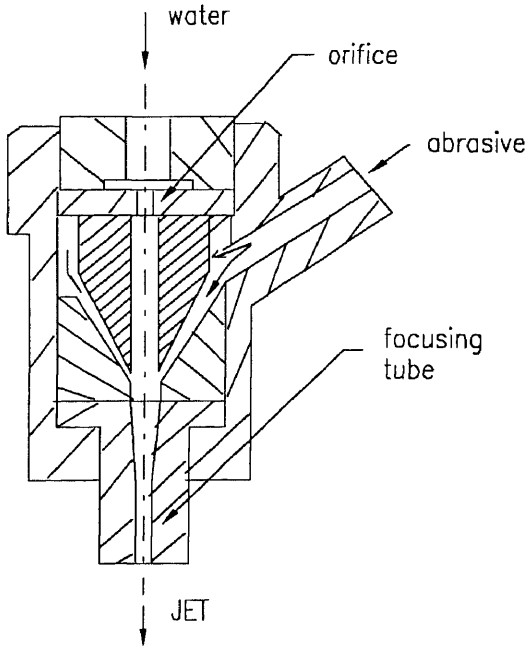

Figure A.8 Schematic of A New Type of AWJ Cutting Apparatus

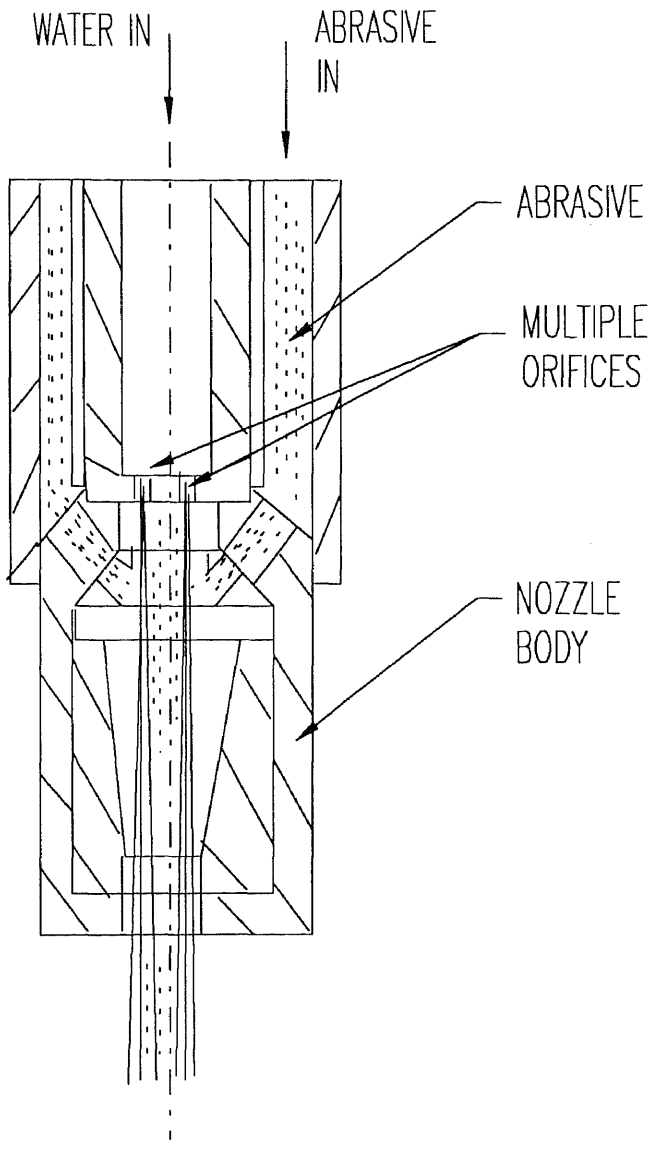

Figure A.9 Schematic of A New Type of AWJ Nozzle

APPENDIX B

RESULTS OF EXPERIMENTAL STUDY OF IMPROVED AWJ NOZZLE

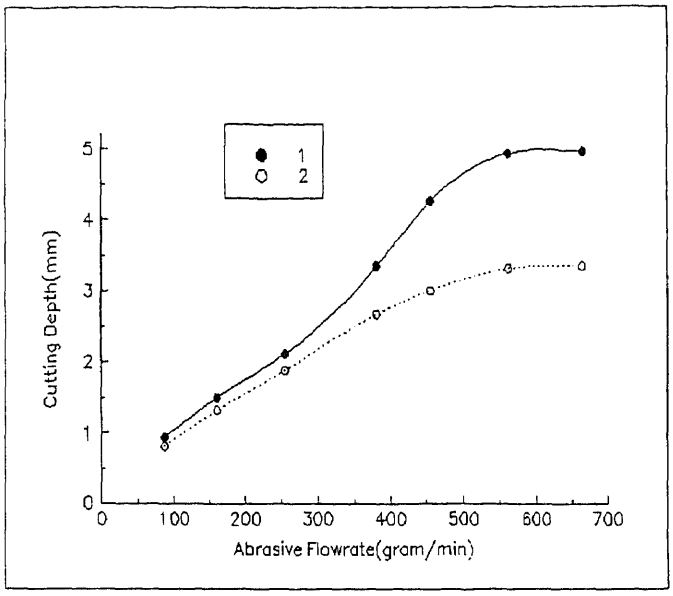

Figure B.1a Effect of Abrasive Flow Rates on Cutting Depth (abrasive: 80 HP; sapphire: #10; carbide : #30; material : reg steel; traverse speed: 25.4 cm / min; 1-- improved nozzle; 2-- conv nozzle) Higher penetration occurs using the improved AWJ nozzle.

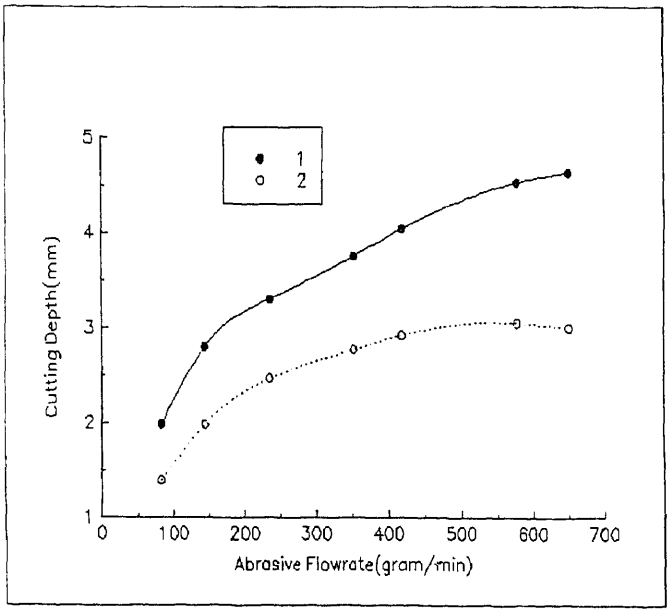

Figure B.1b Effect of Abrasive Flow Rates on Cutting Depth (abrasive: 120 HP; sapphire: #10; carbide : #30; material : reg steel; traverse speed: 25.4 cm / min; 1-- improved nozzle; 2-- conv nozzle) Higher penetration occurs using the improved AWJ nozzle.

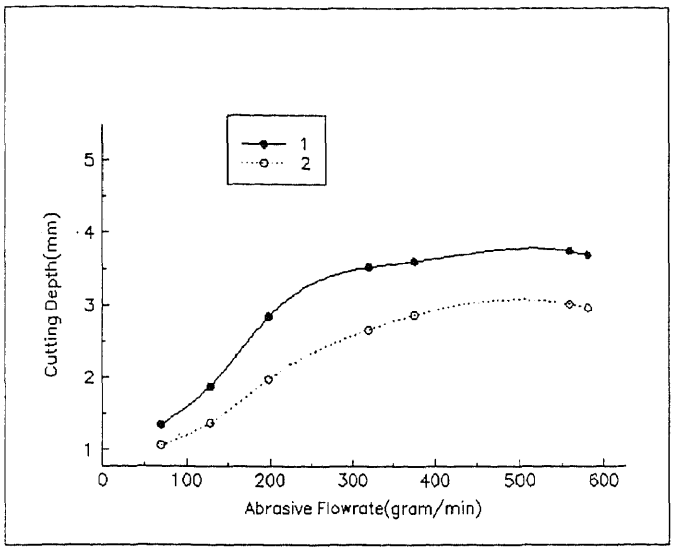

Figure B.1c Effect of Abrasive Flow Rates on Cutting Depth (abrasive: 150 HP; sapphire: #10; carbide : #30; material : reg steel; traverse speed: 25.4 cm / min; 1-- improved nozzle; 2-- conv nozzle) Higher penetration occurs using the improved AWJ nozzle.

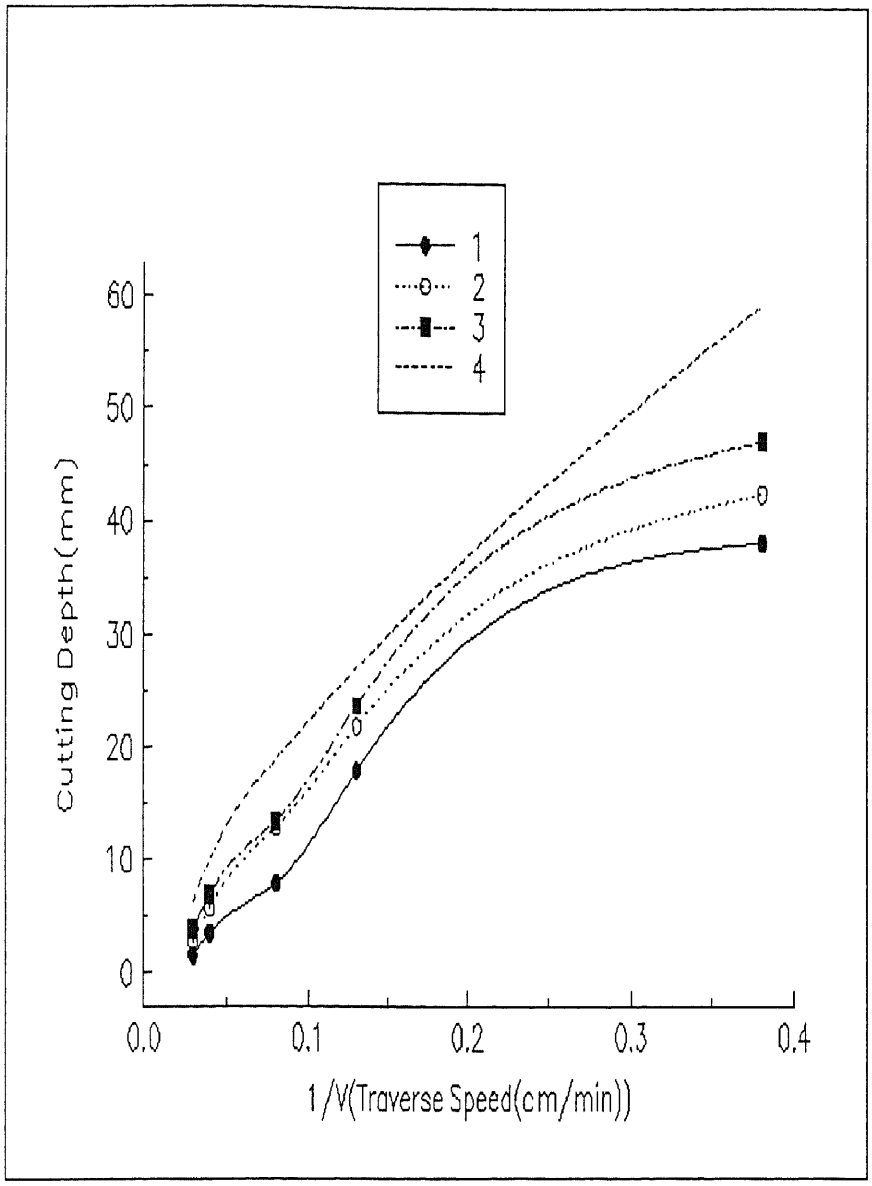

Figure B.2 Effect of Traverse Speed on Cutting Depth (abrasive: 120 HP; sapphire: #10; carbide : #30; material: stainless steel; 1-- conv nozzle (abr flow: 180 g/min); 2-- conv nozzle (abr flow: 210 g/min); 3-- impr nozzle (abr flow: 180 g/min); 4-- impr nozzle (abr flow: 210 g/min)) Higher penetration occurs using the improved AWJ nozzle.

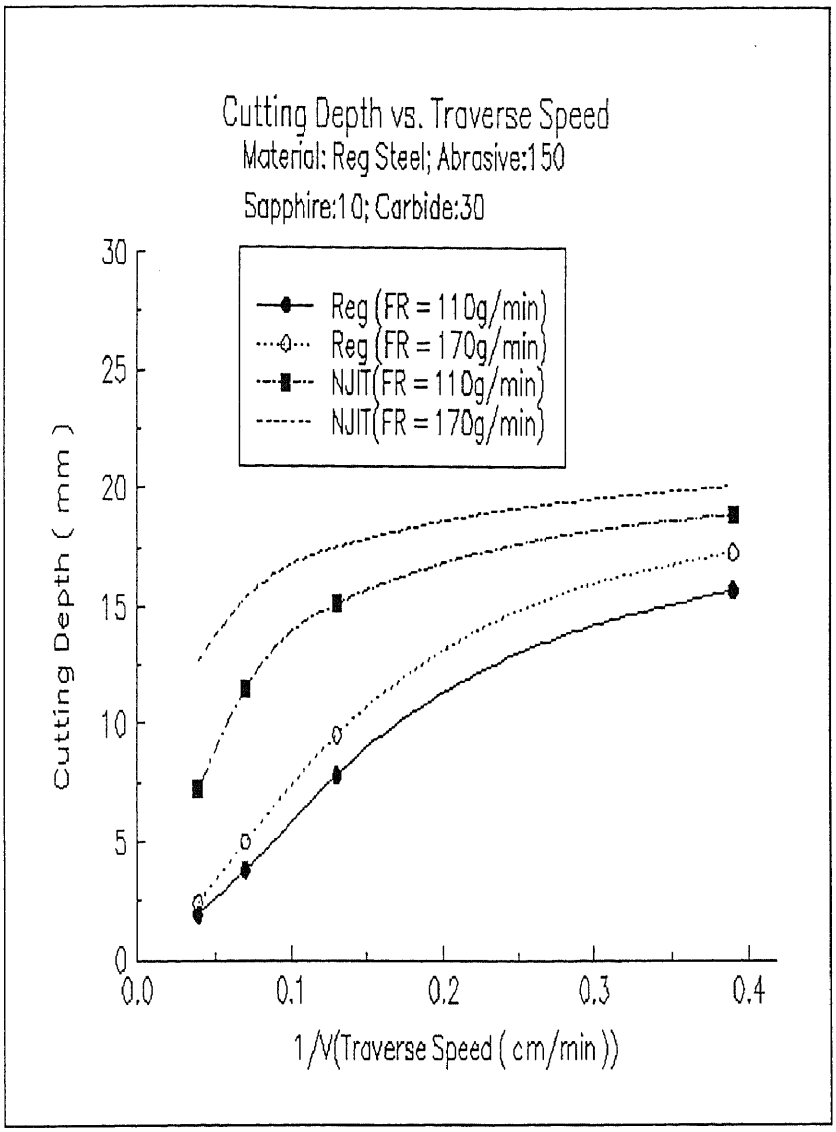

Figure B.3 Effect of Traverse Speed on Cutting Depth (abrasive: 150 HP; sapphire: #10; carbide : #30; material: reg steel; 1-- conv nozzle (abr flow: 110 g/min); 2-- conv nozzle (abr flow: 170 g/min); 3-- impr nozzle (abr flow: 110 g/min); 4-- impr nozzle (abr flow: 170 g/min)) Higher penetration occurs using the improved AWJ nozzle.

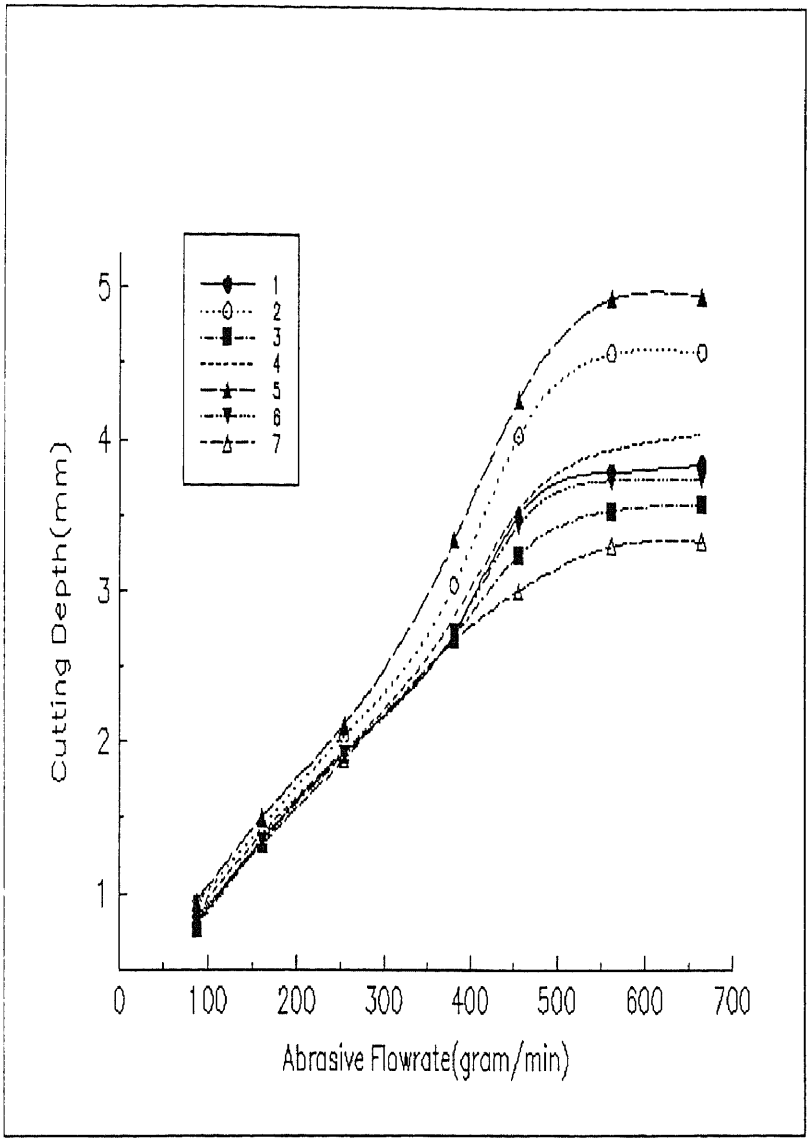

Figure B.4a Effect of Operational Conditions (Abrasive Flow Rates) on Cutting Depth (abrasive: 80 HP; sapphire: #10; carbide:#30; material: reg steel; trav spd: 25.4cm/min; 1-- $\alpha = 30$; H = 0.50 mm; 2-- $\alpha = 30$; H = 1.587 mm; 3-- $\alpha = 30$; H = 3.175 mm; 4-- $\alpha = 45$; H = 0.50 mm; 5-- $\alpha = 45$; H = 1.587mm; 6-- $\alpha = 45$; H =3.175mm; 7-- conv nozzle) Higher penetration occurs using the improved AWJ nozzle.

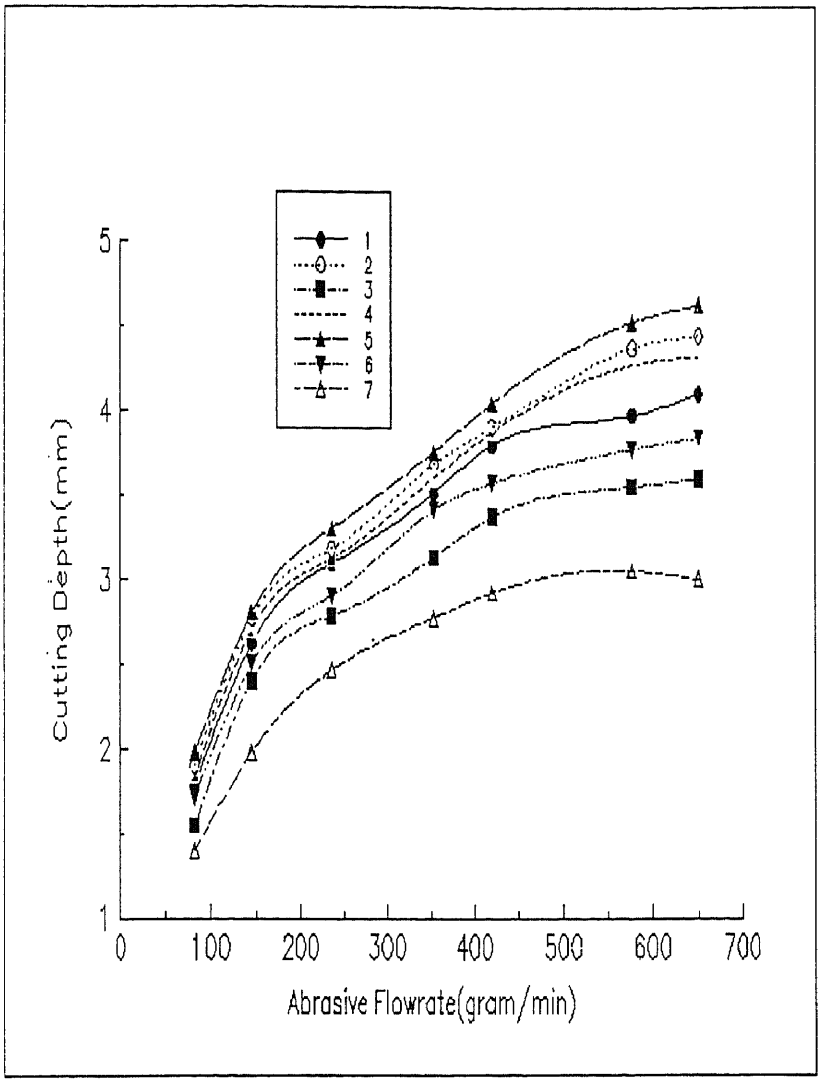

Figure B.4b Effect of Operational Conditions (Abrasive Flow Rates) on Cutting Depth abrasive: 120 HP; sapphire: #10; carbide:#30; material: reg steel; trav speed: 25.4cm/min; 1--α=30; H=0.5 mm; 2--α=30; H=1.587mm; 3--α=30; H=3.175mm; 4--α=45; H=0.5 mm; 5--α=45; H=1.587mm; 6--α=45; H=3.175mm; 7-- conventional nozzle; Higher penetration occurs using the improved AWJ nozzle.

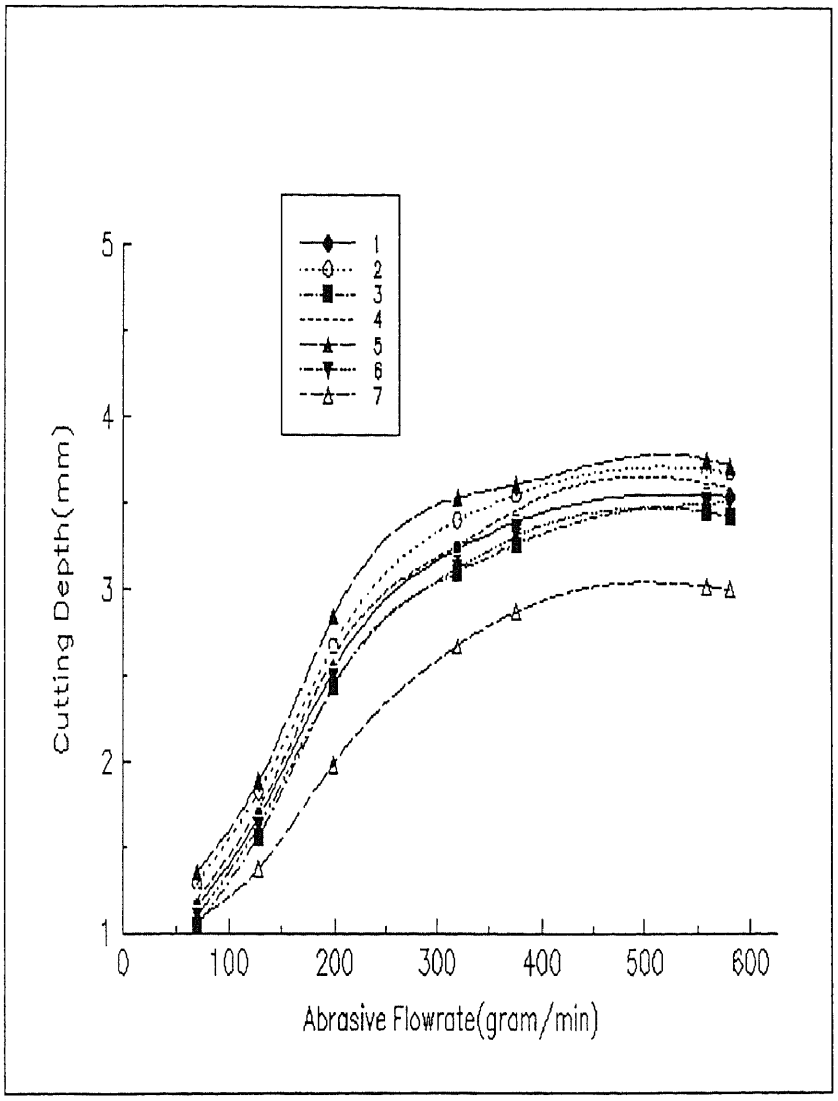

Figure B.4c Effect of Operational Conditions (Abrasive Flow Rates) on Cutting Depth (abrasive: 150 HP; sapphire: #10; carbide:#30; material: reg steel; trav speed: 25.4cm/min; 1--α=30; H=0.5 mm; 2--α=30; H=1.587mm; 3--α=30; H=3.175mm; 4--α=45; H=0.5 mm; 5--α=45; H=1.587mm; 6--α=45; H=3.175mm; 7-- conventional nozzle) Higher penetration occurs using the improved AWJ nozzle.

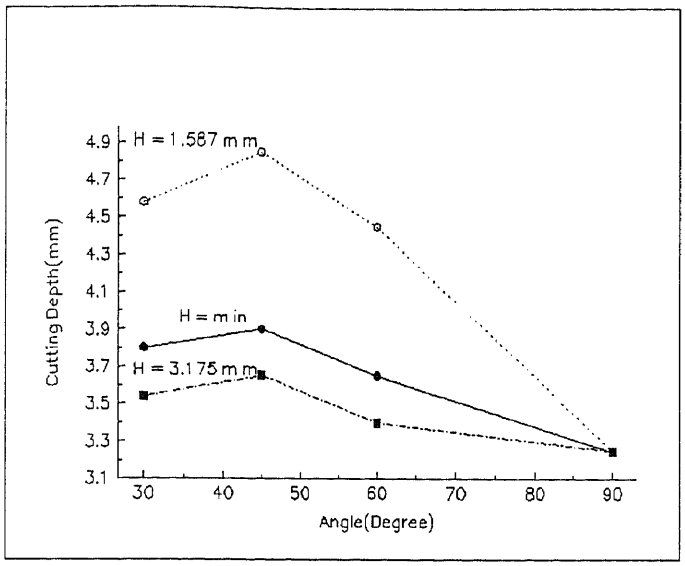

Figure B.5a Effect of α on Cutting Depth (abrasive: 80 HP; abr flow: 561.40 g / min; sapphire: #10; focusing tube: #30; material: reg steel; trav spd: 25.4 cm / min; α = 30, 45 and 60; degree at the modified nozzle; α = 90 degree at the commercial nozzle; (H = min = 0.5 mm)); Optimal angle α is 45 degree.

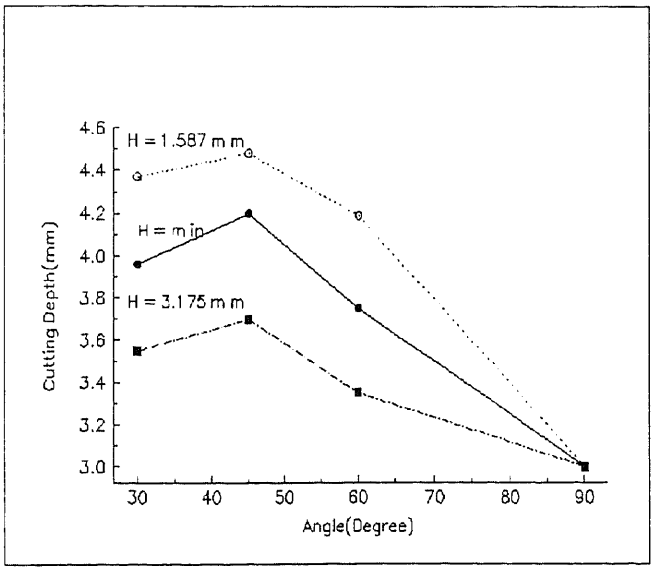

Figure B.5b Effect of α on Cutting Depth (abrasive: 120 HP; abr flow: 577.30 g / min; sapphire: #10; focusing tube: #30; material: reg steel; trav spd: 25.4 cm / min; α = 30, 45 and 60 degree at the modified nozzle; α = 90 degree at the commercial nozzle; (H = min = 0.5 mm)); Optimal angle α is 45 degree.

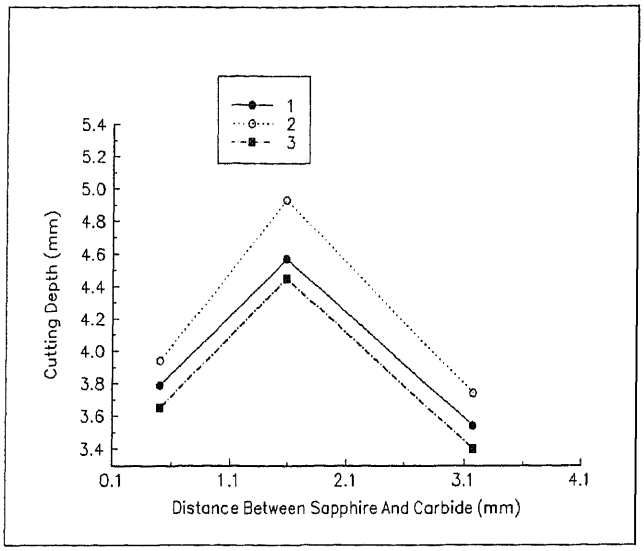

Figure B.6a Effect of H on Cutting Depth (abrasive: 80 HP; abr flow: 561.40 g / min; sapphire: #10; focusing tube: #30; material: reg steel; trav spd: 25.4 cm / min; 1-- $\alpha = 30^0$; 2-- $\alpha = 45^0$; 3-- $\alpha = 90^0$); Optimal stand off distance is 1.587 mm.

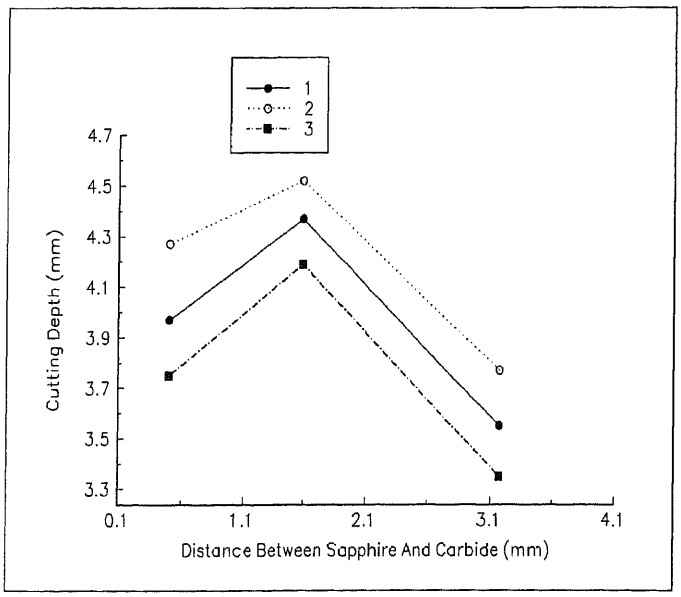

Figure B.6b Effect of H on Cutting Depth (abrasive: 120 HP; abr flow: 577.30 g / min; sapphire: #10; focusing tube: #30; material: reg steel; trav spd: 25.4 cm / min; 1-- $\alpha = 30^0$; 2-- $\alpha = 45^0$; 3-- $\alpha = 90^0$) Optimal stand off distance is 1.587 mm.

Table B.1a Exprimental Data Record for Comparison of Improved and Commercial AWJ Nozzles (Abrasive: #80)

Flowrate(gram/m) / Kind of Abrasive	87.43	160.6	253.7	380.6	455.6	561.4	664.5
New Noz	0.94*	1.5	2.11	3.34	4.27	4.93	4.95
	(0.939)	(1.53)	(2.12)	(3.35)	(4.26)	(4.94)	(4.955)
#80	(0.941)	(1.527)	(2.10)	(3.36)	(4.28)	(4.95)	(4.945)
Conv Noz	0.81	1.32	1.88	2.67	3.00	3.30	3.33
	(0.808)	(1.322)	(1.89)	(2.685)	(2.99)	(3.305)	(3.335)
	(0.812)	(1.328)	(1.87)	(2.665)	(3.01)	(3.295)	(3.325)

Note:
1. Symble * stands for average value of cutting depth.
2. Values in brackets are actual cutting depth.
3. Sapphire nozzle: #10; Focusing tube: #30; Material: Low carbon steel (#c1020); Traverse speed: 25.4cm/min.

Table B.1b Exprimental Data Record for Comparison of Improved and Commercial AWJ Nozzles (Abrasive:#120)

Flowrate(gram/m) / Kind of Abrasive	82.6	144.8	235.2	352.3	419.3	577.3	650.1
New Noz #120	1.98 (1.97) (1.99)	2.84 (2.845) (2.835)	3.25 (3.244) (3.256)	3.63 (3.635) (3.625)	4.04 (4.035) (4.045)	4.52 (4.53) (4.51)	4.62 (4.61) (4.63)
Conv Noz	1.40 (1.39) (1.41)	1.98 (1.985) (1.975)	2.46 (2.465) (2.455)	2.77 (2.765) (2.775)	2.92 (2.916) (2.924)	3.05 (3.044) (3.056)	3.00 (3.01) (2.991)

Note:

1. Symbol * stands for average value of cutting depth.
2. Values in brackets are actual cutting depth.
3. Sapphire nozzle: #10; Focusing tube: #30; Material: Low carbon steel (#c1020); Traverse speed: 25.4cm/min.

Table B.1c Exprimental Data Record for Comparison of Improved and Commercial AWJ Nozzles (Abrasive:#150)

Flowrate(gram/m) / Kind of Abrasive	68.8	128.1	198.5	319.1	374.5	558.5	580.5
#150 New noz	1.35 (1.364) (1.346)	1.88 (1.89) (1.87)	2.84 (2.844) (2.836)	3.53 (3.529) (3.531)	3.61 (3.625) (3.595)	3.76 (3.77) (3.75)	3.71 (3.705) (3.715)
Conv Noz	1.07 (1.066) (1.074)	1.37 (1.374) (1.366)	1.98 (1.978) (1.982)	2.67 (2.665) (2.675)	2.87 (2.88) (2.86)	3.02 (3.015) (3.025)	2.97 (2.985) (2.955)

Note:

1. Symbol * stands for average value of cutting depth.
2. Values in brackets are actual cutting depth.
3. Sapphire nozzle: #10; Focusing tube: #30; Material: Low carbon steel (#c1020); Traverse speed: 25.4cm/min.

Table B.2a Exprimental Data Record of Comparison of Different Combination of Improved AWJ Nozzle (Abrasive: #80)

Flowrate(gram/m) / Kind of Abrasive	angle	dist	87.4	160.6	253.7	380.6	455.6	561.4	664.5
	30	0.50	0.83	1.35	1.93	2.73	3.50	3.79	3.84
	30	1.587	0.93	1.44	2.04	3.04	4.03	4.57	4.58
#80	30	3.175	0.77	1.33	1.91	2.70	3.24	3.54	3.58
	45	0.50	0.87	1.39	1.94	2.83	3.54	3.94	4.04
	45	1.587	0.94	1.50	2.11	3.34	4.27	4.93	4.95
	45	3.175	0.80	1.34	1.92	2.72	3.44	3.74	3.75
	60	0.50	0.82	1.34	1.92	2.72	3.45	3.78	3.83
	60	1.587	0.92	1.43	2.02	3.04	4.01	4.55	4.57
	60	3.175	0.75	1.31	1.90	2.65	3.21	3.52	3.56
	conv	nozzle	0.81	1.32	1.88	2.67	3.00	3.30	3.33

1. Test Conditions:
   Sapphire nozzle: #10; Focusing tube: #30; Mateiral: Low carbon steel (#c1020);
   Traverse speed: 25.4cm/min
2. Units:
   Angle: degree; Distance: mm

Table B.2b Exprimental Data Record of Comparison of Different Combination of Improved AWJ Nozzle (Abrasive: #120)

Flowrate Scale			82.6	144.8	235.2	352.3	419.3	577.3	650.1
Kind of Abrasive									
	angle	dist							
	30	0.50	1.78	2.62	3.09	3.51	3.79	3.97	4.10
	30	1.587	1.90	2.77	3.18	3.68	3.90	4.37	4.44
#120	30	3.175	1.55	2.40	2.78	3.13	3.37	3.55	3.60
	45	0.50	1.84	2.70	3.12	3.60	3.87	4.27	4.32
	45	1.587	1.98	2.80	3.30	3.75	4.04	4.52	4.62
	45	3.175	1.71	2.50	2.90	3.41	3.57	3.77	3.84
	60	0.50	1.77	2.60	3.07	3.50	3.78	3.96	4.08
	60	1.587	1.85	2.75	3.17	3.65	3.89	4.35	4.43
	60	3.175	1.45	2.39	2.76	3.11	3.35	3.53	3.58
	conv	nozzle	1.40	1.98	2.46	2.77	2.92	3.05	3.00

1. Test Conditions:
   Sapphire nozzle: #10; Focusing tube: #30; Mateiral: Low carbon steel (#c1020);
   Traverse speed: 25.4cm/min
2. Units:
   Angle: degree; Distance: mm

Table B.2c Exprimental Data Record of Comparison of Different Combination of Improved AWJ Nozzle (Abrasive: #150)

Flowrate(gram/m)			68.8	128.1	198.5	319.1	374.5	558.5	580.5
Kind of Abrasive									
	angle	dist							
	---	---							
	30	0.50	1.15	1.67	2.53	3.23	3.39	3.55	3.54
	30	1.587	1.29	1.82	2.67	3.40	3.55	3.70	3.68
#150	30	3.175	1.05	1.56	2.43	3.10	3.26	3.45	3.42
	45	0.50	1.20	1.72	2.60	3.25	3.46	3.62	3.59
	45	1.587	1.35	1.88	2.84	3.53	3.61	3.76	3.72
	45	3.175	1.10	1.62	2.44	3.12	3.31	3.50	3.51
	60	0.50	1.13	1.65	2.43	3.18	3.31	3.45	3.44
	60	1.587	1.27	1.73	2.50	3.38	3.45	3.50	3.58
	60	3.175	1.01	1.50	2.39	3.01	3.16	3.33	3.34
	conv	nozzle	1.07	1.37	1.98	2.67	2.87	3.02	3.00

1. Test Conditions:
   Sapphire nozzle: #10; Focusing tube: #30; Mateiral: Low carbon steel (#c1020);
   Traverse speed: 25.4cm/min
2. Units:
   Angle: degree; Distance: mm

APPENDIX C

RESULTS OF EXPERIMENTAL STUDY OF PULSED WJ NOZZLE

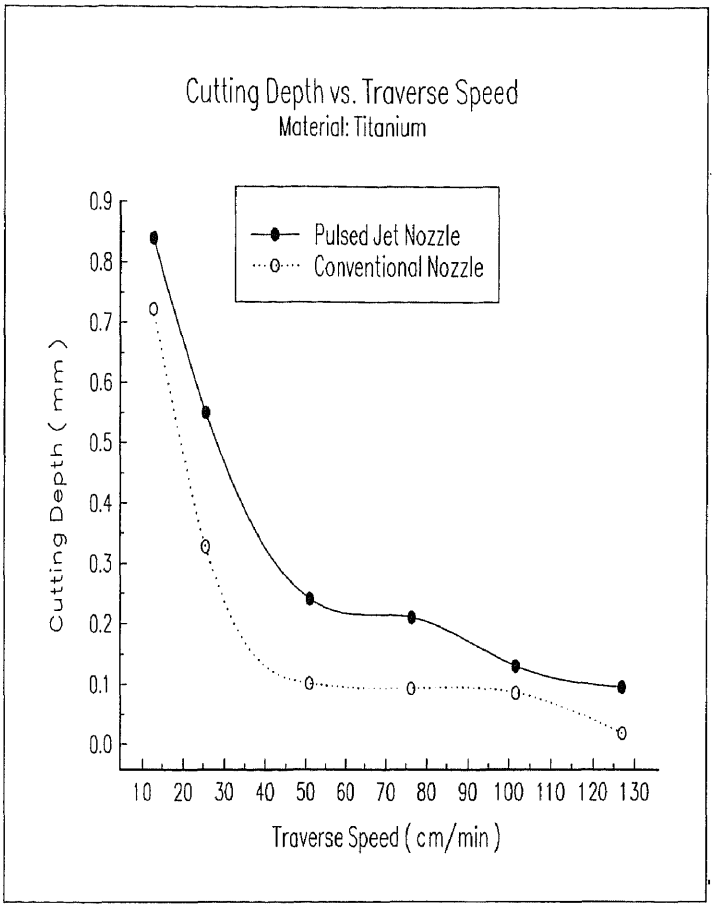

Figure C.1 Comparison of the Performance of Pulsed and Commercial WJ Nozzle at Titanium Milling
(h = 0.75 mm; upstream nozzle: #10(0.254 mm); downstream nozzle: #12(0.305 mm); P = 330.7 Mpa; stand off = 0.50 mm)
Higher penetration occurs using of pulsed nozzle

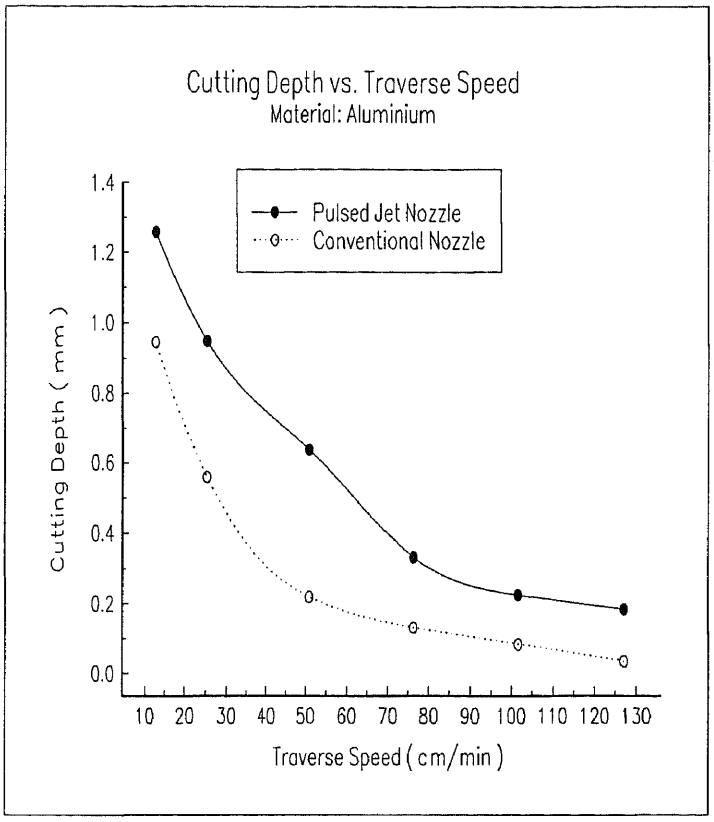

Figure C.2 Comparison of the Performance of Pulsed and Commercial WJ Nozzle at Aluminum Milling
(h = 0.75 mm; upstream nozzle: #10(0.254 mm); downstream nozzle: #12(0.305 mm); P = 330.7 Mpa; stand off = 0.50 mm)
Higher penetration occurs using of pulsed nozzle

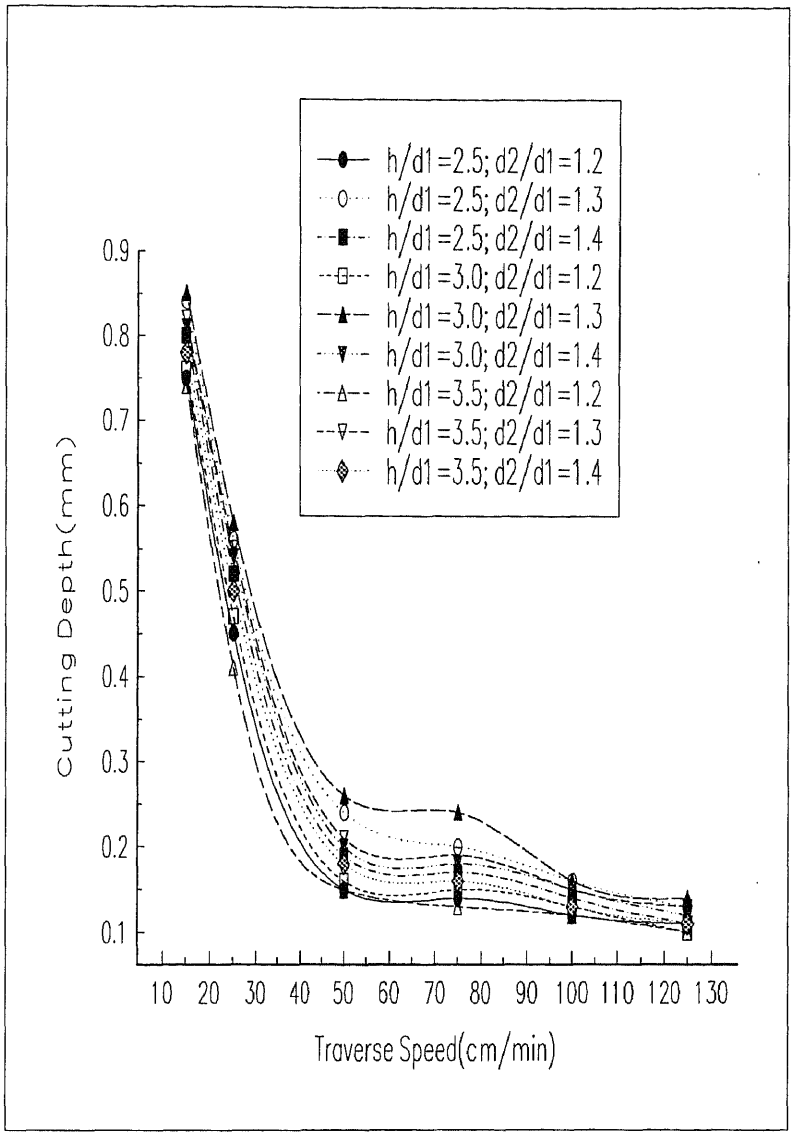

Figure C.3a Effect of the Parameters of Pulsed WJ Nozzle on Cutting Titanium (by experiment)
(P = 330.7 Mpa; stand off distance = 0.50 mm; material: titanium; h: cavity length (mm); d1: diameter of upstream orifice (mm); d2: diameter of downstream orifice (mm))
Optimal parameter of nozzle design is h/d1 = 3.0 and d2/d1 = 1.3.

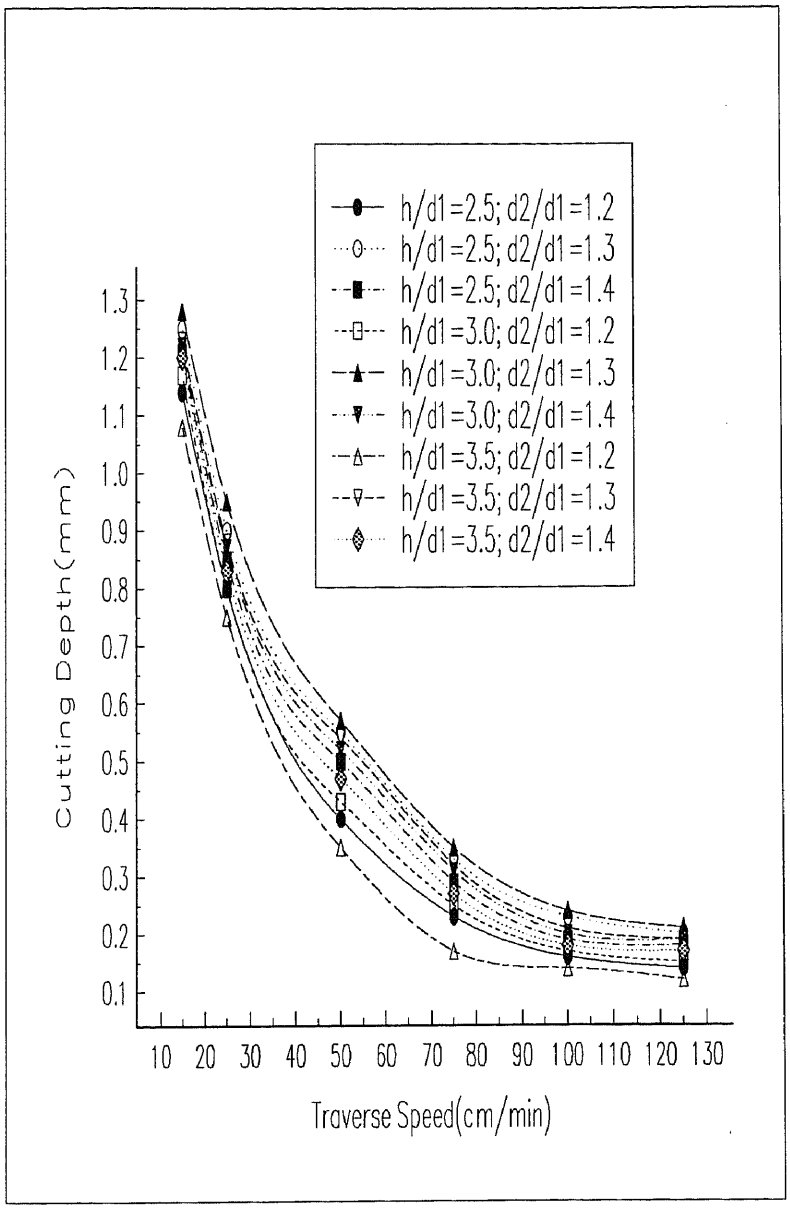

Figure C.3b Effect of the Parameters of Pulsed WJ Nozzle on Cutting Aluminum (by experiment)
(P = 330.7 Mpa; stand off distance = 0.50 mm; material: aluminum; h: cavity length (mm); d1: diameter of upstream orifice (mm); d2: diameter of downstream orifice (mm))
Optimal parameter of nozzle design is h/d1 = 3.0 and d2/d1 = 1.3.

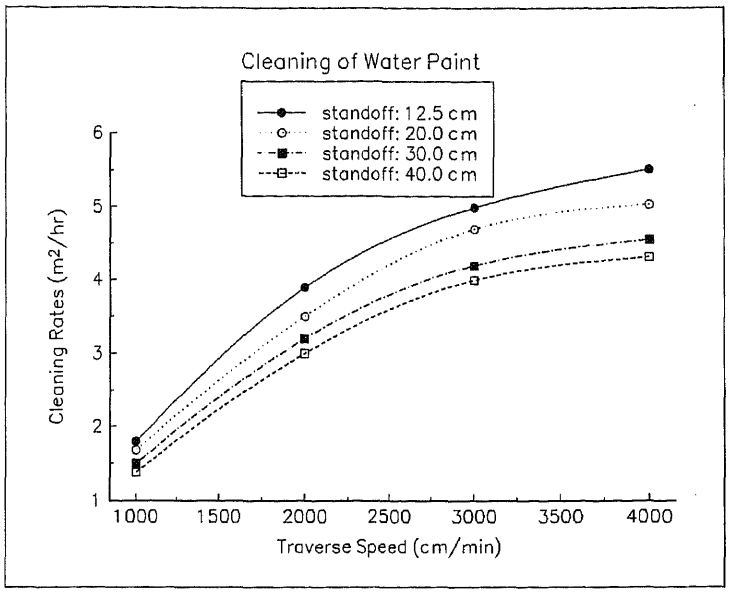

Figure C.4a Cleaning of Water Paint by Pulsed WJ Nozzle at An Extended Stand Off Distance (test conditions are identical to those in Figure C.1)

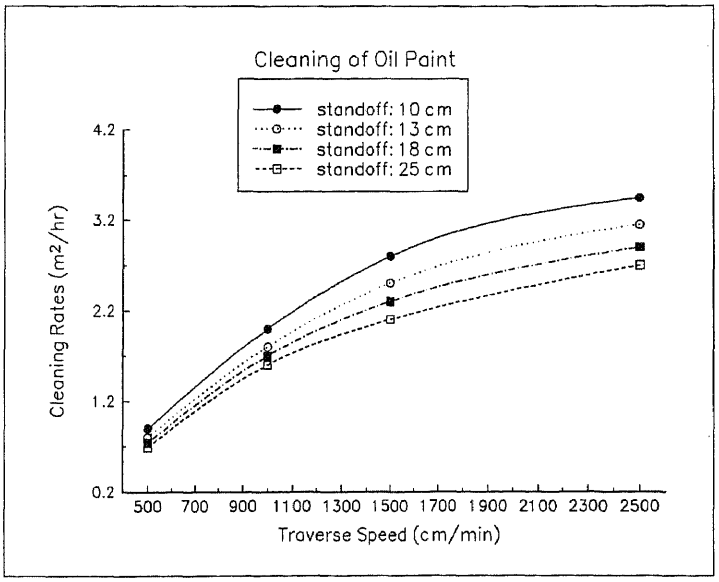

Figure C.4b Cleaning of Oil Paint by Pulsed WJ Nozzle at An Extended Stand Off Distance (test conditions are identical to those in Figure C.1)

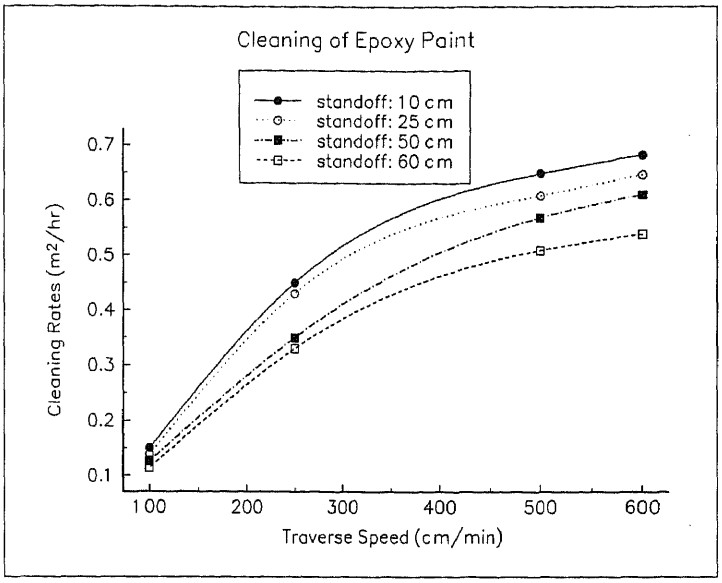

Figure C.4c Cleaning of Epoxy Paint by Pulsed WJ Nozzle at An Extended Stand Off Distance (test conditions are identical to those in Figure C.1)

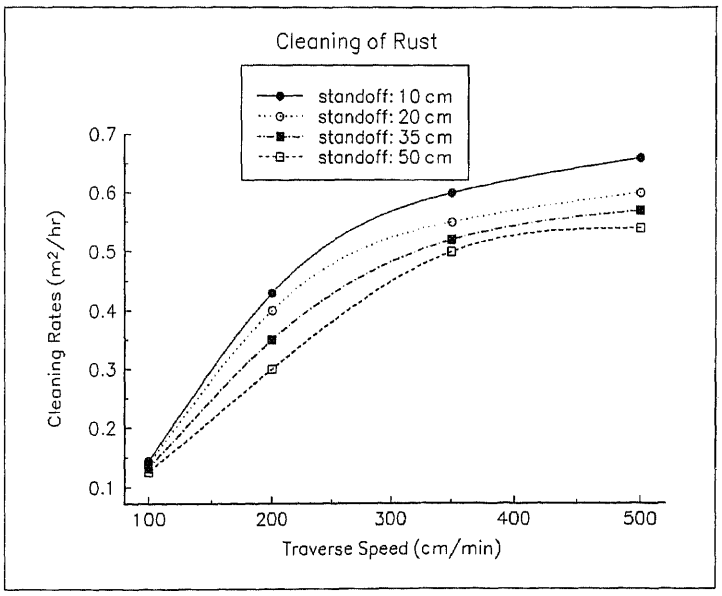

Figure C.4d Cleaning of Rust by Pulsed WJ Nozzle at An Extended Stand Off Distance (test conditions are identical to those in Figure C.1)

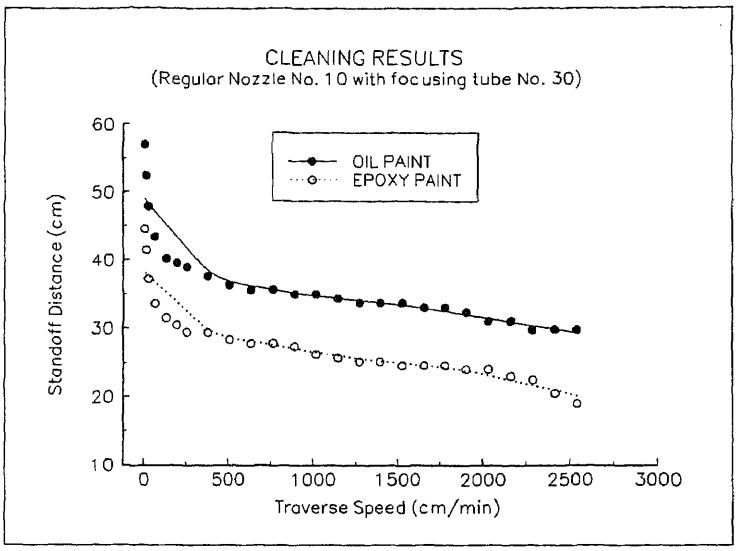

Figure C.4e Cleaning of Oil and Epoxy Paint by Commercial Nozzle (P = 330.7 Mpa; sapphire nozzle: #10 (0.254 mm); focusing tube: # 43 (0.908 mm))
(This result is obtained by people in our laboratory)

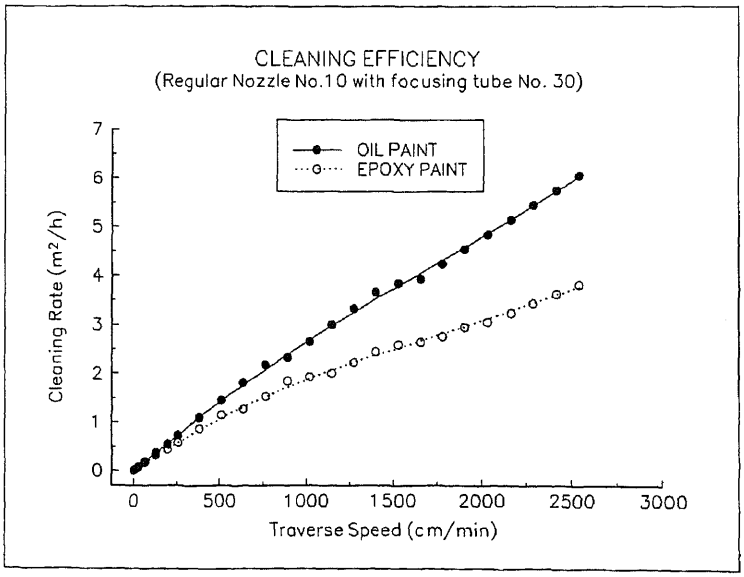

Figure C.4f Cleaning of Oil and Epoxy Paint by Commercial Nozzle at stand off distance of 40 mm and 30 mm respectively (Test conditions are identical to those in Figure C.4e)
(This result is obtained by people in our laboratory)

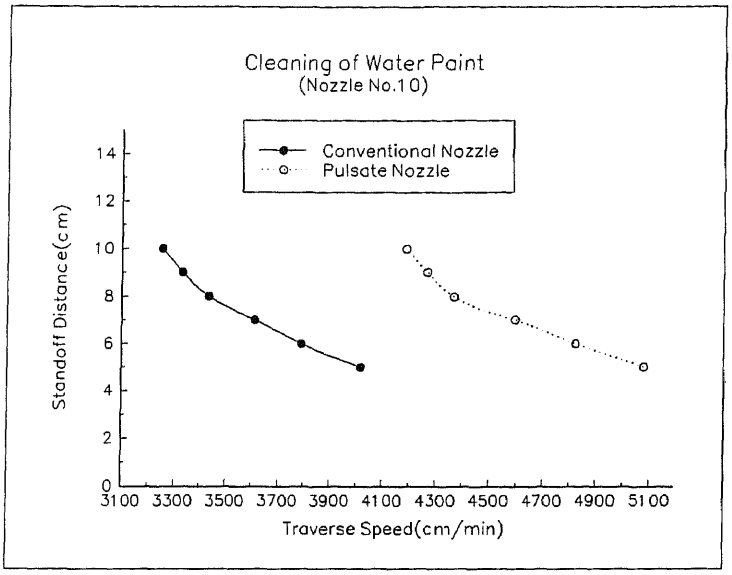

Figure C.5a Comparison of Cleaning of Water Paint by Pulsed and Commercial WJ Nozzle at A Reduced Stand Off Distance (upstream nozzle: #10(0.254 mm); downstream nozzle: #12(0.305 mm); h = 0.75; P = 330.7 Mpa)
Better cleaning performance occurs using pulsed nozzle.

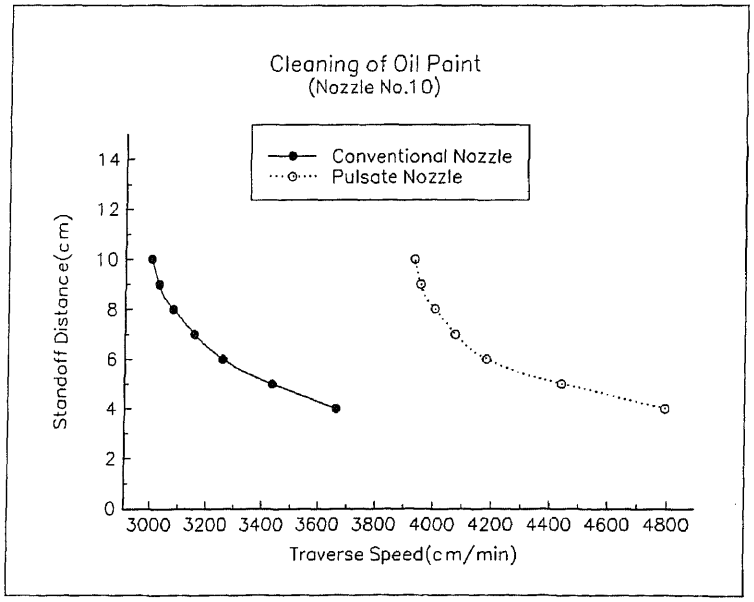

Figure C.5b Comparison of Cleaning of Oil Paint by Pulsed and Commercial WJ Nozzle at A Reduced Stand Off Distance (test conditions are identical to those in Figure C.5a)
Better cleaning performance occurs using pulsed nozzle.

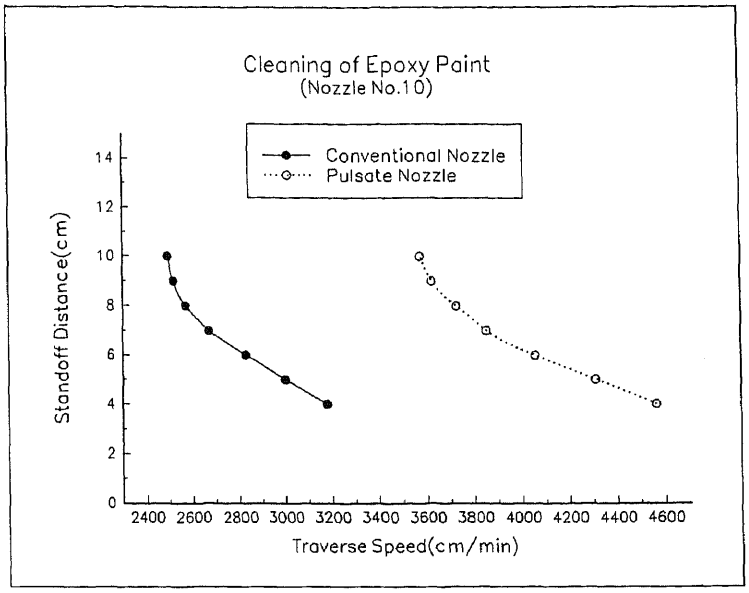

Figure C.5c Comparison of Cleaning of Epoxy Paint by Pulsed and Commercial WJ Nozzle at A Reduced Stand Off Distance
(test conditions are identical to those in Figure C.5a)
Better cleaning performance occurs using pulsed nozzle.

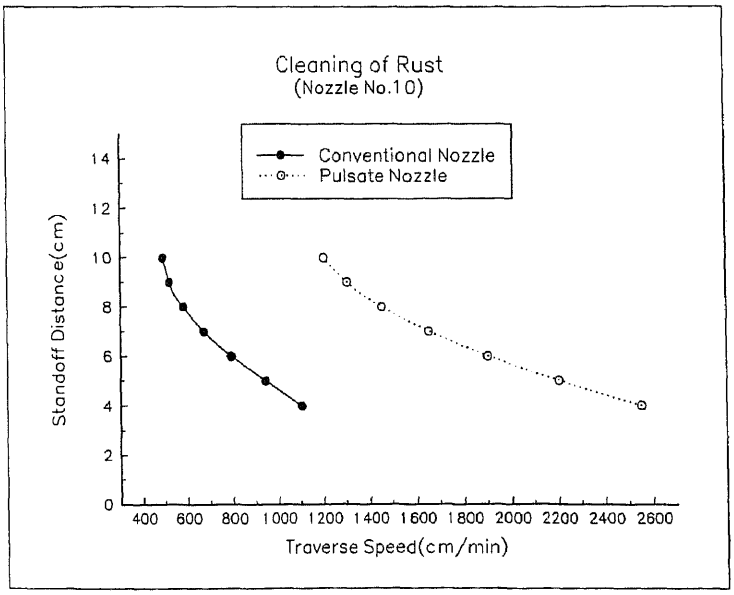

Figure C.5d Comparison of Cleaning of Rust by Pulsed and Commercial WJ Nozzle at A Reduced Stand Off Distance
(test conditions are identical to those in Figure C.5a)
Better cleaning performance occurs using pulsed nozzle.

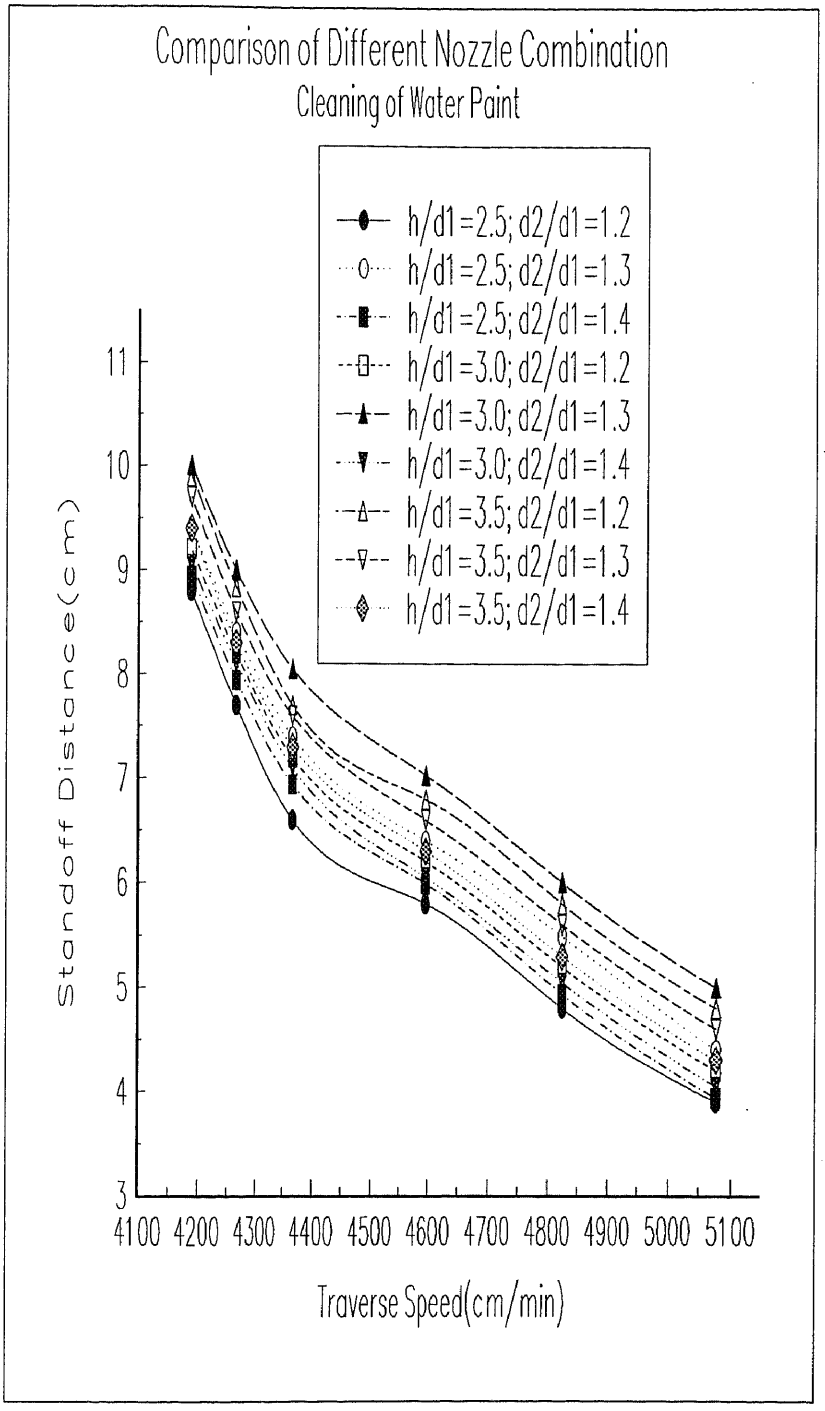

Figure C.6a Effect of the Parameters of Pulsed WJ Nozzle on the Cleaning of Water Paint (by experiment, P = 330.7 Mpa)
Approximately linear correlation between stand off distance and traverse speed is presented. The optimal parameter of nozzle design is h/d1 = 3.0 and d2/d1 = 1.3.

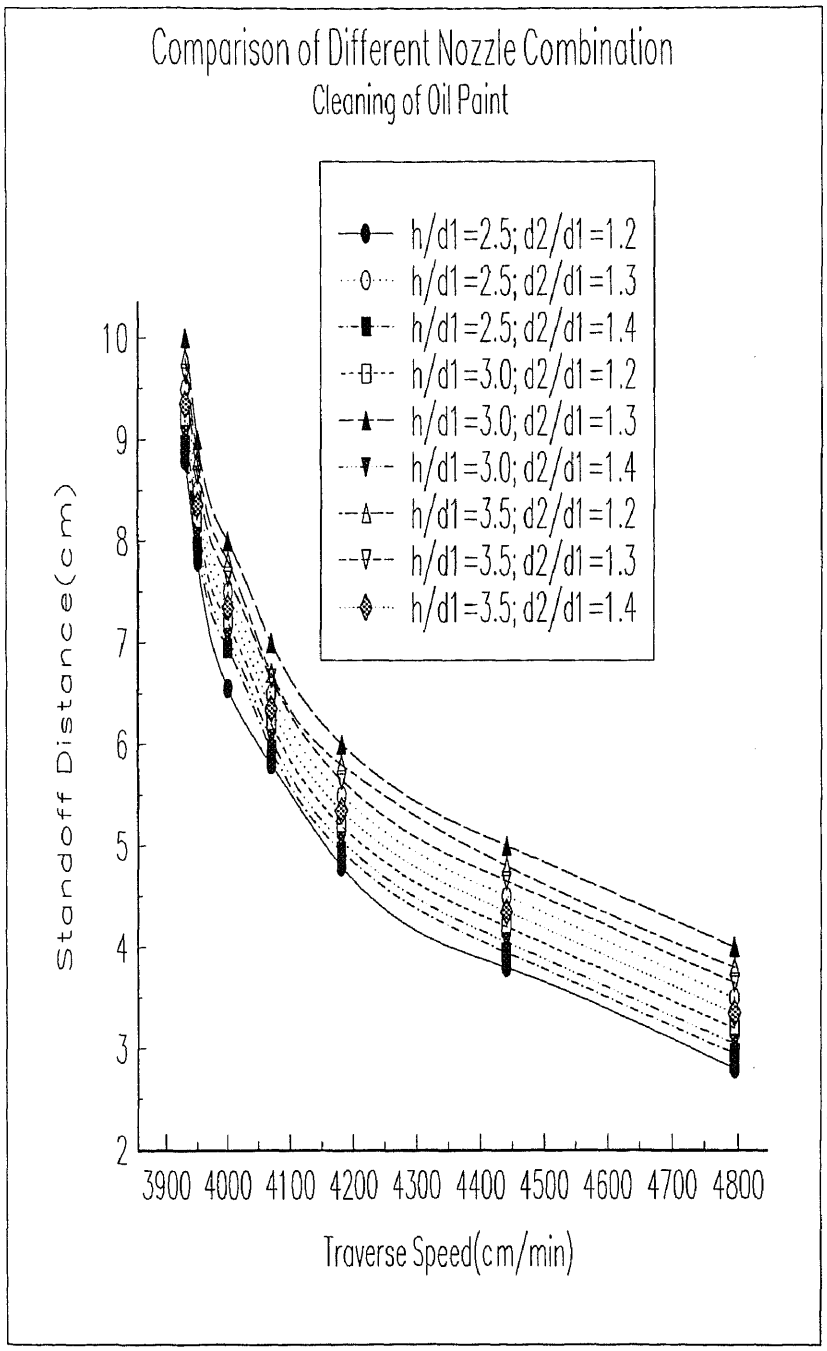

Figure C.6b Effect of the Parameters of Pulsed WJ Nozzle on the Cleaning of Oil Paint (by experiment, P = 330.7 Mpa)
Approximately linear correlation between stand off distance and traverse speed is presented at traverse speed 4100 - 4800 cm/min. Strong effect of cleaning presented at traverse speed less than 4100 cm/min and this is recommended speed zone. The optimal parameter of nozzle design is h/d1=3.0 and d2/d1=1.3.

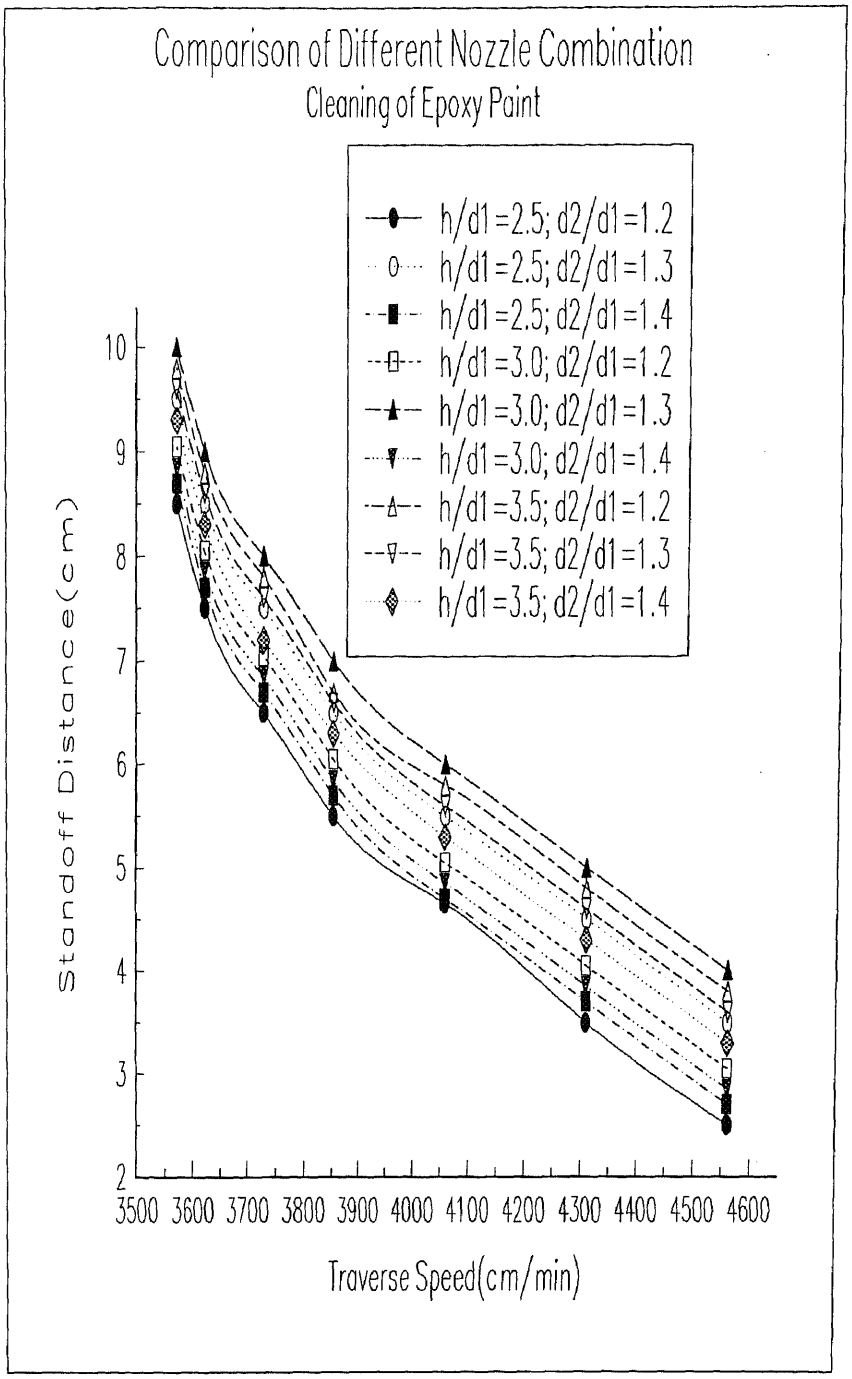

Figure C.6c Effect of the Parameters of Pulsed WJ Nozzle on the Cleaning of Epoxy Paint (by experiment, P = 330.7 Mpa)
Approximately linear correlation between stand off distance and traverse speed is presented at traverse speed 3850 - 4550 cm/min. Strong effect of cleaning presented at traverse speed less than 3850 cm/min and this is recommeded speed zone. The optimal parameter of nozzle design is h/d1=3.0 and d2/d1=1.3.

Table C.1a Experimental Comparison of Different Nozzle Combinations (Titanium Cutting)

trav spd(cm/min) / type	15	25	50	75	100	125
h/d1=2.5; d2/d1=1.2	0.75	0.45	0.15	0.14	0.12	0.11
h/d1=2.5; d2/d1=1.3	0.84	0.56	0.24	0.20	0.16	0.13
h/d1=2.5; d2/d1=1.4	0.80	0.52	0.19	0.17	0.14	0.11
h/d1=3.0; d2/d1=1.2	0.76	0.47	0.16	0.15	0.13	0.10
h/d1=3.0; d2/d1=1.3	0.85	0.58	0.26	0.24	0.16	0.14
h/d1=3.0; d2/d1=1.4	0.81	0.54	0.20	0.18	0.15	0.12
h/d1=3.5; d2/d1=1.2	0.74	0.41	0.15	0.13	0.12	0.10
h/d1=3.5; d2/d1=1.3	0.82	0.55	0.21	0.19	0.15	0.13
h/d1=3.5; d2/d1=1.4	0.78	0.50	0.18	0.16	0.13	0.11
Commercial Nozzle (#10 reg nozzle)	0.72	0.34	0.13	0.12	0.11	0.05

Notes:
Cutting Depth: mm
h: Cavity Length
d1: Diameter of Upstream Nozzle
d2: Diameter of Downstream Nozzle
#10 reg nozzle: diameter of 0.254 mm

Table C.1b Experimental Comparison of Different Nozzle Combinations (Aluminum Cutting)

trav spd(cm/min) / type	15	25	50	75	100	125
h/d1=2.5; d2/d1=1.2	1.14	0.80	0.40	0.23	0.16	0.14
h/d1=2.5; d2/d1=1.3	1.25	0.90	0.55	0.33	0.23	0.20
h/d1=2.5; d2/d1=1.4	1.21	0.85	0.50	0.29	0.19	0.18
h/d1=3.0; d2/d1=1.2	1.17	0.80	0.43	0.25	0.17	0.15
h/d1=3.0; d2/d1=1.3	1.28	0.95	0.57	0.35	0.24	0.21
h/d1=3.0; d2/d1=1.4	1.22	0.87	0.52	0.31	0.20	0.19
h/d1=3.5; d2/d1=1.2	1.08	0.75	0.35	0.17	0.14	0.12
h/d1=3.5; d2/d1=1.3	1.23	0.88	0.54	0.32	0.21	0.19
h/d1=3.5; d2/d1=1.4	1.20	0.83	0.47	0.27	0.18	0.17
Commercial Nozzle (#10 reg nozzle)	0.95	0.55	0.24	0.15	0.13	0.08

Notes:
Cutting Depth: mm
h: Cavity Length
d1: Diameter of Upstream Nozzle
d2: Diameter of Downstream Nozzle
#10 reg nozzle: diameter of 0.254 mm

Table C.2 Evaluation of the Efficiency of Cleaning Rates vs. Water Consumption (cleaning of water paint by pulsate nozzle at an extended stand off distance)

	cleaning rates (m^2 / hr)				**water consumption** [$X10^{-2} (m^3 / m^2)$]			
traverse speed (cm/min)	stdoff 12.5cm	stdoff 20.0cm	stdoff 30.0cm	stdoff 40.0cm	stdoff 12.5cm	stdoff 20.0cm	stdoff 30.0cm	stdoff 40.0cm
1000.0	1.80	1.68	1.50	1.38	4.50	4.81	5.40	5.86
2000.0	3.93	3.52	3.21	3.02	2.07	2.31	2.53	2.71
3000.0	5.01	4.72	4.22	4.01	1.62	1.71	1.93	2.07
4000.0	5.52	5.04	4.56	4.32	1.47	1.60	1.78	1.88

Notes:
Water pressure: 330.7 Mpa
Nozzle type: upstream: #10 (0.254 mm)
downstream: #12(0.305 mm)

Table C.3 Evaluation of the Efficiency of Cleaning Rates vs. Water Consumption (cleaning of oil paint by pulsate nozzle at an extended stand off distance)

	cleaning rates (m^2 / hr)				**water consumption** [X10^{-2}(m^3 / m^2)]			
traverse speed (cm/min)	stdoff 10.0cm	stdoff 13.0cm	stdoff 18.0cm	stdoff 25.0cm	stdoff 10.0cm	stdoff 13.0cm	stdoff 18.0cm	stdoff 25.0cm
500.0	0.91	0.82	0.74	0.69	9.01	10.13	10.93	11.74
1000.0	2.02	1.73	1.68	1.61	4.05	4.52	4.75	5.07
1500.0	2.81	2.52	2.32	2.11	2.89	3.24	3.51	3.85
2500.0	3.45	3.15	2.91	2.72	2.35	2.58	2.79	3.01

Notes:
Water pressure: 330.7 Mpa
Nozzle type: upstream: #10 (0.254 mm)
downstream: #12(0.305 mm)

Table C.4 Evaluation of the Efficiency of Cleaning Rates vs. Water Consumption (cleaning of epoxy paint by pulsate nozzle at an extended stand off distance)

	cleaning rates (m^2 / hr)				**water consumption** $[X10^{-2}(m^3 / m^2)]$			
traverse speed (cm/min)	stdoff 10.0cm	stdoff 25.0cm	stdoff 50.0cm	stdoff 60.0cm	stdoff 10.0cm	stdoff 25.0cm	stdoff 50.0cm	stdoff 60.0cm
100.0	0.15	0.138	0.126	0.114	54.01	58.65	64.27	71.05
250.0	0.45	0.43	0.35	0.33	22.51	23.34	27.64	29.04
500.0	0.65	0.61	0.57	0.51	12.45	13.27	14.21	15.88
600.0	0.684	0.64	0.612	0.54	11.83	12.49	13.47	15.02

Notes:
Water pressure: 330.7 Mpa
Nozzle type: upstream: #10 (0.254 mm)
downstream: #12(0.305 mm)

Table C.5 Evaluation of the Efficiency of Cleaning Rates vs. Water Consumption (cleaning of rust by pulsate nozzle at an extended stand off distance)

	cleaning rates (m^2 / hr)				**water consumption** [X10^{-2} (m^3 / m^2)]			
traverse speed (cm/min)	stdoff 10.0cm	stdoff 20.0cm	stdoff 35.0cm	stdoff 50.0cm	stdoff 10.0cm	stdoff 20.0cm	stdoff 35.0cm	stdoff 50.0cm
100.0	0.144	0.139	0.132	0.126	56.25	58.27	61.35	64.29
200.0	0.43	0.41	0.35	0.31	24.84	26.25	29.14	33.02
350.0	0.61	0.55	0.52	0.49	13.51	14.73	15.58	16.20
500.0	0.66	0.61	0.57	0.54	12.27	13.51	14.22	15.03

Notes:
Water pressure: 330.7 Mpa
Nozzle type: upstream: #10 (0.254 mm)
downstream: #12(0.305 mm)

Table C.6a Evaluation of the Efficiency of Cleaning Rates vs. Water Consumption (cleaning of water paint by pulsate nozzle at an reduced stand off distance)

	cleaning rates (m^2/hr)				**water consumption** $[X10^{-2}(m^3/m^2)]$			
traverse speed (cm/min)	stdoff 5.0cm	stdoff 6.0cm	stdoff 7.0cm	stdoff 8.0cm	stdoff 5.0m	stdoff 6.0cm	stdoff 7.0cm	stdoff 8.0cm
4200.0	10.05	9.38	8.37	7.71	0.53	0.576	0.645	0.71
4400.0	10.20	9.51	8.49	7.82	0.529	0.568	0.636	0.69
4700.0	10.78	10.06	8.99	8.27	0.51	0.536	0.62	0.653
5050.0	11.65	10.87	9.705	8.93	0.463	0.497	0.557	0.605

Notes: Test conditions are identical to those of Table C.2.

Table C.6b Evaluation of the Efficiency of Cleaning Rates vs. Water Consumption (cleaning of water paint by commercial nozzle at an reduced stand off distance)

	cleaning rates (m^2 / hr)				**water consumption** $[X10^{-2}(m^3 / m^2)]$			
traverse speed (cm/min)	stdoff 5.0cm	stdoff 6.0cm	stdoff 7.0cm	stdoff 8.0cm	stdoff 5.0m	stdoff 6.0cm	stdoff 7.0cm	stdoff 8.0cm
3250.0	6.39	5.96	5.33	4.89	1.117	1.198	1.339	1.457
3350.0	6.57	6.13	5.48	5.04	1.086	1.164	1.303	1.417
3600.0	7.02	6.55	5.99	5.38	1.017	1.09	1.192	1.327
4100.0	7.74	7.22	6.45	5.93	0.922	0.989	1.107	1.204

Notes: Test conditions are identical to those of Table C.2.

Table C.7a Evaluation of the Efficiency of Cleaning Rates vs. Water Consumption (cleaning of oil paint by pulsate nozzle at an reduced stand off distance)

	cleaning rates (m^2/hr)				**water consumption** $[X10^{-2}(m^3/m^2)]$			
traverse speed (cm/min)	stdoff 5.0cm	stdoff 6.0cm	stdoff 7.0cm	stdoff 8.0cm	stdoff 5.0cm	stdoff 6.0cm	stdoff 7.0cm	stdoff 8.0cm
3920.0	9.14	8.54	7.62	7.01	0.591	0.632	0.709	0.771
4200.0	9.27	8.66	7.73	7.11	0.585	0.623	0.699	0.759
4400.0	9.63	9.09	8.04	7.39	0.56	0.594	0.672	0.731
4790.0	10.71	10.10	8.99	8.22	0.504	0.535	0.601	0.657

Notes: Test conditions are identical to those of Table C.2.

Table C.7b Evaluation of the Efficiency of Cleaning Rates vs. Water Consumption (cleaning of oil paint by commercial nozzle at an reduced stand off distance)

	cleaning rates (m^2/hr)				**water consumption** $[X10^{-2}(m^3/m^2)]$			
traverse speed (cm/min)	stdoff 4.0cm	stdoff 6.0cm	stdoff 8.0cm	stdoff 10.0cm	stdoff 4.0cm	stdoff 6.0cm	stdoff 8.0cm	stdoff 10.0cm
3000.0	5.94	5.54	4.95	4.55	1.202	1.289	1.443	1.596
3080.0	6.084	5.67	5.07	4.66	1.174	1.259	1.408	1.532
3250.0	6.39	5.96	5.325	4.89	1.117	1.198	1.34	1.46
3660.0	7.71	6.63	5.93	5.44	0.926	1.077	1.204	1.322

Notes: Test conditions are identical to those of Table C.2.

Table C.8a Evaluation of the Efficiency of Cleaning Rates vs. Water Consumption (cleaning of epoxy paint by pulsed nozzle at an reduced stand off distance)

	cleaning rates (m^2/hr)				**water consumption** $[X10^{-2}(m^3/m^2)]$			
traverse speed (cm/min)	stdoff 5.0cm	stdoff 6.0cm	stdoff 7.0cm	stdoff 8.0cm	stdoff 5.0cm	stdoff 6.0cm	stdoff 7.0cm	stdoff 8.0cm
3570.0	8.23	7.68	6.86	6.31	0.656	0.703	0.787	0.855
37500.0	8.50	7.93	7.09	6.60	0.635	0.68	0.762	0.818
4000.0	9.00	8.40	7.51	6.99	0.61	0.643	0.719	0.773
4560.0	9.99	9.33	8.34	7.76	0.54	0.579	0.647	0.696

Notes: Test conditions are identical to those of Table C.2.

Table C.8b Evaluation of the Efficiency of Cleaning Rates vs. Water Consumption (cleaning of epoxy paint by commercial nozzle at an reduced stand off distance)

	cleaning rates (m^2/hr)				**water consumption** $[X10^{-2}(m^3/m^2)]$			
traverse speed (cm/min)	stdoff 5.0cm	stdoff 6.0cm	stdoff 7.0cm	stdoff 8.0cm	stdoff 5.0cm	stdoff 6.0cm	stdoff 7.0cm	stdoff 8.0cm
2490.0	5.04	4.72	4.21	3.86	1.417	1.519	1.71	1.85
2570.0	5.17	4.82	4.31	3.96	1.381	1.481	1.566	1.803
2800.0	5.58	5.21	4.65	4.28	1.280	1.370	1.536	1.668
3180.0	6.26	5.85	5.22	4.81	1.141	1.220	1.368	1.488

Notes: Test conditions are identical to those of Table C.2.

Table C.9a Evaluation of the Efficiency of Cleaning Rates vs. Water Consumption (cleaning of rust by pulsed nozzle at an reduced stand off distance)

	cleaning rates (m^2/hr)				**water consumption** $[X10^{-2}(m^3/m^2)]$			
traverse speed (cm/min)	stdoff 5.0cm	stdoff 6.0cm	stdoff 7.0cm	stdoff 8.0cm	stdoff 5.0cm	stdoff 6.0cm	stdoff 7.0cm	stdoff 8.0cm
1200.0	3.91	3.62	3.21	3.02	1.385	1.501	1.688	1.801
1600.0	4.21	3.92	3.41	3.22	1.286	1.385	1.588	1.688
1900.0	5.11	4.71	4.12	3.91	1.059	1.149	1.317	1.385
2550.0	6.61	6.12	5.31	5.12	0.818	0.885	1.088	1.059

Notes: Test conditions are identical to those of Table C.2.

Table C.9b Evaluation of the Efficiency of Cleaning Rates vs. Water Consumption (cleaning of rust by commercial nozzle at an reduced stand off distance)

	cleaning rates (m^2 / hr)				**water consumption** $[X10^{-2}(m^3 / m^2)]$			
traverse speed (cm/min)	stdoff 5.0cm	stdoff 6.0cm	stdoff 7.0cm	stdoff 8.0cm	stdoff 5.0cm	stdoff 6.0cm	stdoff 7.0cm	stdoff 8.0cm
490.0	2.27	2.11	1.92	1.72	3.145	3.401	3.751	4.202
580.0	2.51	2.32	2.12	1.91	2.856	3.101	3.402	3.758
750.0	2.91	2.72	2.31	2.22	2.462	2.644	3.101	3.245
1100.0	3.41	3.22	2.71	2.51	2.11	2.23	2.644	2.856

Notes: Test conditions are identical to those of Table C.2.

APPENDIX D

RESULTS OF COMPUTATIONAL STUDY OF PULSED WJ NOZZLE

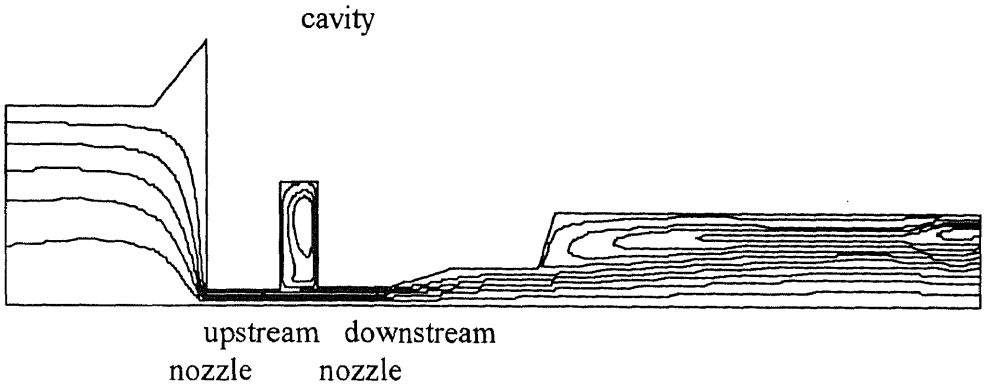

Figure D.1 Streamline Contour Plot for Pulsed Nozzle (contour level: ψ_{max} = 59.75 cm^2 /s and ψ_{min} = 0.00 cm^2 /s) at t=0.5X10^{-3} sec After Initiation of the Pulsate Flow (Test conditions: upstream nozzle: #10 (0.254 mm); downstream nozzle: #12 (0.305 mm); h = 0.75 mm; P = 330.7 Mpa)

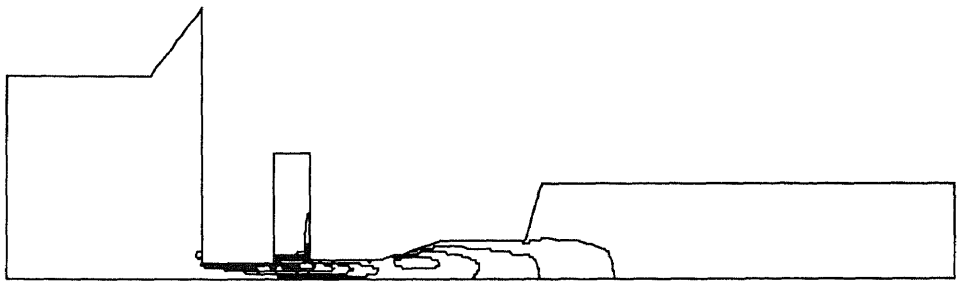

Figure D.2 Turbulent Kinetic Energy Contour for Pulsed Nozzle (Contour Level: k_{max} = 0.249 x 10^9 cm^2 / s^2 and k_{min} = 0.160 x 10^4 cm^2 / s^2) at t = 0.5X10^{-3} sec After Initiation of the Pulsate Flow ; (Test conditions are identical to those in Fig. D.1).

Figure D.3 Turbulent Energy Dissipation Contour for Pulsed Nozzle (Contour Level: $\varepsilon_{max} = 0.237 \times 10^{10} cm^2 / s^2$ and $\varepsilon_{min} = 0.163 \times 10^5$ cm^2 / s^2) at $t = 0.5X10^{-3}$ sec After Initiation of the Pulsate Flow. (Test conditions are identical to those in Fig. D.1).

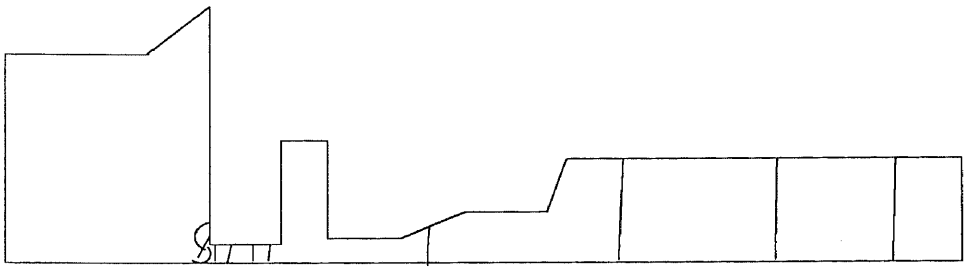

Figure D.4 Pressure Contour for Pulsed Nozzle ($P = -0.1356 \times 10^8$ -- 0.6099×10^{10} gm / cm-s^2) at $t = 0.5X10^{-3}$ sec After Initiation of the Pulsate Flow). (Test conditions are identical to those in Fig. D.1)

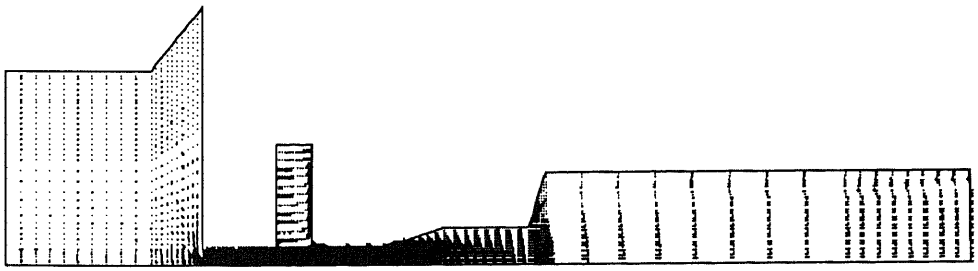

Figure D.5 Velocity Vector Plot for Pulsed Nozzle ($u_{max} = 1002$ m /s and $u_{exit} = 230$ m /s) at $t = 0.5X10^{-3}$ sec After Initiation of the Pulsate Flow). (Test conditions are identical to those in Fig. D.1).

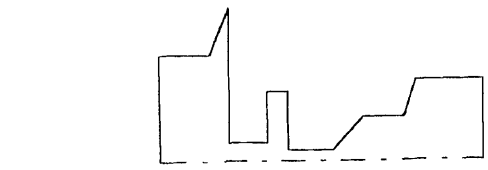

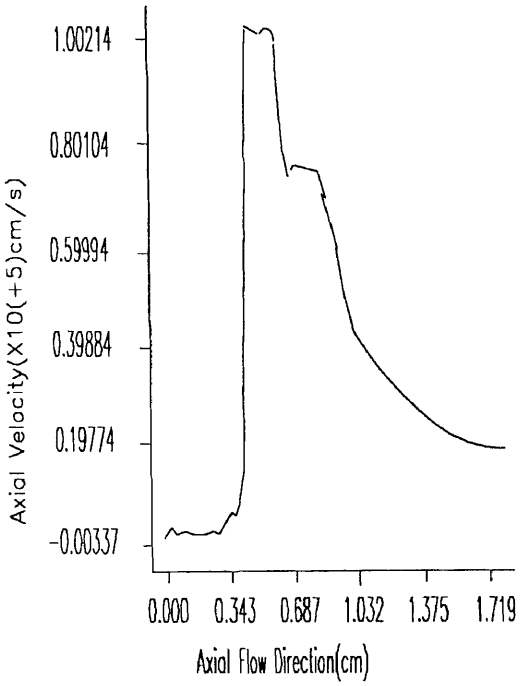

Figure D.6 Axial Velocity Distribution Along the Flow Axis at $t = 0.5X10^{-3}$ After Initiation of Pulsate Flow (test conditions are identical to those in Fig. D.1)

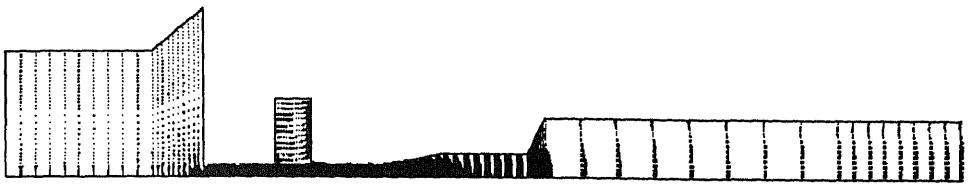

(a) u_{max} = 952 m /s and u_{exit} = 215 m /s at t = $0.1X10^{-3}$ sec

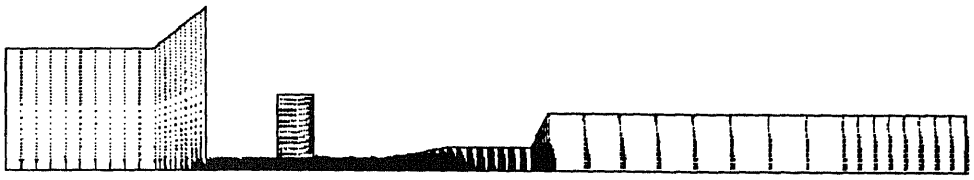

(b) u_{max} = 922 m /s and u_{exit} = 202 m /s at t = $0.5X10^{-2}$ sec

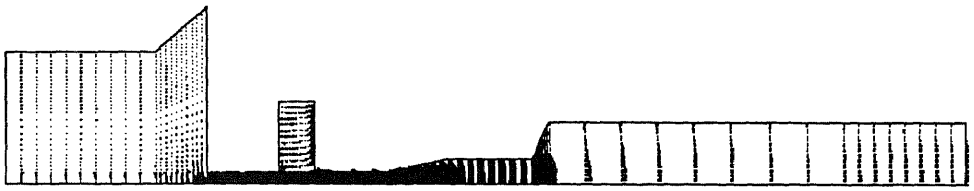

(c) u_{max} = 902 m /s and u_{exit} = 189 m /s at t = $0.1X10^{-2}$ sec

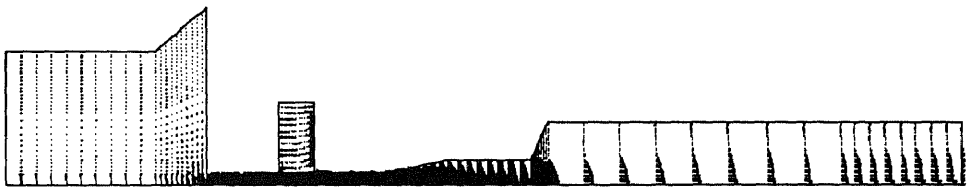

(d) u_{max} = 883 m /s and u_{exit} = 178 m /s at t = $0.5X10^{-1}$ sec

Figure D.7 Velocity Vector Plot for Pulsed Nozzle at Different Time After Initiation of Pulsed Flow (test conditions are identical to those in Fig. D.1)

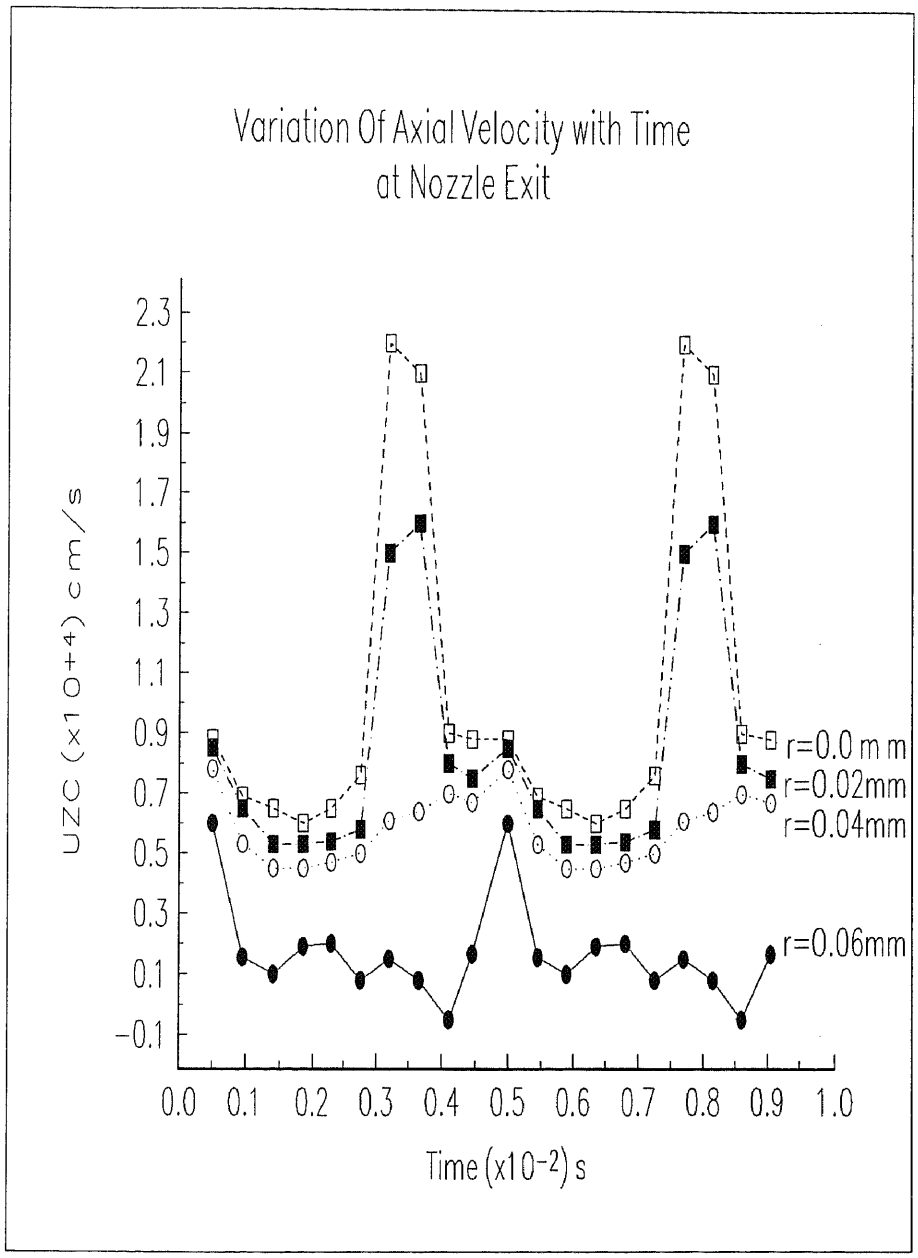

Figure D.8 Variation of Axial Velocity with Time at the Exit of Pulsed Nozzle (by Numerical Simulation).
Maximum axial velocity is presented at the central line of the nozzle and test conditions are identical to those in Fig. D.1.

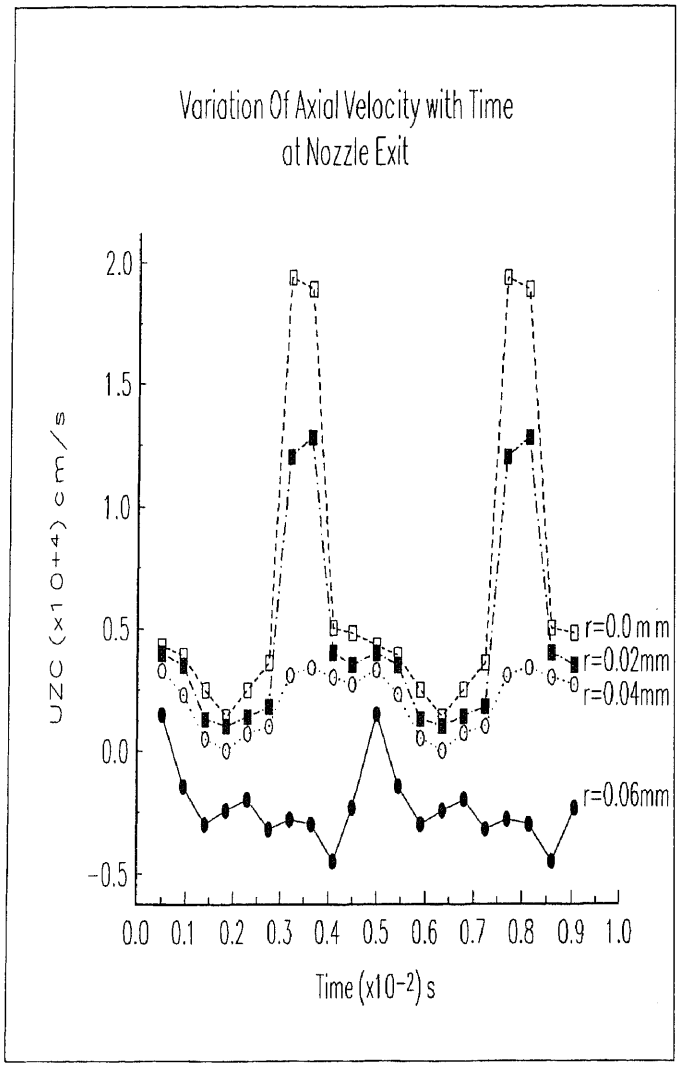

(a) The Length of Downstream Nozzle is 2 mm

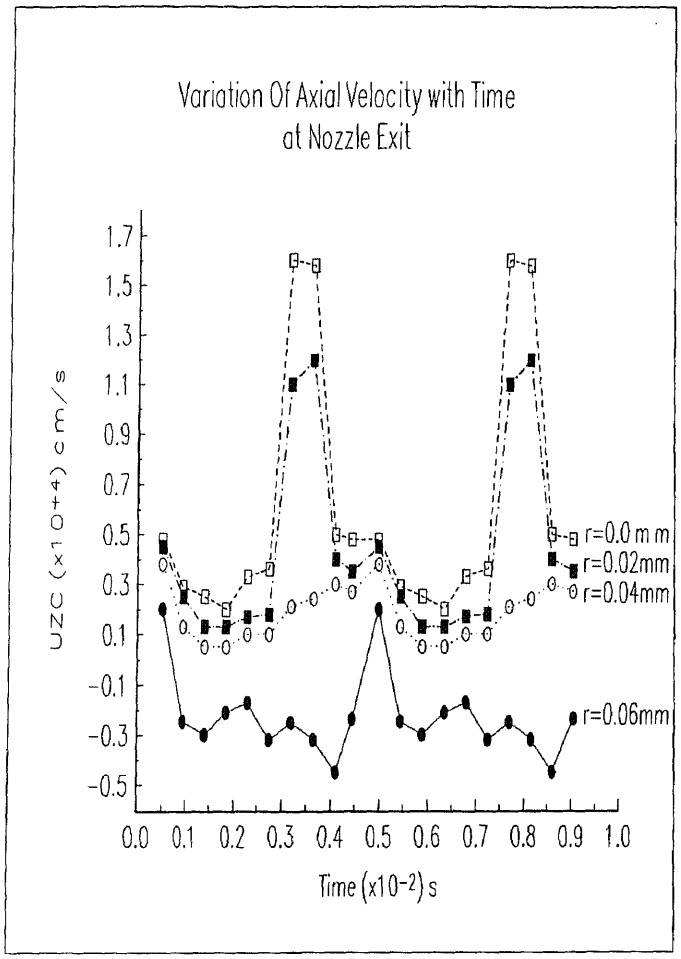

(b) The Length of Downstream Nozzle is 4 mm

Figure D.9 The effect of Downstream Nozzle on Performance of Pulsed WJ Nozzle

APPENDIX E

THE COMPUTATIONAL ANALYSIS OF RECOMMENDED PULSED WJ NOZZLE

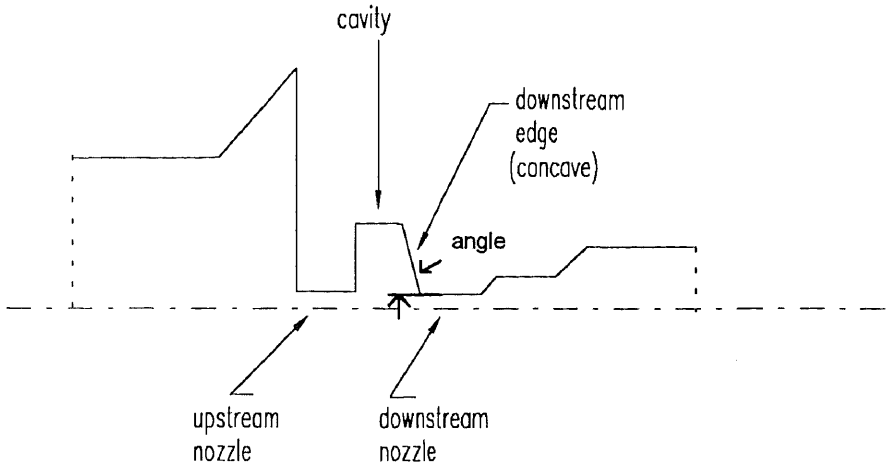

(a) Downstream Edge with Concave Shape

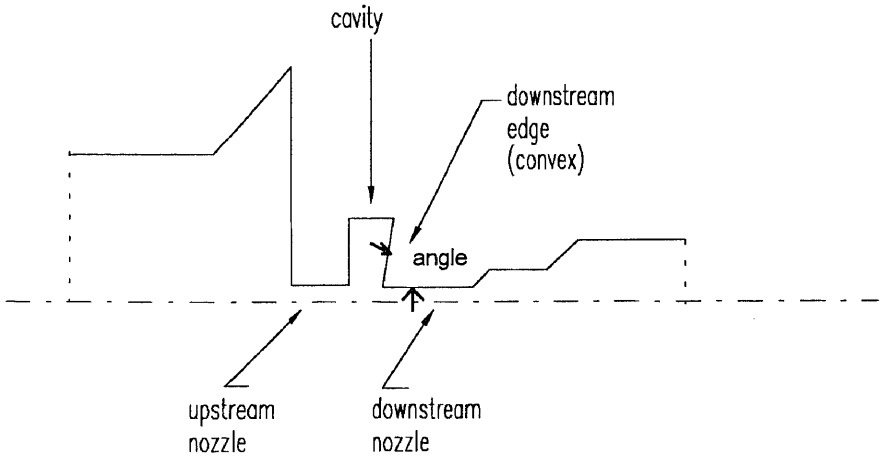

(b) Downstream Edge with Convex Shape

Figure E.1 Schematic of Pulsed WJ Nozzle with Different Geometry of Downstream Edge

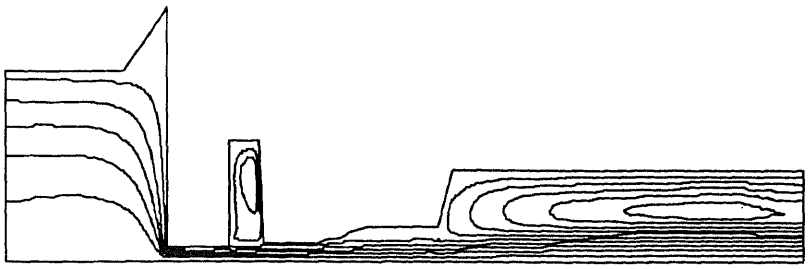

(a) Streamline Contour Plot for Downstream Edge with Concave Shape

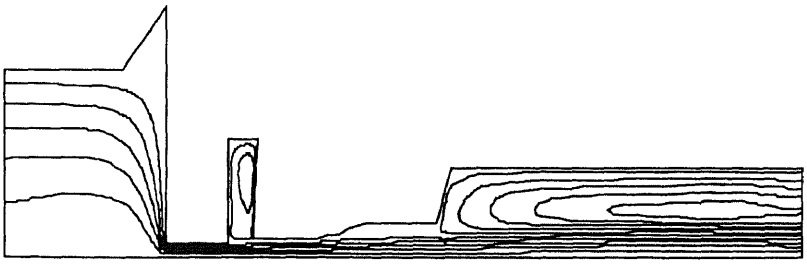

(b) Streamline Contour Plot for Downstream Edge with Convex Shape

Figure E.2 Streamline Contour Plot for Downstream Edge with Different Geometry

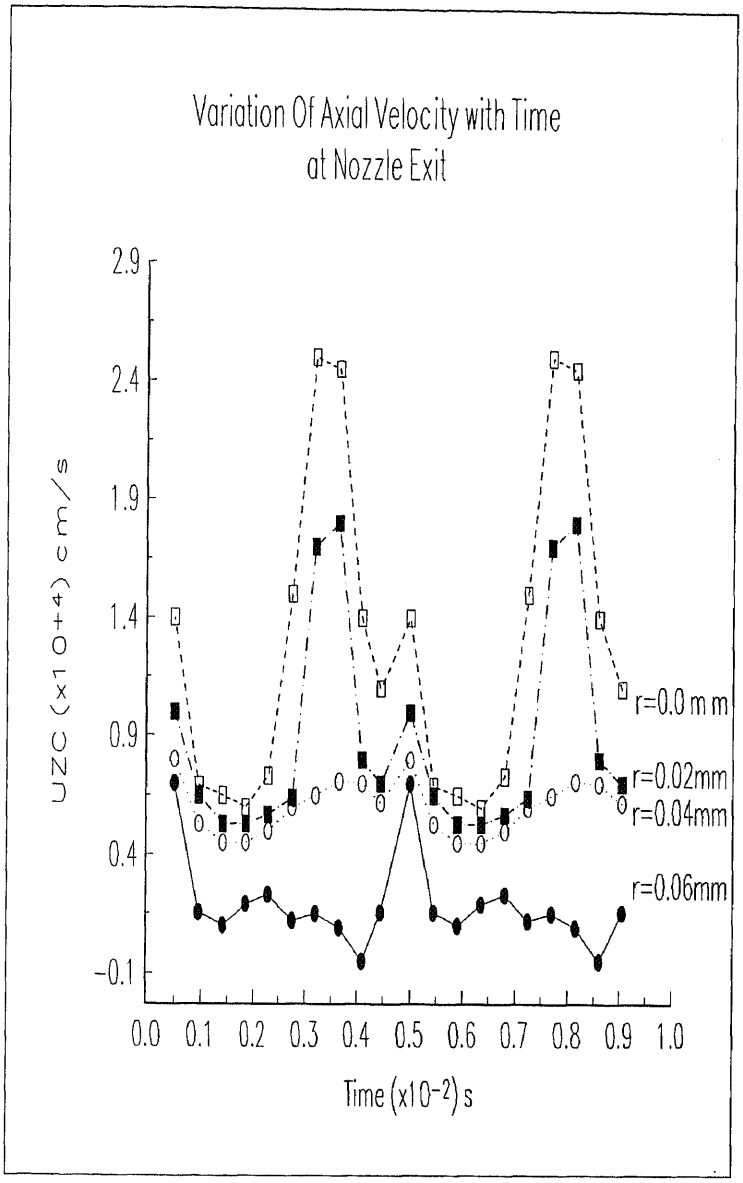

(a) Velocity at the Exit of Nozzle with Concave Shape of Downstream Edge

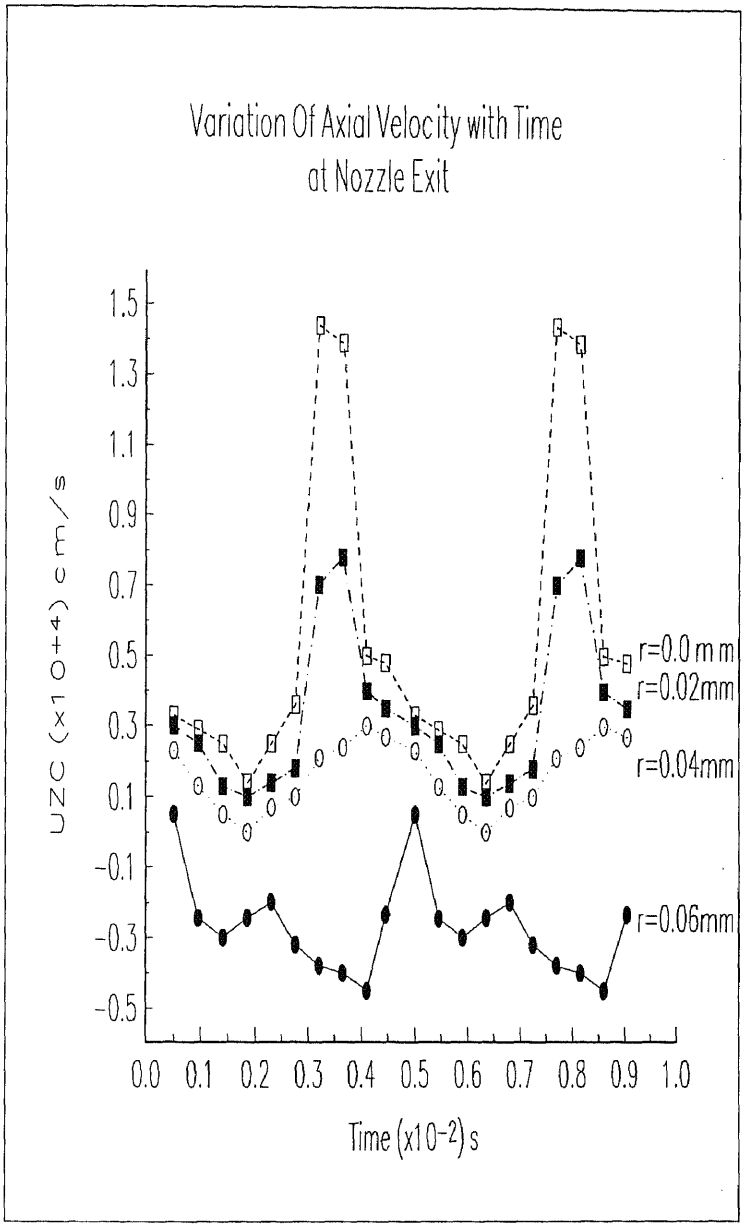

(b) Velocity at the Exit of Nozzle with Convex Shape of Downstream Edge

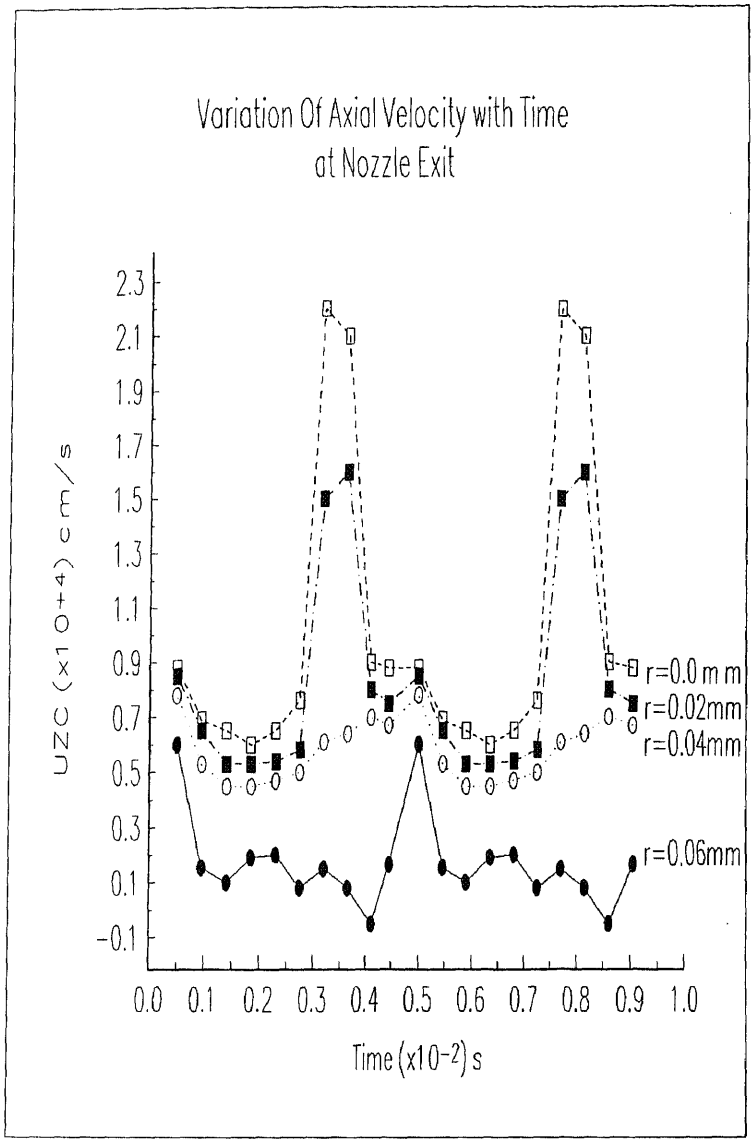

(c) Velocity at the Exit of Nozzle with Plate Shape of Downstream Edge

Figure E.3 The Velocity at the Exit of Nozzle with Different Geometry of Downstream Edge (The results show the best performance of the concave downstream edge)

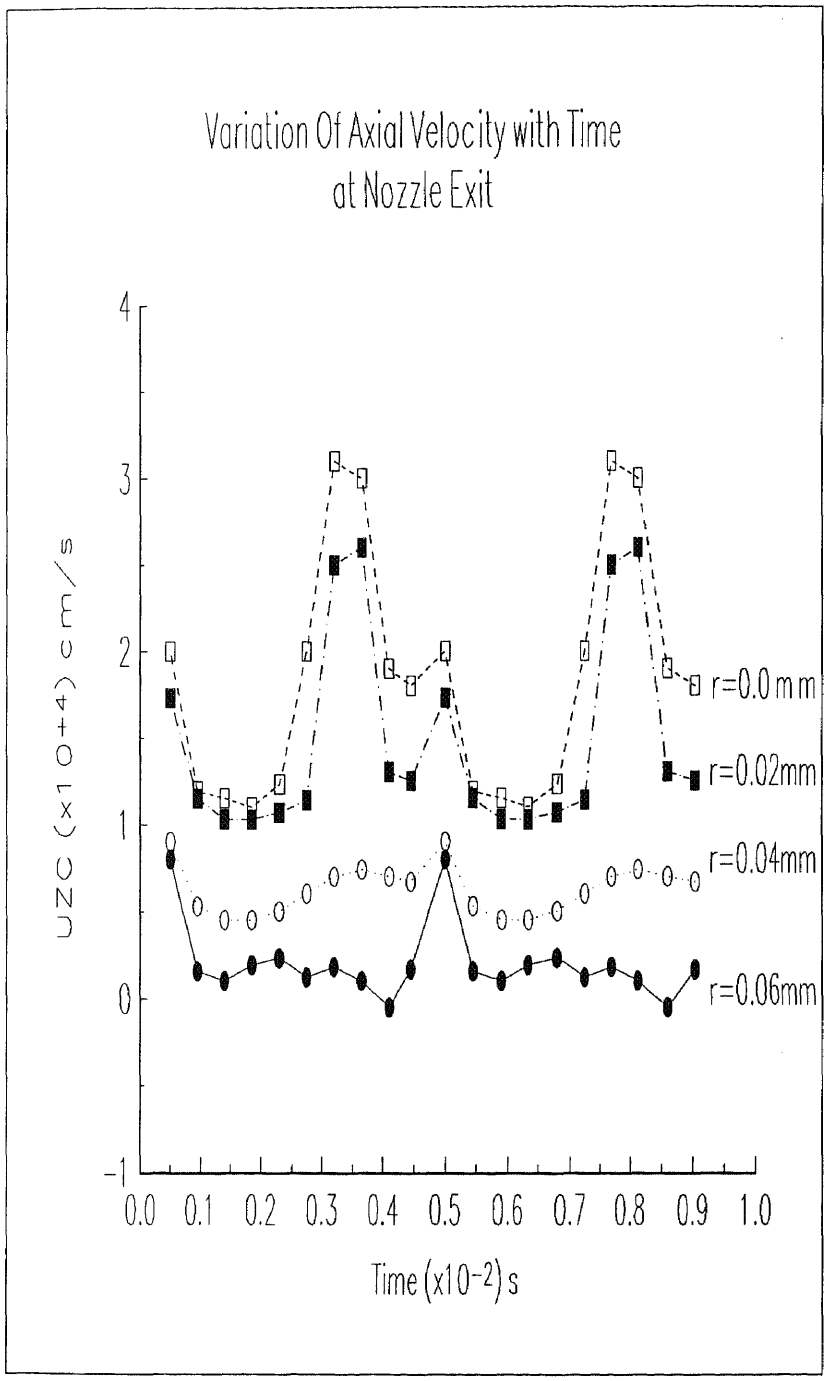

(a) The pulsed jet performance with the angle of downstream edge of 80^0

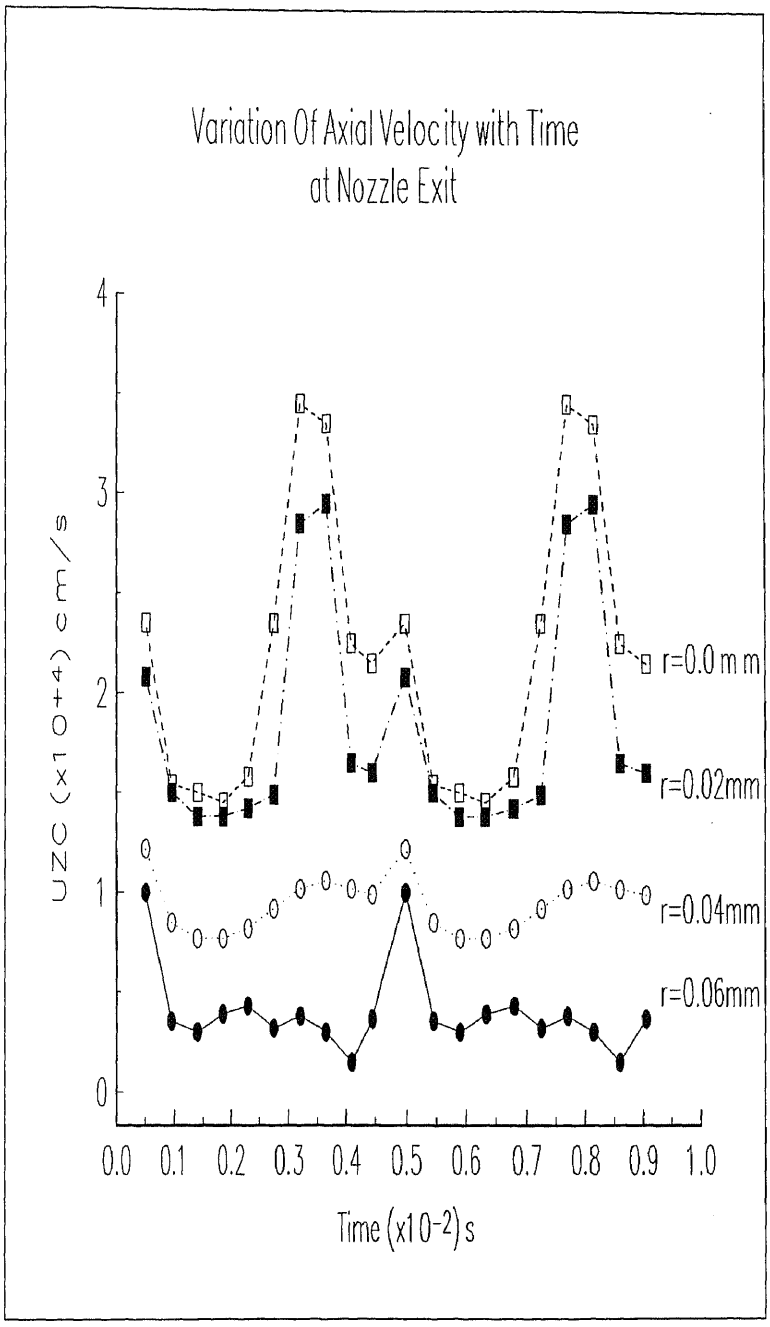

(b) The pulsed jet performance with the angle of downstream edge of 75^{0} .

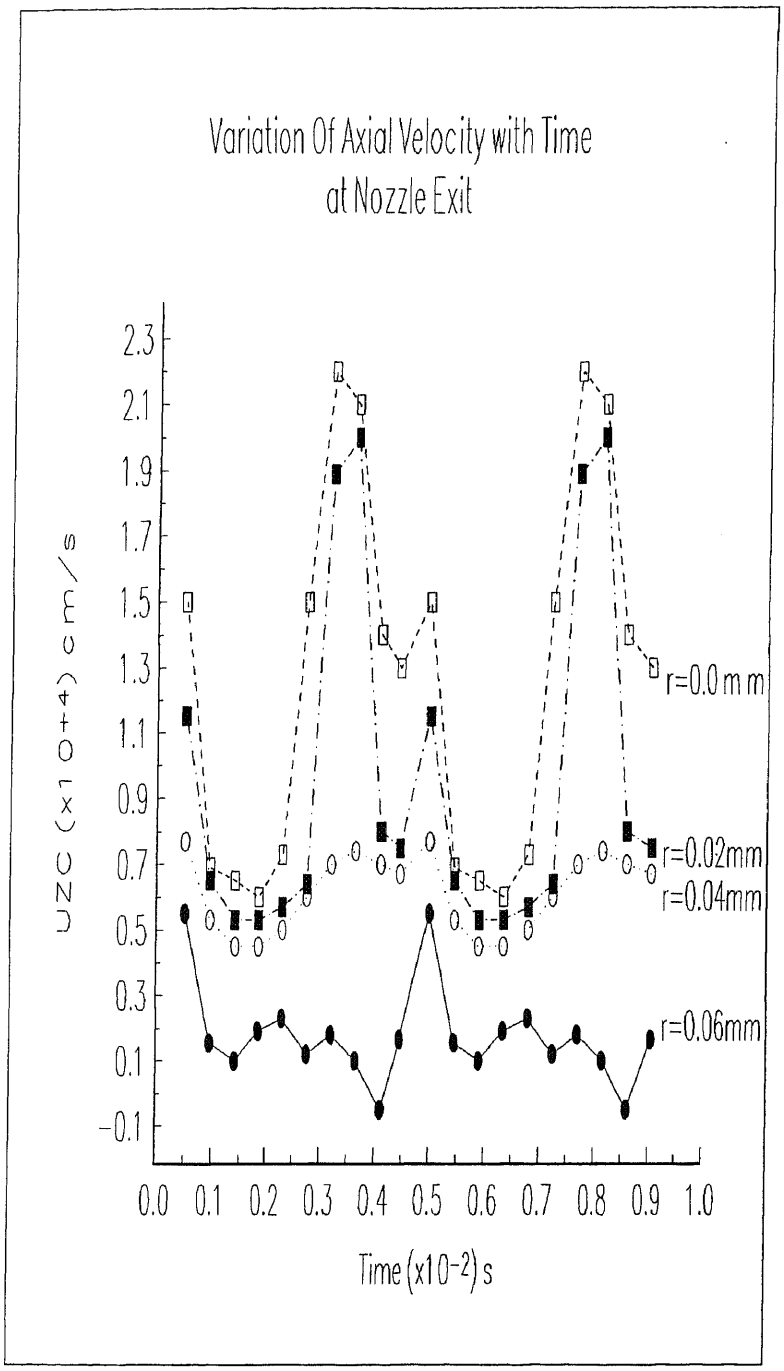

(c) The pulsed jet performance with the angle of downstream edge of 70°.

Figure E.4 The effect of the angle of downstream edge on the performance of pulsed nozzle.

BIBLIOGRAPHY

Abramovich, G. N. *The theory of Turbulent Jets*. Cambridge: MIT Press, 1963.

Bskharone, E. A. "Finite-Eoement Analysis of Turbulent Flow in Annular Exhaust Diffusers of Gas Turbine Engines." *Journal of Fluids Engineering. Transactions of the ASME.* 113: 104-110, 1991.

Chalmers, E. J. "Effect of Parameter Selection on Abrasive Waterjet Performance." *6th American Water Jet Conference*. 345-349, 1991.

Chen, W. L. "Correlation Between Particles Velocities and Conditions of Abrasive Water Jet Formation." Ph.D. Dissertation, New Jersey Institute of Technology, May, 1990

Conn, A.F. and Johnson, V. E. Jr. "Further Applications of the CAVIJET Method." *Proceedings of the 2nd International Symposium of Jet Cutting Technology. BHRA Fluid Engineering.* D2: 14-17, 1974.

Conn, A.F. and Rudy, S.L. "Cutting Coal with the CAVIJET Method". *Proceeding of 3rd International Symposium of Jet Cutting Technology. BHRA Fluid Engineering.* D8: 9-12, 1976.

Conn, A.F., Rudy, S. L. and Mehta, G. D. "Development of a CAVIJET System for Removing Marine Fouling and Rust. "*Proceeding of 3rd International Symposium of Jet Cutting Technology. BHRA Fluid Engineering.* G4: 14-18, 1976.

Conn, A.F. and Rudy, S.L. "Conservation and Extraction of Energy with the CAVIJET." *Proceeding of 4th International Symposium of Jet Cutting Technology. BHRA Fluid Engineering.* H2: 20-24, 1978.

Conn, A.F. and Johnson, V.E. Jr. "The Fluid Dynamics of Submerged Cavitating Jet Cutting." *Proceeding of 5th International Symposium of Jet Cutting Technology. BHRA Fluid Engineering.* A1: 1-14, 1980.

Dunne, B. and Cassen, B. "Velocity Discontinuity Instability of a Liquid Jet." *Journal of Applied Physica.* 27; 6: 577-582, 1956.

Eddingfield, D.L., Evers, J.L. and Setrok, A. "Mathematical Modeling of High Velocity Water Jets." *Ist U.S. Water Conference.* 1: I-3.1 - I-3.14, 1981.

Edwards, D.G., Smith, R.M. and Farmer, G. "The Coherence of Impulsive Water Jets." *6th International Symposium of Jet Cutting Technology.* 6: C4.123 - C4.140, 1982.

Erdmann-Jesnitzer, F., Louis, H., and Schikorr, W. "Cleaning, Drilling and Cutting by Interrupted Jets." *Procedding of 5th International Symposium of Jet Cutting Technology. BHRA Fluid Engineering.* A1: 23-26, 1980.

BIBLIOGRAPHY
(Continued)

Yie, Gene G. and Auburn, Wash. "High Velocity Particular Containing Fluid Jet Apparatus and Process ." *United States Patent.* No. 4,478,368, 1984.

Hashish, M. "Application Of Abrasive-Waterjet To Metal Cutting." *Flow System, 1986.*

Hetsroni, G. and Sokolov, M. "Distribution of Mass, Velocity and Intensity of Turbulence in a Two-Phase Turbulent Jet." *Journal of Applied Mechanics. Transactions of the ASME:* 315-326, 1971.

Hinze, J.O, *Turbulence.* Second Edition. New York: McGraw-Hill, 1975.

Horii, K., Matsumae, Y. and Kim, T.J. et al., "Development of A New Mixing Nozzle Assembly for High Pressure Abrasive Waterjet Applications." *10th International Symposium Jet Cutting Technology,* 1990.

Janakiram, K. S. and Rao, S. B. C. " Studies Of The Characteristics Of Flow And Erosion Due To Plain And Cavijet Impingement." *Proceedings of 5 th International Conference on Erosion by Solid and Liquid Impact.* 70.1-70.9, 1980.

Johnson, V. E. Jr. et al., "The Development of Structured Cavitating Jets for Deep Hole Bits." *SPE* 11060, 1982.

Khan, M. E. H. and Geskin, E.S. "Investigation of Formation and Development of Highly Turbulent Water Jet." Proceedings of Water Jet Technology. Taiwan. 62-63, 1992.

Karamcheti, K. and Bauer, A. B. "Some Features of an Edge-Tone Flow Field." *Basic Aerodynamic Noise Research. NASA SP-207.* 275-304, 1984.

King, J. L., Boyle, P. and Ogle, J. B. "Instability in Slotted Wall Tunnels." *Journal of Fluid Mechanics.* 4: 283-305, 1985.

Kiyoshige, M. and Matsumura, H. "A Study Of Abrasive Waterjet Cutting Using Slurred Abrasives." *Proceedings of 9th International Symposium of Jet Cutting Technology.* 61-65, 1988.

Kohl. R.E. "Rock Tunneling with High Speed Water Jet Utilizing Cavitation Damage." *ASME* 65-PE-42, 1969.

Lai, M.K.Y., Vijay, M.M. and Zou, C. "Computational Fluid Dynamics Analysis of Submerged Cavitating Water Jets." *6th American Water Jet Conference.* 6: 411-426, 1991.

Launder, B.E. and Spalding, D.B. *Lectures in Mathematical Models of Turbulence.* Academic Press, 1972.

BIBLIOGRAPHY
(Continued)

Liao, Z.F. and Lin, T.C. "Theoretical Analysis and Experimental Study of the Self-Excited Oscillation Pulsed Jet Device." *International Water Jet Symposium in Peking, China.* 1987.

Lichtarowicz, A. and Nwachukwu, G. O. "Erosion by an Interrupted Jet." *4th International Symposium of Jet Cutting Technology,* 1978.

Martin, W. W., Naudascher, E. N., and Padmanabhan, M. "Fluid Dynamic Excitation Involving Flow Instability." *Proceedings of ASCE. Journal of Hydraulic Division. No. HY6: 681-698,* 1975.

Masanori Kiyoshige, et al., "Abrasive Water Jet Cutting Apparatus." *United States Patent.* No. 5,018,317, 1991.

Melville, W. K. and Brag, K. N. C. "A Model Of Two Phase Turbulent Jet." *International Journal of Heat Mass Transfer.* 22: 647-656, 1979.

Murphy, J.D. *Turbulence Modeling.* NASA Technical Memorandum 85889, 1984.

Noumi, M. and Yamaoto, K. "Flow Charateristics and Impact Phenomena of Pulsed Water Jets." *3rd Pacific Rim International Conference on Water Jet Technology.* 3: 47-58, 1992.

Pawan, Singh and Jose, Munoz. "The Align Ability of Jet Cutting Orifice and Nozzle Assemblies." *10th International Sympisium of Jet Cutting Technology,* 1990.

Rodi, W. "Turbulence Models and Their Applications in Hydraulics." *International Association for Hydraulic Research, The Netherlands,* 1980

Schlichting, H. *Boundary Layer Theory.* McGraw-Hill, 1979.

Shen, Z.H., Li, G.S. and Zeng, C.Y. "Experimental Study on Rock Erosion by Self-Resonating Cavitating Jets." *International Water Jet Symposium in Peking, China,* 1987.

Swanson, R.K., Kilman, M., Cerwin, S. and Tarver, W. "Study of Particle Velocity in Water Driven Abrasive Jet Cutting." *Proceeding of the 4th U.S. Water Jet Conference.* 4: 103-107, 1987.

Vajay, M.M., Hu, S. G. and Lai, M.K.Y. "Enhancing the Performance of Cavitaitng Water Jets." *7th American Water Jet Conference.* 7: 233-250, 1993.

Woolley, J. P. and Karamcheti, K. "Role of Jet Stability in Edge-Tone Generation." *AIAA Journal. 12: 1457-1458,* 1974.